# Design and Control of a Tactile Stimulator for Real Texture Simulation: Application to Textile Fabrics

Wael Ben Messaoud

N° d'ordre : 42039

## Université Lille 1 : Sciences et Technologies

Ecole doctorale Science pour l'Ingénieur ED SPI 72

# Thèse

Présentée en vue d'obtenir le grade de

Docteur de l'Université des Sciences et Technologies de Lille

**Spécialité Génie Électrique**

par

**Wael BEN MESSAOUD**

Le 6 Juin 2016

# Design and Control of a Tactile Stimulator for Real Texture Simulation: Application to Textile Fabrics

**Composition du jury**

| | | |
|---|---|---|
| **Président** | Pr. Alain BOUSCAYROL | Université Lille1 Sciences et Technologies |
| **Directeurs de thèse** | Pr. Betty LEMAIRE-SEMAIL | Université Lille1 Sciences et Technologies |
| | Pr. Marie-Ange BUENO | Université de Haute Alsace |
| **Rapporteurs:** | Pr. Philippe LUTZ | Université de Franche Comté |
| | Dr. Vincent LE HOUEROU | Université de Strasbourg |
| **Examinateurs:** | Pr. Antoine FERREIRA | INSA Centre Val de Loire |
| | Dr. Anthony GALLIANO | Ingénieur R&D à L'Oréal Saint Ouen |

Laboratoire d'Electrotechnique et d'Electronique de Puissance de Lille -- L2EP -- EA 2697
Laboratoire de Physique et Mécanique Textiles -- LPMT -- EA 4365

# Remerciement

Les travaux de recherche présentés dans ce manuscrit ont été effectués au laboratoire d'Électrotechnique et d'Électronique de Puissance (L2EP), Université de Lille 1 au sein de l'Institut de recherche sur les composants logiciels et matériels pour l'information et la communication avancée de Lille (IRCICA) et au laboratoire de Physique et Mécanique Textiles (LPMT), Université de Haute Alsace Mulhouse au sein de l'École nationale supérieure d'ingénieurs Sud Alsace (ENSISA). Je tiens tout d'abord à remercier les laboratoires et les universités pour leur accueil et pour l'ambiance de travail agréable.

Je remercie chaleureusement les régions Nord Pas de Calais et Alsace pour le financement de ce projet. Sans ces fonds, nous ne pourrions pas avoir été en mesure de maintenir cette recherche de doctorat et d'atteindre ses objectifs.

Je suis très honoré que Monsieur Philippe LUTZ, Professeur à l'Université de Franche-Comté et Monsieur Vincent LE HOUEROU, Maître de Conférences HDR à l'Université de Strasbourg aient accepté d'être rapporteurs de ma thèse. Je les remercie vivement pour l'intérêt qu'ils ont porté à mon travail et pour les remarques constructives sur la poursuite de mes travaux. J'associe à ce remerciement, mes examinateurs Monsieur Antoine FERREIRA, professeur à l'INSA Centre Val de Loire, Monsieur Alain BOUSCAYROL, professeur à l'Université de Lille 1, et Monsieur Anthony GALLIANO, Ingénieur R&D à L'Oréal Saint Ouen, pour l'intérêt qu'ils ont porté à mon travail de thèse.

Je suis grandement reconnaissant à mes directrices de thèse, madame la professeure Betty Lemaire-Semail et madame la professeure Marie-Ange Bueno, qui m'ont encouragé tout au long de la thèse. Je lui suis très reconnaissant de m'avoir assuré un encadrement rigoureux tout au long de ces années, tout en me donnant toutefois la possibilité de trouver par moi-même mon cheminement personnel. Madame Lemaire-Semail et Madame Bueno m'ont dirigé mes travaux avec beaucoup de disponibilité et d'intérêt. Elles m'ont toujours accordé généreusement le temps nécessaire pour partager avec moi des idées créatives. Merci pour leurs analyses soignées et leurs commentaires judicieux qui m'ont permis de raffiner davantage certains points de l'analyse et de l'interprétation de mes données.

Je suis aussi redevable à la contribution de monsieur Frédéric Giraud qui m'a dirigé au début de cette thèse. Il a consacré beaucoup de temps et d'énergie pour son avancement. Je remercie également monsieur Michel Amberg de m'avoir apporté les moyens techniques durant le travail de la thèse.

La validation de cette étude n'aurait pas été possible sans la collaboration des participants dans les expériences psychophysiques de toucher tactile qui ont accepté avec beaucoup d'ouverture, au travers de leurs engagements, de consacrer du temps et me prêter leurs doigts pour la science.

Mes remerciements vont particulièrement à mon père, Mohamed et ma mère Faouzia, qui m'ont constamment encouragé et soutenu tout au long de ces années. Je ne saurai passer sous silence l'apport inestimable des autres membres de ma famille qui m'ont soutenu, de près ou de loin durant mes études doctorales.

Les mots me manquent pour remercier, à sa juste valeur, mon épouse Taysir, pour ses soutiens moral et psychologique indispensables pour maintenir ce projet à flot au travers des aléas de la vie et pour avoir cru en mes capacités intellectuelles pour le réaliser.

Je ne saurais terminer sans souligner le soutien amical et chaleureux de mes collègues des deux laboratoires qui m'ont soutenu durant ce parcours de thèse : Sofiane Ghenna, Eric Vezzoli, Clément Nadal, Ehsan Enferad, Mathieu Decrette, Antoine Vaesken, Houssem Eddine Gassara, Claire Guignier et Donia Chetouane.

Merci à toute personne ayant contribué de près ou de loin à la réalisation de ce projet.

# Design and control of a tactile stimulator for real texture simulation: Application to textile fabrics


## Abstract

The friction modulation produced by ultrasonic vibrations is one of the methods which produces the tactile stimulation. The vibration amplitude is modulated depending on the finger position to give the illusion of touching a texture. This thesis aims at developing a tactile device able to simulate the sensation of touching complex textures such as textile fabrics. For this aim, we modelled first the vibration behaviour and proposed a new strategy to track the resonance frequency of the tactile device and to improve the robustness of the control. On the other hand, the relationship between the tribological aspects of interaction finger / stimulator and the perception of stimuli is assessed to define the most perceived tribological criteria. The tribological parameter named “friction contrast” is introduced. Following this tribological study, we developed a new tactile device called SmartTac integrating new force sensors to measure and control directly the coefficient of friction and to make it adaptive to the user’s finger. Last, a method for extracting the tribological properties of three various textile fabrics is applied to simulate them. Our method is validated by conducting a psychophysical experiment with a success rate of 78%, matching the simulated surfaces to real surfaces.



**Keywords:** Tactile stimulation, Ultrasonic vibration, System modelling, Closed-loop control, Tribology, Textile.

# Développement et contrôle d'un stimulateur tactile pour simuler des textures réelles : application aux surfaces textiles


## Résumé

La modulation de frottement par vibrations ultrasoniques est une des méthodes utilisées pour produire une stimulation tactile. L'amplitude de vibration est modulée en fonction de la position du doigt pour donner l'illusion à l'utilisateur de toucher une texture. L'objectif de cette thèse est de développer une interface tactile permettant de simuler la sensation tactile de textures complexes telles que des surfaces textiles. Pour ce faire, nous avons tout d'abord implanté une méthode de contrôle robuste du stimulateur tactile du L2EP grâce au développement d'un modèle du comportement vibratoire. Ce contrôle assure également le suivi de la fréquence de résonance afin d'optimiser l'efficacité énergétique du dispositif. Dans un second temps et après avoir évalué la relation entre les aspects tribologiques de l'interaction doigt/stimulateur et la perception des stimuli, nous avons prouvé par une étude statistique que le «contraste en frottement» est le paramètre le plus significatif et donc celui à programmer pour qualifier la variation de perception du frottement. Cette étude nous a menés à concevoir un nouveau dispositif tactile appelé SmartTac, intégrant des nouveaux capteurs de force permettant de mesurer et contrôler directement le coefficient de frottement pour qu'il soit adaptatif au doigt du sujet. Enfin, après avoir décrit une méthode d'extraction des propriétés tribologiques de trois surfaces textiles très différentes, la simulation de ces textures est entreprise avec le SmartTac. Notre approche est testée par la réalisation d'une expérience psychophysique sur la correspondance entre surfaces simulées et surfaces réelles: un taux de réussite de 78% valide notre démarche.



**Mots clés:** Stimulation tactile, Vibration ultrasonique, Modélisation des systèmes, Contrôle en boucle fermée, Tribologie, Textile.

# Table of contents

# List of figures

# List of tables

# Glossary

| | |
|---|---|
| **FA** | Fast adapting mechanoreceptors |
| **SA** | Slow adapting mechanoreceptors |
| **TPO** | Polymeric thermoplastic olefins |
| **DSP** | Digital Signal Processor |
| **PWM** | Pulse-width modulation |
| **COF,** $\mu$ | Coefficient of friction |
| **JND** | Just noticeable difference |
| **IQR** | The boxplot interquartile range |
| **VA** | Vibration amplitude |
| **PtP** | Peak to Peak |
| **VEL** | Velvet fabric |
| **VEL1** | The along pile direction of the Velvet fabric |
| **VEL2** | The against pile direction of the Velvet fabric |
| **SCOT** | Cotton twill fabric |
| **SPET** | Polyester twill fabric |
| $\boldsymbol{R_a}$ | Roughness |
| $\boldsymbol{c}$ | Stiffness parameter |
| $\boldsymbol{m}$ | Modal mass |
| $\boldsymbol{d_s}$ | Modal damping |
| $\boldsymbol{N}$ | Electromechanical conversion factor |
| $\underline{\boldsymbol{V}}$ | The ceramics supply voltage vector |
| $\underline{\boldsymbol{W}}$ | The vibration amplitude vector |
| $\boldsymbol{W_d}$ | The real part of the vibration vector |
| $\boldsymbol{W_q}$ | The imaginary part of the vibration vector |
| $\boldsymbol{V_d}$ | The real part of the voltage vector |
| $\boldsymbol{V_q}$ | The imaginary part of the voltage vector |
| $\boldsymbol{F_e}$ | Excitation frequency |
| $\boldsymbol{F_r}$ | Resonant frequency |
| $\boldsymbol{\omega}$ | Angular frequency |
| $\boldsymbol{\omega_0}$ | The resonant angular frequency |
| $\boldsymbol{\tau}$ | Time constant of the first order transfer function |
| $\boldsymbol{K}$ | Static gain of the first order transfer function |
| $\boldsymbol{V}$ | Sliding Velocity |
| $\boldsymbol{F_1}$ | Force sensor located in the North West $NW$ |
| $\boldsymbol{F_2}$ | Force sensor located in the South West $SW$ |
| $\boldsymbol{F_3}$ | Force sensor located in the North East $NE$ |

| | |
|---|---|
| $\boldsymbol{F_4}$ | Force sensor located in the South East $SE$ |
| $\Delta \boldsymbol{F_t}$ | The difference in friction force between the excited and the unexcited parts |
| $\boldsymbol{F_{t0}}$ | Initial friction force without vibration |
| $\boldsymbol{F_{t1}}$ | Friction force when vibration is switched on |
| $\boldsymbol{F_{n0}}$ | Initial normal force without vibration |
| $\boldsymbol{F_{n1}}$ | Initial normal force when vibration is switched on |
| $\Delta\mu$ | The difference in the coefficient of friction |
| $\mu_0, \mu_{max}$ | Initial coefficient of friction without vibration |
| $\mu_1$ | The reduced coefficient of friction |
| $\mu_{1_{ref}}$ | The reference value of coefficient of friction |
| $\boldsymbol{FFC}$ | Friction Force Contrast |
| $\boldsymbol{FC}$ | Friction Contrast |
| $\boldsymbol{FC_{S-F}}$ | Friction Contrast between the SmartTac and the user's finger |
| $\boldsymbol{FC_{F-F}}$ | Friction contrast between the real fabrics and the finger or the artificial finger |
| $\boldsymbol{FC_{F-F\,tot}}$ | The total friction contrast to be reproduced |
| $\boldsymbol{FC_{F-F\,sha}}$ | The shape of the Friction Contrast |
| $\boldsymbol{FC_{F-F\,tex}}$ | The fine texture of the friction contrast |
| $\boldsymbol{k_{FC}}$ | The adaptation constant between $FC_{S-F}$ and $FC_{F-F}$ |
| $\boldsymbol{k'}$ | The adaptation constant between $FC_{F-F}$ and $W$ |
| $\boldsymbol{A}$ | The amplitude of texture in percent |
| $\boldsymbol{V}$ | The sliding velocity |
| $\boldsymbol{E}$ | The error of the friction coefficient controller |
| $\boldsymbol{C_\mu}$ | The controller of the coefficient of friction |
| $\boldsymbol{C_W}$ | The controller of the vibration amplitude |
| $\boldsymbol{W_{ref}}$ | The reference of the vibration amplitude controller |
| $\boldsymbol{Mad}$ | Mean absolute deviation |

# Introduction

The touch perception of surfaces enables us to identify their characteristics and explore the world around us. In fact, this sense is used in diverse fields in everyday life to facilitate the interaction between the subject and the surface. Notably, the textile field is considered to be one of the important fields where the tactile interaction plays a crucial role in our judgment. For a long time ago, textile trade has been commonly used among people due to the importance of fabrics whereby clothes and carpets, for instance, are made. This kind of trade has been developed nowadays from selling in a real market to an online trade of textile offering many advantages. The online textile trade is a time-saving operation that can be conducted at anytime and anywhere in the world. Additionally, it is an easier way of trading as it gives more possibilities to choose the suitable fabric in a short time compared to the traditional trade. This type of shopping has significantly increased in the last decade and become indispensable for the consumers. However, despite the technological progress of the textile trade, one of the most important aspects is still missing which is the touch feeling.

Haptic devices are able to simulate the touch perception of the real surfaces in order to reproduce their features. Nowadays, numerous types of tactile stimulation devices have been developed which are different in the way of stimulating tactile signals as well as sense of touch. Tactile stimulators can simulate for example: texture, temperature, shape, etc. Each of these tactile stimulators has to be designed with different actuators and a different mechanical design depending on the dedicated way of touch.

To build a realistic tactile simulation, many interconnected domains must be investigated extensively:

- The mechanical field is used to design the stimulator dedicated to the specific type of stimulation.
- The electrical and control field is operated to generate the control signals and actuate the different parts of the device.
- The control processing and the computer programming are utilized to optimise the interface between the user and the device and to prepare an automatic way to save data and measurements.
- The signal processing from tribological measurement is employed to study the real textile surfaces and to extract their features to be simulated.
- The analysis of the effect of the stimuli on the subjects' perception is operated to realize psychophysical experiments which aim at validating the stimulation for the subjects.

This thesis entitled “Design and control of a tactile stimulator for real texture simulation: Application to textile fabrics” is a collaboration between the Laboratory of Electrical Engineering and Power Electronics (L2EP), Lille University and the Laboratory of Physics and Textile Mechanics (LPMT), University of Haute Alsace, Mulhouse. The thesis has been performed thanks to the financial support from the Nord Pas de Calais and Alsace regions.

Actually, the aim of this research work is the design and control of a tactile feedback device able to simulate a specific type of surfaces. This topic is multidisciplinary as it brings together the expertise of the two laboratories in different domains. The L2EP has started working on this subject in 2004 by designing different prototypes of tactile stimulation devices based on the friction modulation. The optimized stimulator called Stimtac made in 2011 was used to simulate different textures such as gratings, fish scales, and a first attempt of velvet simulation, already done in collaboration with the LPMT. On the other hand, the expertise of LPMT in tribology and tactile of textile fabrics is investigated. Being specialized in a specific field and having a specific expertise, each laboratory contributes to the improvement of the application by creating an adequate atmosphere for research to design a tactile stimulation device able to simulate the real textile fabrics.

The present manuscript is organized as follows:

Chapter 1 presents the state of art of the different types of the tactile feedback devices. The chapter opens with a classification of the stimulators into two types which are the local and the global stimulations, depending on the discretization of the stimulation area induced in the finger. Then, the stimulators based on the friction modulation and their different types and principle of operation are presented. Finally, it ends with a presentation of the particularity of the textile fabrics when extracting their features and their characteristics’ dependence on the sliding parameters.

Chapter 2 focuses on the development of a new approach to control a large version of a tactile stimulator based on the friction reduction. The first part of the chapter begins with an introduction of the stimulators developed previously in the laboratory. In the second part, the robustness of the stimulator in open loop is studied after showing the design specifications. Then, in a third part, in order to perform the closed loop control of the stimulator and to cope with the disturbance influence, the model of system is established, enabling to find the transfer functions. In the following part, the closed loop control of the vibration amplitude is implemented to improve the robustness and dynamics of the system. Finally, the last part of the chapter ends with an evaluation and a validation of the performances obtained by the closed loop thanks to experimental measurements and by the use of a psychophysical study.

Chapter 3 concerns the analysis of the relation between human perception and friction in the tactile stimulation. This analysis is performed to integrate the tribological field between the controlled vibration amplitude and the perception. It is necessary to investigate more thoroughly the perception of a simulated surface relative to the user's finger. The first goal of the chapter is to determine the tactile perception's threshold as a function of the vibration amplitude by operating a psychophysical experiment. Then, we aim at determining the most relevant tribological criterion relative to the tactile perception. Finally, the dependence of this friction criterion called "the friction contrast" on the initial coefficient of friction and the exploration velocity is studied.

Chapter 4 proposes a new high fidelity tactile device called SmartTac. The particularity of this device lies in the fact that it includes new force sensors allowing to measure in real time the friction force and then the coefficient of friction. Thus, this stimulator is able to control in real time the coefficient of friction, which is in agreement with the conclusion of the third chapter in order to simulate textile surfaces. Tribological validation of the coefficient of friction control is proved by an experiment on subjects showing a stable and desired level of friction with a variable response time between 3 and 5 ms. A first attempt to control the friction contrast is shown but a limitation of the SmartTac is found, due to the variability of the initial coefficient of friction. Therefore, a solution to reduce this variability is introduced and tested.

The final chapter evaluates the performances of the developed and controlled tactile stimulator for textile fabrics simulation. The chapter opens with a fabric feature extraction with a multilevel approach allowing to evaluate the friction between real fingers or an aluminium slider and the surfaces to be simulated. Two psychophysics experiments are operated: The first experiment aims at calibrating the amplitude of the haptic signal from a series of trials performed on 11 subjects. The second experiment is performed on 21 volunteers aiming at validating the simulated fabrics. Three various textile fabrics are chosen which are: a pile fabric (velvet), a fabric with a texture and a standard hairiness (cotton twill woven fabric) and a fabric with a fine texture and without hairiness (polyester twill woven fabric). This experiment gives satisfactory results with an average of 78% for the matching rates between the simulated and the real surfaces, which validates the simulated surfaces strategy.

The manuscript ends with conclusions of the research work along with perspectives that are envisaged.

# Chapter 1

# State of the art

# 1 State of the art

## 1.1 The sense of touch

The sense of touch represents one of the five human senses (sound, sight, touch, smell, and taste). Through touch, humans can enter into contact with the environment and can perceive the objects around them. Its importance lies in its ability to detect and make a difference between the objects that interact with. This sense plays the role of intermediary between the environment and the brain when entering in contact with objects. The sensation perceived when touching is performed by the activation of different receptors inside the skin, sensitive to external stimuli. Each type of sensory receptors can be classified according to its ability to detect various stimuli such as mechanoreceptors for touch, thermoreceptors for temperature (whether cold, warm or hot) and nociceptors for pain. The receptors cover the skin surface and play a crucial role in preventing the brain from touching surfaces that can affect the skin. Without the sense of touch, the skin cannot be protected against harmful sensations such as hotness or pain that can burn or injure the skin when touching some surfaces or the hand cannot catch an object safely. The information we receive from the objects surrounding us through the sense of touch are huge. Although we do not yet know all the elements that affect skin when touching something, the sense of touch is considered very important, and enables to explore the world around us.

Even if there is a lot of discussions about the role and sometimes the existence of some mechanoreceptors, they will be presented in this manuscript in the most common way. Mechanoreceptors perceive sensations of pressure, vibration, and texture. There are four types of mechanoreceptors. Each of them has a specified function. The four mechanoreceptors types are: Merkel discs, Meissner's corpuscles, Ruffini corpuscles and Pacinian corpuscles as shown in Figure 1-1.

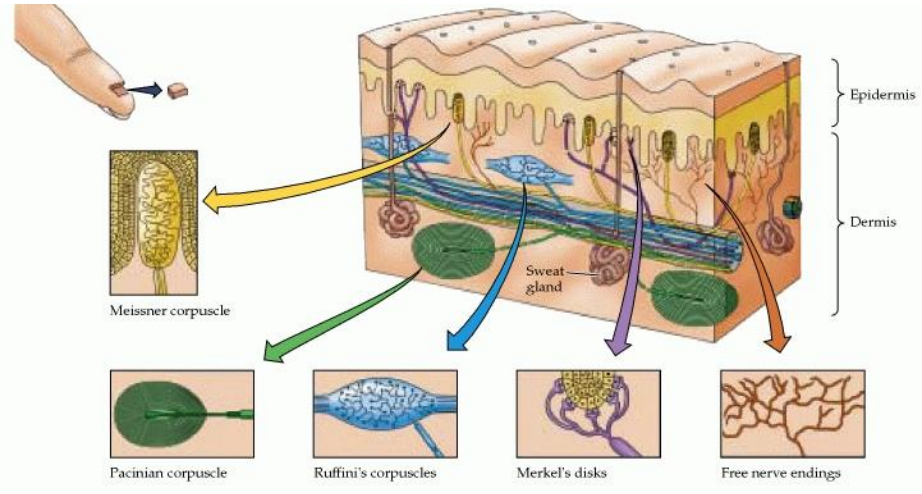


Figure 1-1: Finger mechanoreceptors (Darian-Smith, 1984)

The mechanoreceptors in the skin can be separated into distinct categories: the fast adapting (Pacinian and Meissner) and the slow adapting (Merkel and Ruffini) mechanoreceptors.

The fast adapting mechanoreceptors (FA), like the Pacinian Corpuscles, detect rapidly small and quick changes in the stimulus sensed by the human skin with a response time less than 0.1 second. This sensitive type of mechanoreceptors is found principally in the subcutaneous layer of the skin, to be protected against injuries that may affect the skin. These receptors are used in the surface roughness perception, as the fingertips are dragged across a surface, or to detect small and quick vibration levels. As the skin acts to distribute the forces applied by the surfaces with a maximum sensitivity, it is not necessary to have a high surface density of these receptors, even if they are located rather far from the surface.

The Meissner's Corpuscle is a type of moderate adaption receptor. These receptors are located near the skin surface; their response time is about 1 second. For example, these receptors are able to detect insects on the skin (mosquitoes, flies, etc.).

Ruffini Endings and Merkel's Cells are examples of slow adapting (SA) mechanoreceptors. These receptors are generally located close to the surface of the skin, and they are responsible for the static perception capabilities. For instance, they are used to feel changes on the skin such as static pressure and to maintain grip on an object, all situations which have usually slow adaptation times. The time scale of the adaptation of these cells can be 10 to over 100 seconds.

## 1.2 Tactile feedback devices

The tactile feedback devices are a type of haptic devices, as haptic includes tactile and force interaction. A bidirectional interaction is perceived between the finger and the haptic device. This means that it is not just an interaction from the user's finger towards the surface or the screen that can be made, but it is also an interaction from the surface towards the finger. The main objective of the tactile feedback devices is the reproduction of the sense of touch of real surfaces using a programmable device. The ways to touch are related to what we want to feel. There are two types of finger stimulation: local and global stimulations. Each of these stimuli corresponds to different types of tactile feedback devices.

### 1.2.1 Local stimulation

Local stimulation can reproduce a local physical sensation under the finger of the user, differentiated at the level of the fingerprint grooves. To achieve this aim, this family of tactile stimulators is operating as follows: the finger is placed statically on the interface in motion. Typically, the stimulation is based on the programming of a matrix of pins; the normal movement on the surface of these pins is programmed to stimulate the finger when it touches the active surface of the device. In some cases,

the pins are working in a quasi-static mode, rather to simulate shape (Velazquez et al., 2005). In most cases, they vibrate with a frequency less than the mechanoreceptors threshold (400 Hz) typically between 10 and 200 Hz and with a displacement of the order of a few micrometres. The main application for this type of tactile display is the development of the Braille display (Echenique et al., 2010) to help blind people to read texts. Generally, blind readers use the sound output to access to the texts (Coutinho et al., 2012; Supriya and Senthilkumar, 2009). But, the sound output is limited in term of scientific equations, graphic or music. Additionally, (Varao Sousa et al., 2013) demonstrated that the fact of listening to text is fundamentally different from actively reading for visual readers. They report that more active modes of reading (such as reading silently or reading aloud) lead to less mind-wandering and greater comprehension than when participants passively listened to the text being read to them. Recently, researchers have investigated on the development of a low cost refreshable Braille display able to help blind reader to read texts and other materials (Russomanno et al., 2015).

Various techniques exist for powering pins. The electromagnetic technologies are the more common (Benali-Khoudja et al., 2004; Lee et al., 1999; Streque et al., 2010).Using a pneumatic pump for expelling air through microvalves (Asamura et al., 1998) proposed a stimulator with 2 mm of diameter and 0.5 mm of thickness. Piezoelectricity is also a good candidate to actuate tactile displays. One of the most famous piezoelectric device is the OPTACON (Efron, 1977) dedicated to blind people who can perceive on their finger the Braille translation of a camera read text (Nye, 1976). Another type of local stimulation device using piezoelectric technology has been proposed in 2000 by (Hayward and Cruz-Hernandez, 2000). It differs from the preceding as it stretches the skin. Indeed, the pins are actuated in a lateral movement; this device is called the STReSS. Figure 1-2 illustrates the final assembly of 6 * 10 piezoelectric bimorph with a spatial resolution of 1.8 * 1.2 mm

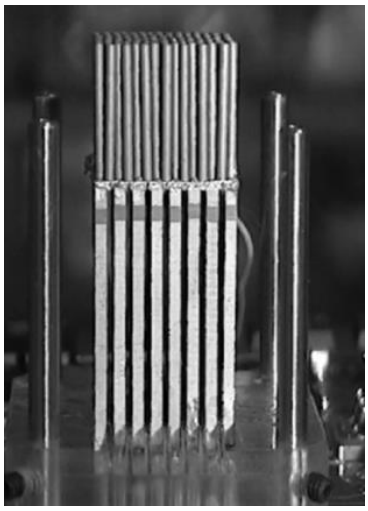

Figure 1-2: STReSS lateral skin tactile display (Hayward and Cruz-Hernandez, 2000).

In general for local stimulation, it must be noted that this technique is effective and does give a good sensation only if the pins' matrix density is high. The main difficulty is that each pin must be controlled independently, which makes this technique complex in terms of manufacture and expensive in terms of cost.

### 1.2.2 Global stimulation

In contrast to the local stimulation, the global stimulation consists of having the same stimulation on the whole finger. To perceive changes in stimuli, the finger must be in motion on the tactile device, and the physical parameter which may be controlled is the friction between the moving finger and the surface. By modulating the friction according to the finger position, it is possible to produce the illusion of touching various surfaces such as smooth or rough surfaces (Watanabe and Fukui, 1995). The finger position is a highly important parameter because the simulation is based on it.

This type of devices is dedicated mainly to improve the tactile touch screens like smartphones, tablets or touch screen pc by adding a tactile feedback. This feedback from the tactile device towards the user's finger will give more realistic touch conditions. For example, it will be felt a textured image on an LCD screen when entering in contact with the image Figure 1-3.

Figure 1-3: A developed tactile feedback device used to render 3D surfaces (Disney Research) by (Kim et al., 2013).

## 1.3 Stimulators based on the friction modulation

### 1.3.1 Tactile stimulation principle

These devices belong to the global stimulation device family. We can distinguish two techniques to control the friction which are Ultrasonic Vibrations and Electrovibration. The Electrovibration generates an attractive force between the

finger and a polarized surface. A high voltage must supply the plate which is covered with an insulator to polarize the finger. This electrostatic force attracts the finger and increases the coefficient of friction, which gives a modified sensation from the non-supplied surface (Kaczmarek et al., 2006).

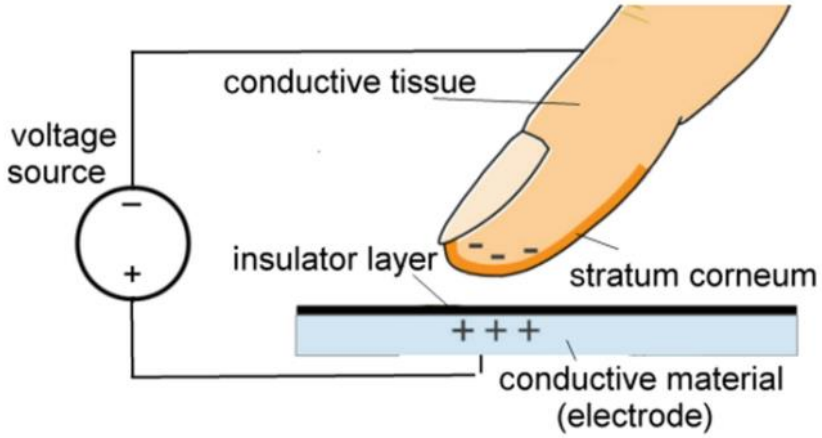


Figure 1-4: Representation of the electrovibration principle from (Vezzoli et al., 2014).

Different devices have been designed based on the electrovibration effect, we can cite for example TeslaTouch illustrated in Figure 1-5 (Bau et al., 2010), 3D rendering texture by Disney research (Kim et al., 2013) or the Senseg device (Wijekoon et al., 2012). It must be noted that no physical movement of the surface is required to create the tactile feedback using this type of devices because the effect is based on electrostatic attraction.

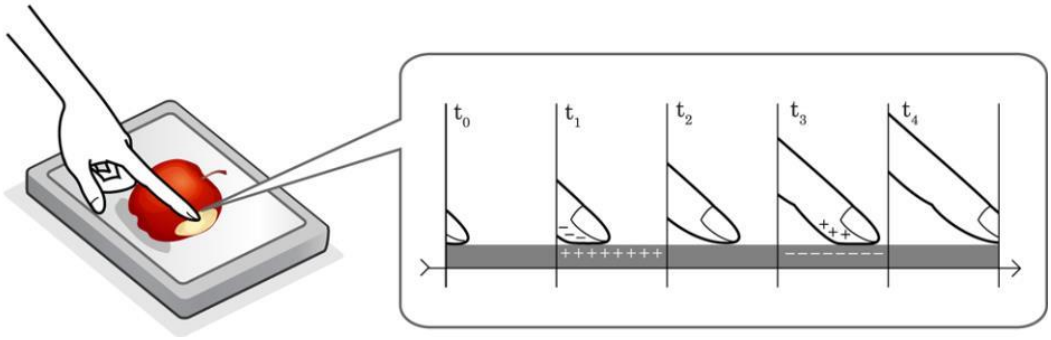


Figure 1-5: TeslaTouch device controlling electrostatic forces to modulate the friction from (Bau et al., 2010).

On the other hand, the other family of the friction modulation devices, on which this thesis is focused, relies on ultrasonic vibrations, which constitute an alternative technique to modulate the friction. A first physical explanation for the friction reduction using ultrasonic vibration is given by the squeeze film theory (Biet et al., 2007; Watanabe and Fukui, 1995; Winter et al., 2013): ultrasonic vibrations generate an air film between the fingertip and the stimulator which acts as a lubricant between the surface and the finger, and reduces the friction. This air film created by the plate

is modulated by the amplitude of the ultrasonic vibrations of the surface. More recently, some studies proposed other causes for friction reduction, based on an intermittent contact mechanical approach (Dai et al., 2012; E. Vezzoli et al., 2015b). For ultrasonic excitation, piezoelectric ceramics are utilized to provide a vibration at the whole system mechanical resonance frequency; this type of actuators is chosen for its high responsivity and its low power consumption. The first device based on this principle was developed by (Watanabe and Fukui, 1995) twenty years ago.

Some conditions have to be respected to produce this effect. The first one is that the vibration frequency should be more than 25 kHz and the second condition relies on the vibration amplitude that should be superior to 1 μm peak to peak to generate friction reduction (Biet et al., 2007). A standing wave is created when the plate is excited at a specific mechanical resonance frequency of the vibrating plate. This frequency is defined by its material, its geometry and the number and the position of the piezoelectric ceramics actuators. The resonance frequency can be pre-determined using a FEM analysis. Then a vibrometer is operated to check the simulated results.

Different tactile feedback devices have been proposed and evaluated, we can cite for example (Wiertlewski et al., 2014; Winter et al., 2013). The TPad project from Northwestern university was one of the first proposal, (Winfield et al., 2007) and was based on a small circular piezoelectric bending element. From this first prototype, E. Colgate's team went on working on the topic and in 2013, the principle has been implemented in a Kindle Fire™ (Figure 1-6) tablet computer having a large screen area (88 mm x 152 mm) to increase the range of potential applications.

Figure 1-6: The TPad fire (Mullenbach et al., 2013)

Figure 1-7: The optimized Stimtac version connected by a USB connection

The Stimtac project developed in the L2EP laboratory started in 2004 has proposed multiple tactile feedback devices based on the ultrasonic friction modulation. This project recorded several notable changes from the first prototype, fully glued by piezoelectric actuators (Biet et al., 2007), to an optimization of the actuator number to reduce the power consumption in (Giraud et al., 2010). The finger position sensing has been evolved from the use of a 1D LVDT sensor to a 2D position sensing using four force sensors which can also measure the normal force applied by the user. A transparent tactile stimulator has been also developed using a glass material plate in (Giraud et al., 2012). An optimized tactile device connected to the PC by an USB cable has been developed in (Amberg et al., 2011), a picture of the Stimtac device is illustrated in Figure 1-7.

It may be noted that all these global stimulation devices allow only the tactile feedback on a single finger, as the active surface is in the same state at a given time. To allow multi touch tactile feedback with global stimulation devices, another approach has been studied recently, which aims at creating different touch sensations in the same surface. This method, which is based on ultrasonic vibration using a multimodal approach, consists in exciting several vibration modes at the same time corresponding to different mechanical resonant frequencies (Ghenna et al., 2015). The superimposition of several modes allows to produce different tactile stimulations on several fingers located in different positions. Another approach based on the multi-touch stimulation using electrovibration is reported in (Nakamura and Yamamoto, 2014).

As the two effects, Electrovibration and Ultrasonic Vibrations, modulate the friction in an opposite way (one increases and the other effect decreases it), it seems interesting to couple the two effects together in order to increase the range of the

modulated friction. The idea to couple the two effects has been applied and implemented for the first time in the same device by (Frederic Giraud et al., 2013). The two effects, using different principle are compatible. A tribological measurement confirmed that by giving step references of ultrasonic vibration and electrovibration (Figure 1-8), it was possible to increase and decrease the friction. It is also technically possible to produce almost the same modulation level using the two effects.

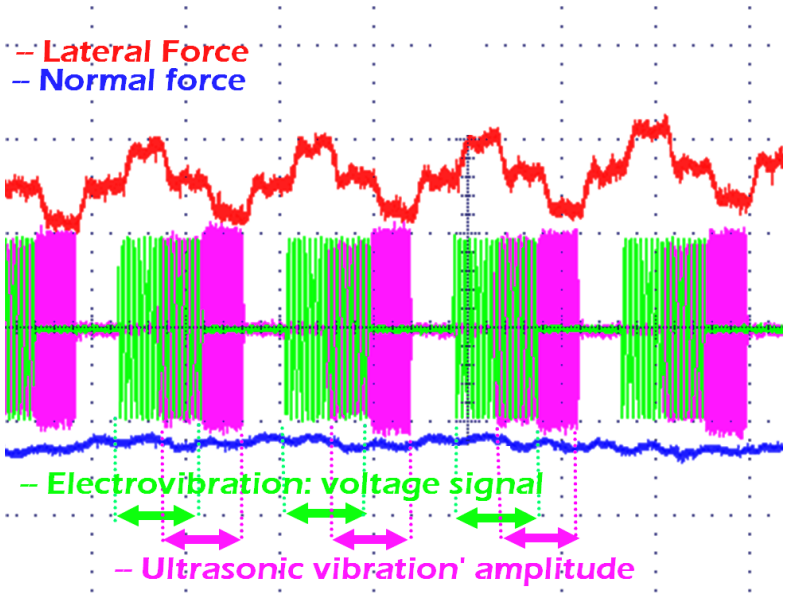


Figure 1-8: Combined stimulation with electrovibration and ultrasonic vibrations in the same device (Frederic Giraud et al., 2013).

A recent contribution by (Meyer et al., 2014) has investigated the dynamic behaviour of the two friction modulation effects, with three different velocities 20, 40 and 80 mm/s of the finger on the device. The results show that the dynamic behaviour of the electrovibration effect is faster than the ultrasonic vibration one. However, authors confirm that even if the dynamic of the ultrasonic vibrations is lower, the range of the friction modulation using this effect can be larger than the one obtained from electrostatic friction modulation. Nevertheless, it must be noted that the response time has been measured between the applied voltage to piezoelectric ceramics and the resulting friction force, which means that the mechanical response time of the vibrating plate was included in the response time of the effect.

In our recent paper (E. Vezzoli et al., 2015a), the compatibility of both effects to be implemented in the same device were proven at three levels: static, dynamic and perceptual. The static independence confirmed the possibility to couple the two effects to enhance the range of lateral force modulation experienced by the finger (Eric Vezzoli et al., 2015a). Moreover, it has been demonstrated that if the influence on the lateral force by the two effects is considered as similar, it is possible to obtain a friction modulation equal to zero while coupling them in phase. The measurements confirm the physical independence of the two effects and confirm the validity of the

equation (1.1) relating the normal, lateral and the electrostatic forces and the coefficient of friction.

$$F_t = (\mu - \Delta\mu)(F_n + F_e) \tag{1.1}$$

where $\mu$ is the coefficient of friction between the finger and the plate, $\Delta\mu$ is the induced variation of the coefficient of friction performed by ultrasonic vibrations, $F_n$ is the normal force applied by the finger and $F_e$ is the induced normal force between the finger and the plate by electrostatic force.

In the range of induced modulation, it is possible to conclude that the two effects are purely complementary, and cannot influence each other.

The dynamic behaviour has been also investigated using a vibrating plate with a fast response time(Ben Messaoud et al., 2014b), about 1.5 ms, which is 10 times faster than that used in (Meyer et al., 2014). The response time has been measured between the vibration amplitude and the lateral force to investigate the dynamic behaviour of the effect decoupled to the dynamics of the mechanical system. With these conditions, the dynamic response of the two effects has been evaluated from a statistical analysis. The experiment confirms that in most of the cases considered, the rising times of the two effects are comparable as shown in Figure 1-9. Hence, they can be successfully coupled additively in static and also in dynamic.

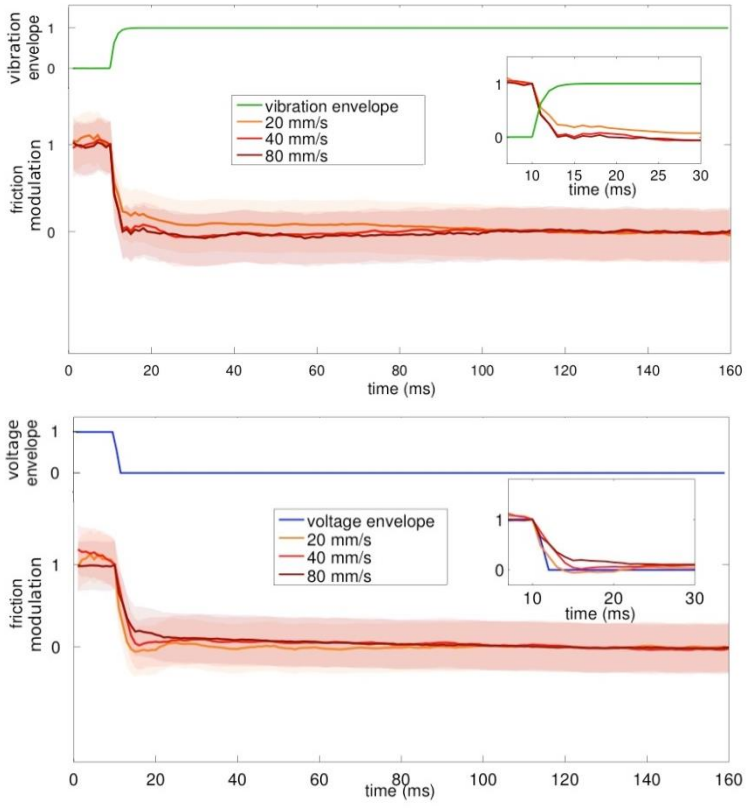


Figure 1-9: Friction modulation for different finger speeds related to the measured plate vibration or voltage envelope reported in the figure. The shadowed area represents the measure standard deviation. **a),** descending friction ultrasonic devices**, b)** increasing friction electrostatic devices

The last level of coupling validation which is the perceptual validation was also proven. A psychophysical experiment on the two coupled effects confirms that it is always possible to find a level where the two effects fully compensate each other. The experiment demonstrates that the two friction modulation techniques are perceived in the same way by the users.

## 1.4 Simulation of real surfaces: case of textile fabrics

### 1.4.1 Applications of the texture simulation

The principal goal of the texture simulation is the reproduction of the touch sense of textures. Different applications where the sense of touch is very important can be targeted using the tactile feedback devices. For instance, in the e-commerce shopping, one of the significant differences between reality and virtual shopping is the impossibility for the purchaser to touch products before buying (Bingi et al., 2000; Lee, 2002). Another application which can be also targeted is the virtual prototyping as design assistance (Fontana et al., 2004), or tactile deficiency detection and rehabilitation (Bueno, M.-A. et al., 2015).

For textile industry, the texture and colour simulations on the computer screen are used for the designers of fabrics without having the touch feeling of the surface. Additionally, the textile industry exchanges a great number of fabric samples between the designers of objects (garment, upholstery …) and the fabric producers. Virtual tactile textures simulation could facilitate these transfers by adding the touch feeling of the surfaces. Furthermore, the tactile simulation could be used by the final consumer to choose the textile material sold through the internet (Peck and Childers, 2003; Varadarajan and Yadav, 2002). In the future, the textile fabrics samples can be simulated to have their own 3D body shape (Loker et al., 2008). In other words, it would be possible to choose online a fabric in terms of colour, texture and drape, to choose a garment shape and to simulate individual avatars wearing virtual garments (Fontana et al., 2004; Luginbühl et al., 2011).

To build realistic tactile virtual textures, it is required to measure the real surfaces then transform them to a digital signal. This signal called haptic texture has to be implemented in the tactile device. Haptic textures have been investigated extensively by characterizing the surface roughness and friction. Some psychophysical studies have shown that the surface properties are more important for haptic exploration of the surface than vision (Klatzky et al., 1987). The friction and texture can be used to enhance the haptic simulation. However, several difficulties must be faced to obtain the measurement of the real surfaces. First, the mechanics of contact have to take into consideration the sliding parameters such as the velocity and the normal force to construct accurate physical models. Second, the measurement tool (the slider) must be well chosen to characterize the real surface.

### 1.4.2 Texture feature extraction

Various methods of texture feature extraction exist in literature. The first one is the measurement of the acceleration of a probe tip in contact with the surface to characterize. An accelerometer must be attached to the probe to measure this contact parameter. Several researchers use this technique to characterise the texture surface; in (Pai and Rizun, 2003), a wireless haptic texture sensor (illustrated in Figure 1-10) has been designed to measure the contact force and the acceleration with the selected textures.

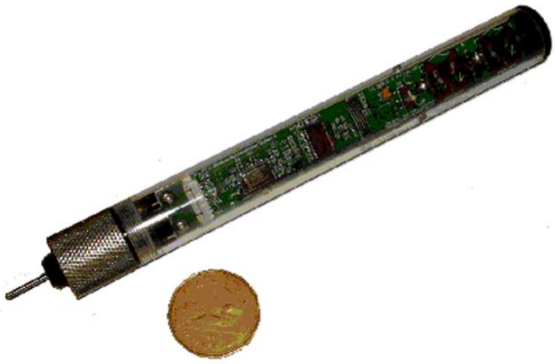

Figure 1-10: The WHaT prototype used to measure the contact force and the acceleration between the device and the real surface (Pai and Rizun, 2003).

In (Strese et al., 2015), an accelerometer was also employed by sliding a rigid tool over a surface. The vibrations induced on the tool, representing the interaction between the tool and the surface texture, were measured.

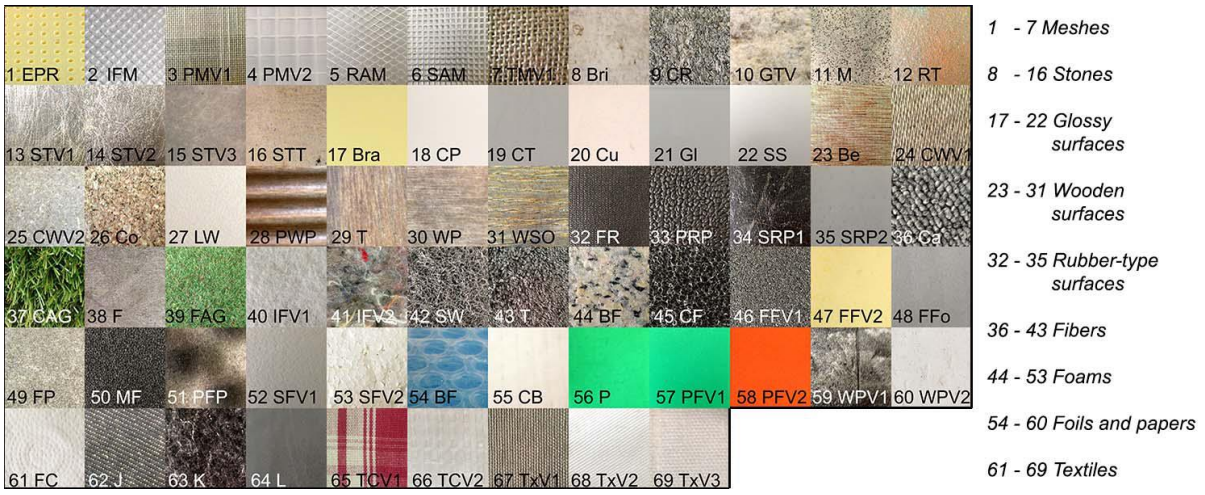


Figure 1-11: Materials included in the haptic surface database in (Strese et al., 2015), freely accessible at http://www.lmt.ei.tum.de/texture

The acceleration signal can be used to recognize or to classify object surface textures. As different parameters influence the sliding process, such as the applied force and the velocity, the used measurement device characterizes the texture for different normal applied forces, with controlled constant velocity and free movement of the slider. Afterwards, a haptic texture database has been established for 69 different textures to have digital signals of the textures ready for use in haptic stimulation devices. A photo of the studied textures is illustrated in the Figure 1-11.

As we can see, usually, the characterization of the surface is done by sliding a rigid tool on it; the measurement of the slider's acceleration is done using an accelerometer. It can be noted that the signal extracted from this measurement cannot characterize adequately the surface in terms of tactile perception because it is a characterisation of a rigid tool and not a measurement of an interaction between real fingers and the surfaces. To resolve this problem, (Martinot, 2006, p. 110) operated a high sensitivity accelerometer attached to the user's finger, to approach the touch conditions Figure 1-12. The application was not to characterize the textures but to feel the vibration caused by a rotating wheel imitating a regular texture. The accelerometer was attached to the nail of the finger, to be as close as possible to the friction area and the weight of the accelerometer was light enough to be glued to the nail. The author deduced that the measurement system cannot be precise to sense the vibrations unless the angle between the finger and the surface is larger than 60 degrees. Three other angles were evaluated also 0, 30 and 45°, giving a low sensitivity of the accelerometer to the vibration. We can conclude that the idea to glue the measurement system is validated but it shows a limitation when the angle is low as the accelerometer must be as close as possible to the surface.

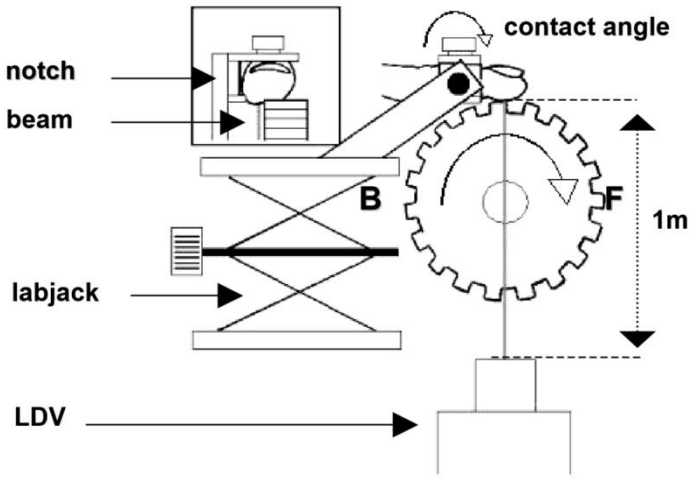


Figure 1-12: Photo of the experimental setup used to measure the acceleration when the finger is in contact with a rotatory wheel (Martinot et al., 2006).

The real texture can be characterized also by extracting the friction between the surface and the slider. Few works exist in literature using the friction characterization to be applied in the case of tactile reproduction. As the friction is not a characteristic

of the material only, a slider must be used to determine the friction test between the surface and the slider. The friction measurement depends greatly on the material of the slider. The measurement of the friction needs a tribometer able to measure the lateral force by applying a known normal force and velocity. The origin of the present thesis has begun from the collaboration between the laboratories L2EP and LPMT when trying to simulate the velvet fabric using the Stimtac tactile device (Amberg et al., 2011). In the work of (Bueno et al., 2014), a tribological measurement of the contact between a probe slider and the velvet has been realised. Depending on the direction of motion, against and along pile, a difference of the coefficient of friction adapted to the velvet real characteristics has been noticed and measured. A transition phase when moving from one direction to the other was observed which is different between the three velvet fabrics as shown in Figure 1-13. The measured friction profile was transformed to a digital signal and implemented to the Stimtac device. This signal includes the shape of the measured signal and the fine textures of the velvets are modelled as a square signals. After that, to validate the simulated surfaces, a psychophysical experiment was conducted to compare the real and simulated velvets.

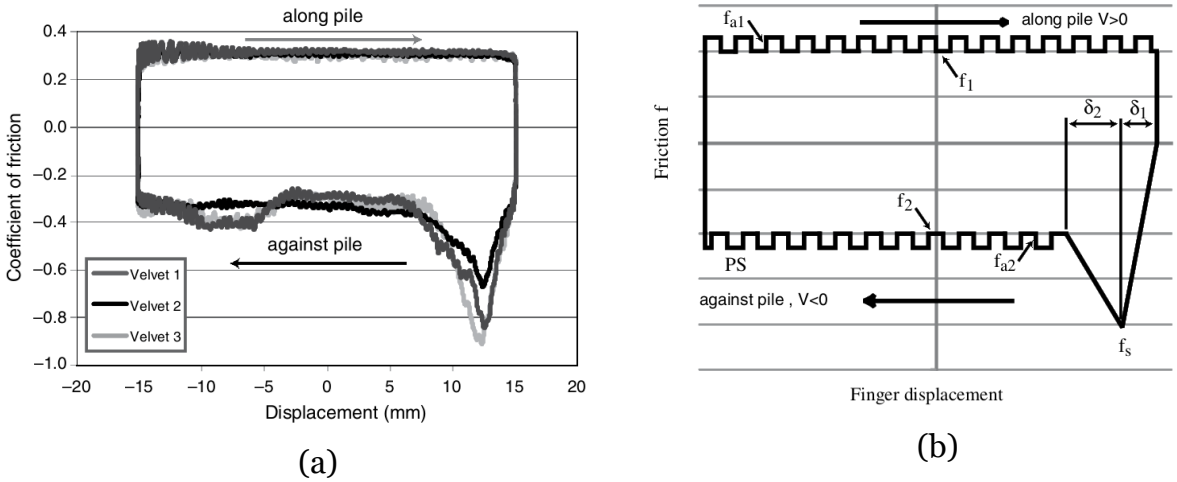


Figure 1-13: (a) The measured coefficient of friction between the slider and the three velvet fabrics as a function of the slider position. (b) The determined signal implemented on the Stimtac tactile device. From (Bueno et al., 2014).

### 1.4.3 Dependence of the friction on the sliding parameters

It was observed using the accelerometer that the sliding conditions influence the extracted signal. By measuring the friction when sliding a tool on a surface, it was also observed in several studies that the sliding conditions such as the normal applied force ($F_n$) and the velocity ($V$) affect the coefficient of friction noted μ. The variability of μ as a function of the sliding parameters depends highly also on the shape and the material of the slider. Several researches analyse the effect of μ by using different probes or real finger and for different ranges of $F_n$ and $V$. The following Table 1-1 sums up the evolution of the coefficient of friction (COF) depending on normal force and the slider materials.

Table 1-1: The evolution of the coefficient of friction when the normal force increases for different sliders and different velocities.

| **Publication** | **Surface** | $F_n$ [$N$] | **Velocity** | μ % $F_n$ |
|---|---|---|---|---|
| (Al-Samarai et al., 2012) | aluminium–silicon | 10-30 | 200-300-400 rpm | ↘ |
| (Darden and Schwartz, 2013) | Elastomer-texture | 2.5-17.8 | 200 mm/s | ↘ |
| (Pascoe and Tabor, 1956) | | Very small | | ↘ |
| (Jiang et al., 2008) | Thermoplastic olefins - Rough surface | 5-20 | 100 mm/s | ↗ |
| (Souza et al., 2014) | Polyester composite | 1-10 | 100 et 200 rpm 21-42 mm/s | ↗ |
| (Sivamani et al., 2003) | Skin hand / surface | 0.05-0.45 | | ↘ |
| (Koudine et al., 2000) | Skin /glass pad | 0.02-0.8 | | ↘ |
| (Fagiani et al., 2012) | Finger / Aluminium | 0-2 | 10-20 mm/s | ↘ |
| (Tang et al., 2008) | Hand skin / polypropylene probe | 0.1-0.9 | 1 mm/s | ↗ |
| (Liu et al., 2013) | Finger / surface | 2-25 | 10-28 mm/s | ↗ |

In (Al-Samarai et al., 2012), when sliding a silicon with aluminium surface, authors found that the coefficient of friction decreases when the normal force increases for a range of the studied $F_n$ between 10 and 30 N. In another study (Darden and Schwartz, 2013), the coefficient of friction between the silicon and a non-textured surface is linked to the normal force by $\mu = K\,{F_n}^{-0,26}$ for a range of normal force between 2.5 and 17.8 N and a scanning speed of 200 mm/s. The same result was found also in (Pascoe and Tabor, 1956). Conversely to these studies, the authors of (Jiang et al., 2008) rubbed polymeric thermoplastic olefins (TPO) against different surfaces with different roughness $R_a$ between 0.5 and 17.8 microns, they concluded that the coefficient of friction μ increases as the normal force increases from 5 to 20 N for all the used surfaces with different roughnesses. It is noticed in this study that the surface has been scratched during the experiment that may cause this augmentation. In (Souza et al., 2014), the study was carried out on the composite polyester, the coefficient of friction increases with the normal load in the load range between 1 and 10 N.

(Sivamani et al., 2003) found that μ decreases as $F_n$ increases when the skin is in contact with a surface, following a relationship expressed as follows: $\mu = K\,{F_n}^{-0,32}$. According to (Koudine et al., 2000) the coefficient of friction can be expressed as

$\mu = K\,F_n{}^{-0,28}$. (Fagiani et al., 2012) have measured the coefficient of friction between a finger and an aluminum surface, the same conclusion is found that μ decreases as $F_n$ increases ($\mu = K\,F_n{}^{-0,27}$) for a scanning velocity of 10 mm/s and with a coefficient -0.24 for a speed of 20 mm/s. However, in (Tang et al., 2008) the coefficient of friction increases with the normal charging by rubbing a polypropylene ball on the skin of the hand, which is explained by authors because not only the adhesion counts but also the deformation of the skin and the contact material plays. In (Liu et al., 2013), the authors also found that the coefficient of friction increases with the load applied in the case of a human finger to friction of the support forces between 2 and 25 N.

From these studies, we can conclude that the friction evolution depends critically on the sliding parameters such as the normal force, the velocity and the slider material. When the slider is the finger, the evolution depends also on the finger parameters such as the humidity. This significant dependence is a real issue when we want to add the tactile feedback in tactile stimulation devices. In the case of the tactile feedback devices based on the friction reduction, a special attention must be paid on the dependence of the friction on these different parameters.

## 1.5 Conclusion

The first chapter focused on the state of the art of different types of tactile feedback devices. The difference between the local and the global stimulation has been first mentioned which is based on the stimulation location on the fingertip. Next, the tactile feedback devices based on friction modulation type are identified and a brief state of the art of some prototypes based on this technology was presented. Then, some texture feature extraction methods for extracting the haptic signal are presented and compared. Finally, the dependence of the friction on the different sliding parameters is mentioned, which can present a real issue when we want to add the tactile feedback in tactile stimulation devices. The next chapters will analyse the possibility to design a tactile stimulator able to simulate textures especially fine fabric textures.

# Chapter 2

# Design and Control of the tactile stimulation device

# 2 Design and Control of the tactile stimulation device

In this chapter, our aim is to design a friction controlled tactile stimulator and to improve its performance so as to be able to simulate the sensation of touching real surfaces. As seen in the previous chapter, ultrasonic vibration stimulators are able to reduce the friction between the finger and the surface. The intensity of the ultrasonic vibration can be modulated depending on the finger position or following a temporal variation. When the amplitude increases, the finger feels that the lubricated surface becomes more slippery.

We will first introduce the stimulators previously developed in the laboratory of Electrical Engineering and Power Electronics (L2EP). Then, we will analyse their robustness in open loop after giving their design specifications. After that, in order to perform the closed loop controls of the stimulators, we will develop the system modelling leading to the transfer functions able to predict the system's behaviour in response to a voltage excitation. Following that, the control of the vibration amplitude will be implemented after identifying the transfer functions. Finally, the performances obtained by the closed loop will be evaluated thanks to experimental measurements and by a psychophysical study.

## 2.1 Previous studies on ultrasonic tactile devices in L2EP

The former tactile stimulation devices developed in the L2EP laboratory are mainly based on the ultrasonic vibration. This vibration with an amplitude of a few micrometres creates the feeling of a smoother surface. By just adjusting its intensity depending on the finger position, it is then possible to recreate the sensation of touching a textured surface. This slippery feeling of the finger when sliding on the surface was first explained by the creation of the squeeze film effect theory which proved that an air film is created between the finger and the surface (Watanabe and Fukui, 1995; Wiesendanger, 2001). However, some recent studies have been focused on the physical explanation of this friction weakening effect (Eric Vezzoli et al., 2015b; Xiaowei Dai et al., 2012). Even if squeeze effect may occur between the vibrating surface and the fingertip, some other phenomena such as intermittent contact together with stochastic adhesion seem to be influent (Ben Messaoud et al., 2015b; Eric Vezzoli et al., 2015b).

Several prototypes of ultrasonic friction modulation devices are developed worldwide (Winfield et al., 2007; Winter et al., 2013), and in L2EP, since 2007, under the name "Stimtac". The first Stimtac was developed by (Biet, 2007) and made up of copper. This device had the dimension 83 mm × 49 mm and was fully glued in its reverse side by piezoelectric ceramics forming an array of actuators to produce a

stationary wave at its resonance frequency. It was designed to stimulate gratings regardless of the power consumption. This first prototype used 1D LVDT sensor to track the finger position, so the simulation was just in one direction. This device was liable to thermal heating due to unoptimized design of the copper plate. An analytical modelling of the air pressure between the finger and a vibrating surface characterized by its roughness, wavelength, vibration amplitude, and resonance frequency was developed. In 2008, to determine the finger position, a custom-made 2D sensor built from two white LEDs with a set of mirrors replaced the LVDT sensor. A Digital Signal Processor was used to estimate the finger position from its shadow according to the (x, y) axis with a frequency of 120 Hz. This principle increased the finger position precision and allowed the 2D stimulation. However, heating problems remained.

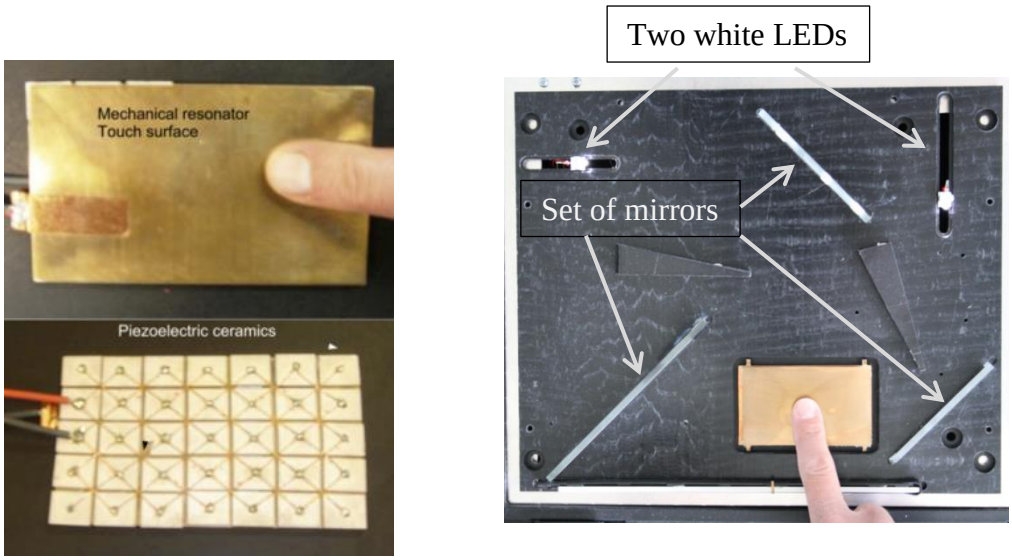


(a) (b)

Figure 2-1 : (a) The first tactile stimulation device called Stimtac developed by (Biet, 2007), (b) The finger position sensing using a custom-made 2D optical sensor (2008).

The following study (Giraud et al., 2010) which focused on the design optimization of the plate allowed a reduction in the power consumption by 90% without influencing the tactile sensation. This outstanding result was obtained thanks to the accurate choice of the piezoceramics and plate thickness, and by the optimization of the number and location of piezoceramics. Another solution was proposed and implemented to reduce the bulkiness of the Stimtac: the 2D optical sensor was substituted by force sensors. On the other hand, the serial port was replaced by a USB connection to provide read/write communication signals and power supply. Demo applications were implemented so that they detect the finger displacement and adapt the vibration amplitude based on the color of the pointed pixel in order to give the illusion of touching a displayed texture (Amberg et al., 2011).

In 2012, a glass material has been utilized as a vibrating plate to make the surface transparent (Giraud et al., 2012). The transparency of the plate allows the device to

simulate a more realistic tactile feedback by displaying the simulated surface on a LCD screen under the transparent surface. Force sensors have been employed to estimate the finger force in one direction and the finger position as well.

(a) (b)

Figure 2-2 : (a) The optimized Stimtac version connected by a USB connection (Amberg et al., 2011) (b) The transparent tactile stimulator developed by (Giraud et al., 2012).

The finger position measurement plays a very important role in the simulation of textures. The use of force sensors to deduce the finger position, despite its accuracy, needs a minimum level of finger pressure and the precision may derive with the time. Moreover, this kind of sensor is not suitable for current transparent mobile screens which are equipped either with resistive sensors, or more often with capacitive sensors. Thanks to collaboration between the L2EP Lab. and STMicroelectronics Company, two other Stimtac have been designed using respectively a resistive and a capacitive screen, with piezoceramics glued at the edges of the vibrating surface (Figure 2-3).

(a) (b)

Figure 2-3: The improvement of the finger sensing using resistive (a) and capacitive (b) sensors.

The size and the shape of the tactile stimulators have also been changed. In 2013, a haptic knob was made to produce programmable tactile effects in order to reproduce the illusion of manipulating a rotating knob (Frédéric Giraud et al., 2013). It was made of a ring shape active area which vibrated in order to reduce the friction. In this work, when operating in open loop control, it was observed that the fingertip has an influence on the vibration. On this device, when maintaining a constant voltage $V$ excitation and a same angular frequency $\omega$, the vibration amplitude as a function of the normal force reduces to 50% of its nominal value for a normal force higher than 1.5 N. Consequently, the sensation can be significantly changed from one user to another if they do not apply the same force on the device. For that purpose, a first order model of the vibration behaviour as a function of the voltage excitation was developed when exciting the device at a vicinity of resonance. Then, a control of the vibration amplitude $W$ was implemented in order to make the device robust against force variation (Giraud et al., 2012).

A first attempt to use a large surface of the Stimtac was made by (Yang, 2013). The large tactile plate has a dimension of (198mm × 134mm) and is able to produce a vibration amplitude above 1 µm to be detectable by the users. Even if this plate is opaque, the reverse side is not fully glued with piezoceramics: a developed model shows that the power consumption is related to the location of the piezoelectric ceramics (Yang et al., 2015). So, much effort was made to find the optimal location on the reverse side of the resonator where piezoelectric actuators should be placed. Psychophysics experiments have also been conducted to evaluate the tactile feedback capability of the device to produce detectable tactile stimulation. Despite the large size of the device which can simulate the sensation of touching of a large surface, the stimulator suffered from a response time relatively long of about 5 ms which reduced the device's ability to simulate fine texture details.

(a) (b)

Figure 2-4 : (a) The developed haptic knob (Frédéric Giraud et al., 2013) (b) The large area of the Stimtac developed by (Yang, 2013).

However, the large workspace provided by this version of Stimtac may be comfortable if we want to simulate real textures and especially fabrics. That's why, for the following, we decided to investigate and to improve the capabilities of this device.

## 2.2 Design of the tactile stimulator

This part focuses on the use of the large Stimtac version and evaluates its performances and ability to reproduce the sensation of texture despite its large response time.

### 2.2.1 Mechanical structure of the tactile stimulator

To produce a friction modulation that gives the tactile sensation, it is required to generate an ultrasonic vibration on a mechanical resonator. This vibration is non-perceptible by the cutaneous mechanoreceptors of the fingertip whose bandwidth is below 400 Hz (Darian-Smith, 1984) but the resulting sliding effect on the plate is easily perceivable. In order to create this vibration, piezoelectric ceramics are used as actuators by means of the inverse piezoelectric effect. They are made of PZT and the dimension of each ceramic is 14*6*0.5 $mm^3$. They are glued under the aluminium plate. The size of the plate used in this study is 198*134*1.2 $mm^3$ (9.5 inches). Twenty ceramics were glued under the active surface, most are used as actuators to produce the vibration and some can be used as sensors in order to measure and control the instantaneous vibration amplitude. It must be noted that in wide thin plates, many resonant modes exist with closed frequencies. The desired resonant mode is illustrated in Figure 2-7. If only one ceramic is chosen as a sensor, it was noticed that this sensor detects several near modes as illustrated in Figure 2-5. This curve is plotted by varying the excitation frequency around the resonant frequency which was 32300 Hz at 24°C.

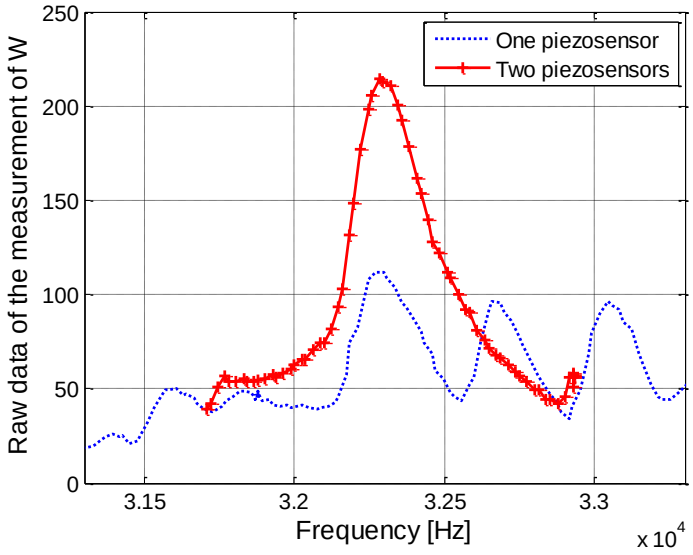


Figure 2-5: Comparison between using one or two piezo sensors when exciting the plate around resonance. The two-sensor approach emphasises the desired mode.

In that case, the ceramic in the opposite side gives an antiphase deformation. By using two sensors, the two signals are added and the result is the single mode that we are looking for which is then validated by the laser vibrometer. The two curves are extracted for the same excitation voltage giving 1.4 µm of vibration amplitude at the resonance. The y label of the curve represents the raw data of the measurement of *W* before the calibration of the laser vibrometer. The two sensors are placed in the first anti-nodal line from the left side of the plate at the two corners (Figure 2-6).

20 piezoceramics are glued on the plate: 18 are used as actuators and 2 as sensors. The 18 piezoceramics used as actuators are connected in parallel, so they are supplied by a single sinusoidal voltage source. The actuators are arranged into four columns, two in each border. Each column is composed by five ceramics distributed over the whole width of the plate as illustrated in Figure 2-6. The plate is maintained using four attachment points placed at the nodes to fulfil the free vibration boundary condition. The piezoelectric actuators are positioned at the antinodes to produce the standing wave with some microns of amplitude. The two sensors are placed in the left column and the four attachment points join together the vibrating plate and the fixed part.

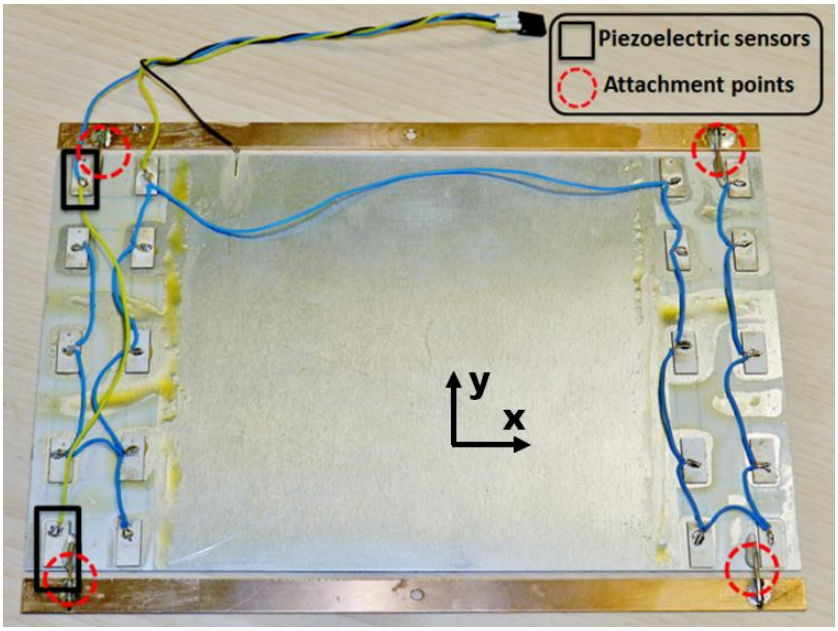


Figure 2-6: The reverse side of the vibrating plate composed by 20 piezoelectric ceramics.

When the actuators are excited at the mechanical resonant frequency of the chosen bending mode, a standing wave is generated as depicted in Figure 2-7. In this figure, a 154 V peak to peak voltage is applied to produce 1 µm of vibration amplitude. The mechanical resonant frequency of the metal plate is defined by its material and its geometry. The resonant frequency is pre-determined by a FEM analysis. The modal analysis gives many vibrational modes, but we choose one mode providing a flexural vibration with nodal lines along the width of the plate, and respecting the

criteria defined by (Biet et al., 2008) to obtain the friction reduction at ultrasound frequency and with a minimum of nodes. In our case, this resonant mode has a frequency at 32.3 kHz in ambient temperature. The measurement of the instantaneous vibration amplitude is carried out using the two piezoelectric ceramics as sensors. They are positioned at the anti-node of the vibration and they convert the deformation of the plate into a voltage proportional to the vibration amplitude. The sensors are calibrated using a vibrometer in order to find the linear relation between the sensors response and the instantaneous vibration amplitude.

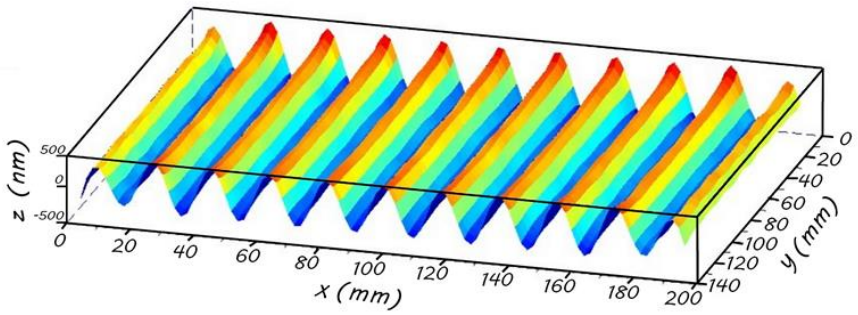


Figure 2-7 : The chosen bending vibration mode when the system is excited at the resonance

### 2.2.2 Finger position measurement

In order to simulate textures, the level of the lubrication which reduces the friction between the finger and the plate needs to change according to the fingertip position. The method used to estimate the finger position is an extension of the method developed in one of the previous work (Giraud et al., 2012). In this previous work, this method has been implemented using two force sensors to estimate the x position, using the equations of force and moment equilibrium. The method developed and employed is a generalization to a 2D surface to calculate the position defined by the coordinates (x, y). This method was also used in the Stimtac device.

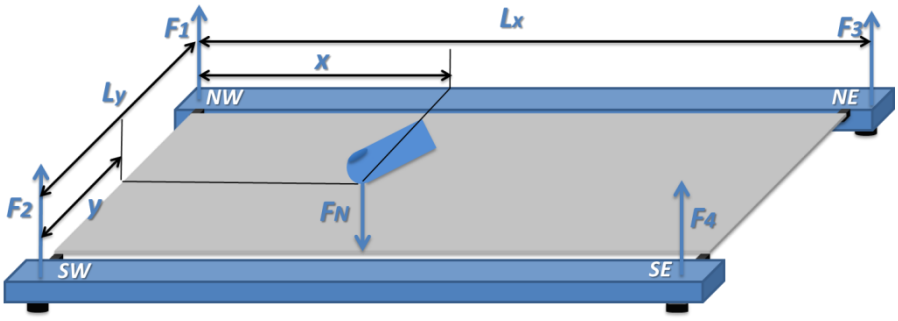


Figure 2-8: The designed configuration of the finger position estimation in x and y axes using four force sensors located in different locations: *NW (North West), SW (South West), NE (North East)* and *SE (South East)*.

The force equilibrium equation can be written as follows:

$$F_1 + F_2 + F_3 + F_4 = F_N \tag{2.1}$$

With $F_1, F_2, F_3, F_4$ the forces respectively measured by the sensors located in $NW, SW, NE, SE$ and $F_N$ is the normal force applied by the finger. The equations of moment equilibrium in the contact point in the x and y axes are the following:

$$x(F_1 + F_2) - (L_x - x)(F_3 + F_4) = 0 \tag{2.2}$$

$$y(F_2 + F_4) - (L_y - y)(F_1 + F_3) = 0 \tag{2.3}$$

Then x and y are deducted from the equation (2.1), (2.2) and (2.3) giving:

$$x = L_x \frac{F_3 + F_4}{F_1 + F_2 + F_3 + F_4} \tag{2.4}$$

$$y = L_y \frac{F_1 + F_3}{F_1 + F_2 + F_3 + F_4} \tag{2.5}$$

The finger position in the two directions x and y is therefore determined as a function of the signal of the force sensors type FSS1500 from Honeywell. The whole system induces a noise to the sensors which disturbs the measurement of the forces. To evaluate the amount of the noise, the normal force is measured for different normal loads from 7 cN to 250 cN and the noise noted $Er$ expressed in the equation (2.6).

$$Er = \frac{[\max(F_N) - \min(F_N)] / 2}{\overline{F_N}} \tag{2.6}$$

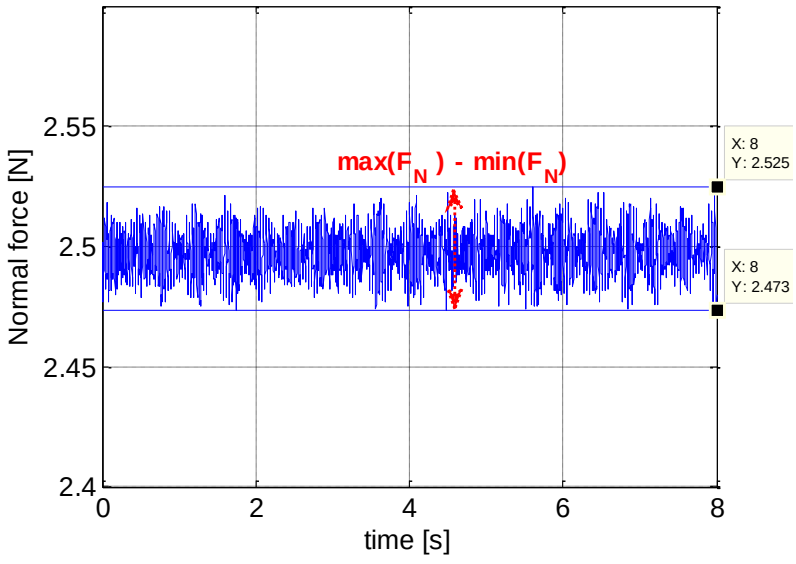


Figure 2-9: The force measurement when applying a weight of 2.5N on the plate.

The normal force which is a function of time is illustrated in Figure 2-9. The evolution of $E_r$ as a function of different loads is illustrated in the Figure 2-10 showing a decrease of $Er$ from 25% for very small loads to less than 2.5% for loads higher than 0.5 N. Each point of the curve represents the percentage of the deviation compared to the average value of the force.

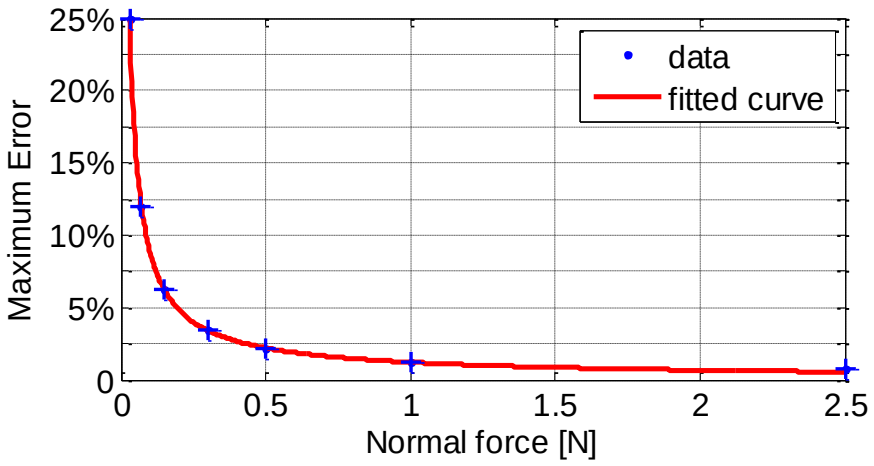


Figure 2-10: The decrease of the error in the measurement of $F_N$ for different values of the normal applied force.

The error in the position detection is 2 times higher than the error of the force measurement; this error is calculated from the equations (2.4) and (2.5) and from the uncertainty propagation of the error. Figure 2-10 shows that a minimum normal force around 0.5N must be applied in order to limit the position error lower than 2.5%.

The acquisition frequency of the finger position is 1 kHz. The vibration amplitude (of few µm) is then modulated as a function of the fingertip position in order to simulate textures.

### 2.2.3 Control of the tactile plate

On a practical point of view, the tactile plate is controlled using a DSP (Digital Signal Processor) type STM32F4 from STMicroelectronics which generates the numerical control signal. The DSP plays the role of the interface between the device and the computer to display on the screen the response of the tactile stimulator – i.e. the vibration amplitude – which is measured through the sensors of the plate and then converted using an ADC to be operated by the DSP. The operating point can be programmed through an emulated serial port. Figure 2-11 shows the main components of the system.

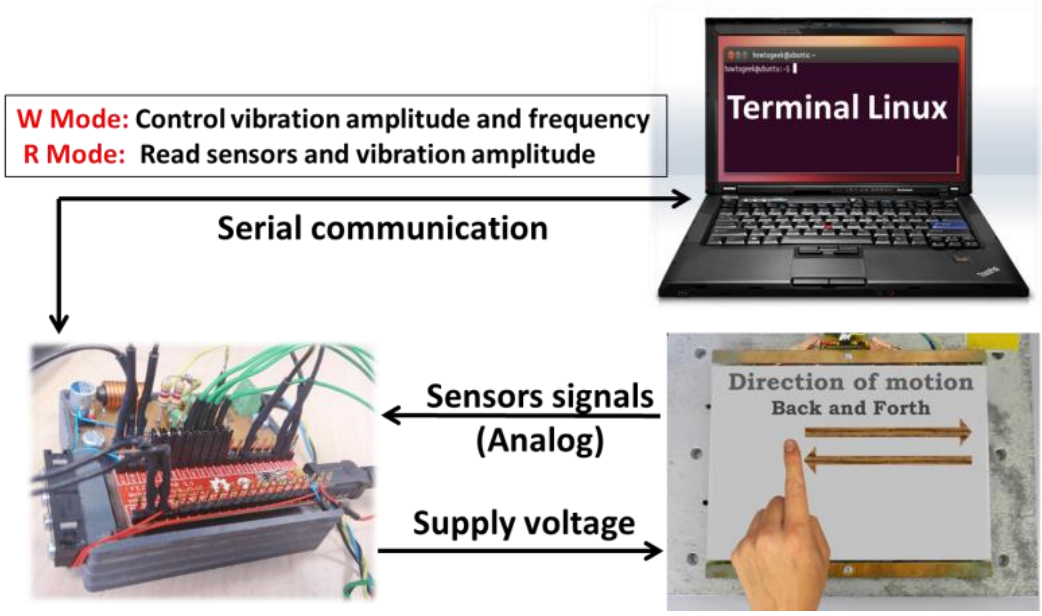


Figure 2-11: Operation principle of the tactile stimulator

In order to supply the piezoceramics with a sinusoidal excitation voltage controlled in amplitude and frequency, we consider a DC voltage source (5 V). Then a two leg inverter is operated to produce a three level Pulse-width modulation (PWM) voltage signal. This signal is controlled both in frequency by changing the timer of the DSP and in amplitude by modifying the commutation moment of the PWM signals (see Appendix A1 for more details). After that, a filter is employed to deliver a sinusoidal voltage from the three level signal. Finally, a step-up transformer is used to produce the required level of voltage able to excite the piezoelectric ceramics to produce vibration amplitude in the range of micrometres (µm).

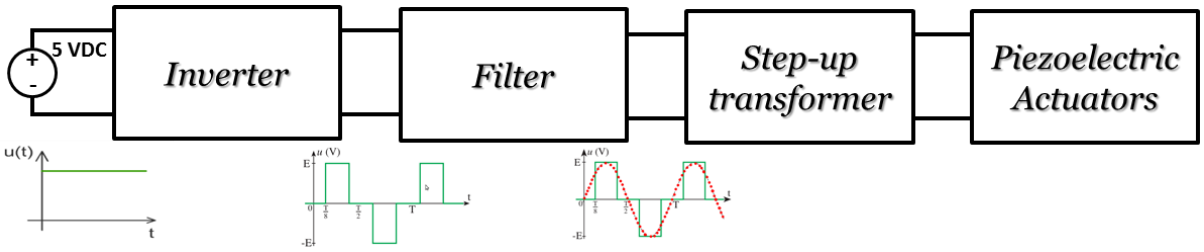


Figure 2-12: The power circuit to excite the piezoelectric ceramics by a controlled sinusoidal signal in amplitude and frequency.

## 2.3 Robustness analysis

First studies on friction reduction based tactile devices were carried out in open loop, the wave amplitude was not controlled (Giraud et al., 2012) (Frederic Giraud et al., 2013) (Amberg et al., 2011). However, in recent publication (Wiertlewski et al., 2014) and our recent article (Ben Messaoud et al., 2014a), it was highlighted that some external factors such as the finger normal force and the temperature variation can disturb those devices while modifying the vibration amplitude and the resonant frequency. These disturbances influence the damping and stiffness properties of the

vibrating plate as it is also found in (Kang et al., 2012) even if they work in another range of frequency (less than 500 Hz). The measurements we performed on our tactile plate highlight that the vibration can be damped by 50% with an applied normal force of about 1.5 N (Figure 2-13). In this figure, the percentage of the vibration amplitude variation $A_V$ is plotted as a function of the time, during an increase of the normal force.

$$A_V = 100 * \left(\frac{A}{A_d} - 1\right) \tag{2.7}$$

$A_d$ is the desired vibration amplitude (i.e. the one expected without any normal force applied) and $A$ is the actual vibration amplitude.

Moreover, this variation is quite fast, as fast as the normal force variations. As an example, it has been measured in (Ben Messaoud et al., 2014a) that the normal force variations can reach 1 N in 0.1 second. Additionally, another factor modifies the vibration amplitude in open loop by changing the resonant frequency of the plate: the variation of the external temperature. By increasing the temperature, the mechanical structure becomes softer, which decreases the stiffness parameter $c$ (see later, eq (2.8)) leading to decrease the resonant frequency (Lin, 2012). It should be noted that piezoelectric ceramics characteristics are much less sensitive to the temperature than the resonator itself. Indeed, Figure 2-14 shows the vibration amplitude as a function of the frequency at two different temperatures (24°C and 33°C). It shows that the resonant frequency is decreased from 32.3 kHz to 32.2 kHz when the temperature increases. This variation of 9°C of temperature is supposed to be similar as the variation between the room temperature (24°C) and the temperature of the finger skin (33°C). In practical, this curve was plotted after putting the plate in an oven and varying the temperature from 24°C to 33°C by steps of 1°C. During this experiment, we found a linear relation between the temperature and the resonant frequency.

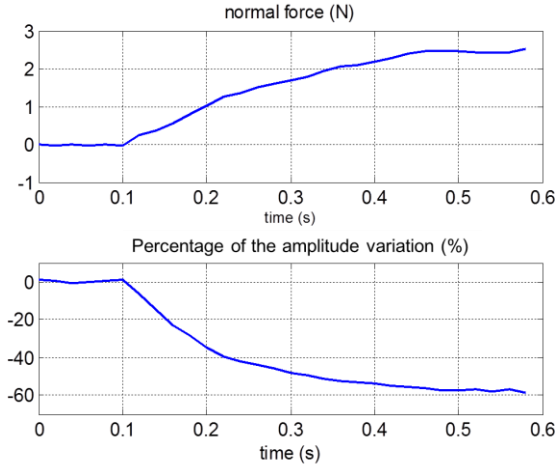


Figure 2-13: Percentage of the amplitude variation $A_V$ as a function of the normal force applied

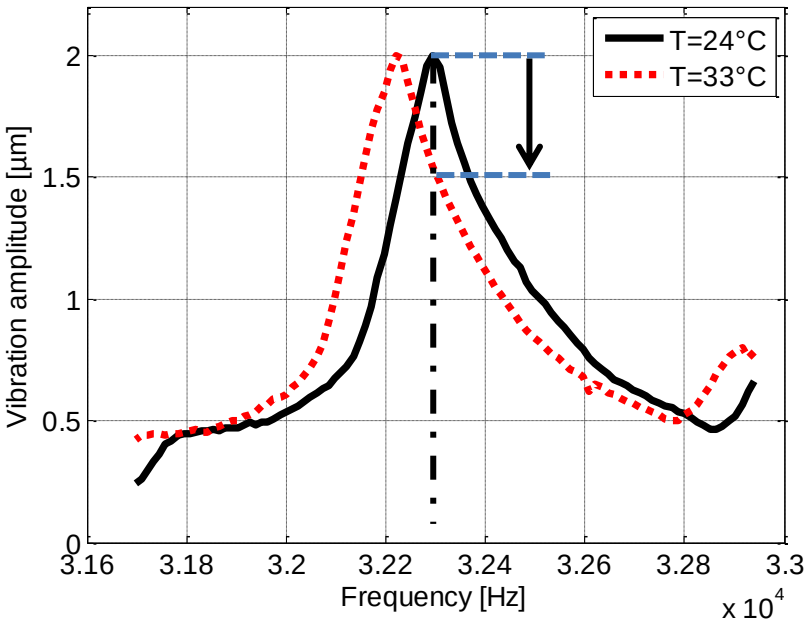


Figure 2-14: Frequency response around one mode for two stimulator's temperatures: 24°C (continuous, black line) and 33°C (dotted, red line).

Hence, for a constant supply frequency adjusted to the resonant frequency at the lower temperature, the vibration amplitude decreases when the temperature increases. Moreover, despite the small frequency shift (0.3% for the example above), the effect is not negligible, and the amplitude of vibration is reduced by 25% from its initial value. At the end, an experimental study shows that the vibration amplitude reduction may reach up to 8% for only a 4°C variation.

To cope with these issues, it is necessary to track the resonant frequency. This can be done by adjusting the phase difference between the courant and the voltage (Gokcek, 2003; Liu et al., 2015; Mortimer et al., 2001). More recently, other groups of researchers have investigated the frequency tracking and the amplitude control of ultrasonic devices using digital circuits based on DSP when controlling Langevin ultrasonic transducer (Takasaki et al., 2007) or when controlling ultrasonic frequency in Biological Decomposition field (Shi et al., 2015). These methods are mainly based on PID discrete digital controller with manually tuned parameters in order to minimize the ratio between the supplied voltage and the vibration amplitude.

Besides, the aforementioned sensitivity to external factors, added to the slow response time drawback already mentioned lead us to propose a closed loop control of the vibration in addition to the tracking of the resonant frequency, in order to obtain the robustness of the system at each operating condition (Ben Messaoud et al., 2016b). As a consequence, the modelling of the system in order to achieve the control is the next step of this study.

## 2.4 System modelling

The vector control will be used here because this method acts simultaneously on the wave amplitude and on the frequency or on the instantaneous phase shift of the standing wave. A d-q frame will be defined to represent the system in a rotating frame, and the control will occur in this specific frame. Then, the sinusoidal voltage supply will be computed thanks to a frame transformation.

### 2.4.1 General equations in d-q frame

Around the resonant frequency of the vibrating plate in a chosen bending mode, and under purely sinusoidal excitation, the evolution of the vibration amplitude W(t) can be modelled by a second order equation. The vibratory behaviour of the plate is assumed as an equivalent circuit of a piezoelectric actuator. This actuator is modelled with two ports of interaction, a voltage port on the electrical side and a force port on the mechanical side (Goldfarb and Celanovic, 1997). The electrical port is driven by a voltage source and the mechanical port by a force source, which represents input command voltage and external mechanical load, respectively. With respect to the mechanical side of the transformer, since the actuator model is concerned only with endpoint displacement, the piezoelectric actuator is assumed to have a modal mass and a linear material stiffness and damping. This model can be expressed in the complex form (Pigache et al., 2006):

$$m\underline{\ddot{W}} + d_s\underline{\dot{W}} + c\,\underline{W} = N\,\underline{V} - \underline{F} \tag{2.8}$$

with $m$ the modal mass, $d_s$ the modal damping, $c$ the modal stiffness, $N$ is the electromechanical conversion factor, $F$ represents the effect of the external force applied to the system, $\underline{V}$ is the ceramics supply voltage and $\underline{W}$ is the vibration amplitude. The latter and the voltage can be represented with their complex form and we name $W_d$ and $W_q$ ($V_d$ and $V_q$) the real and imaginary parts of the vibration (and of the voltage respectively) as follows:

$$\underline{W} = (W_d + j\,W_q)e^{j\omega t} \tag{2.9}$$

$$\underline{V} = \left(V_d + j\,V_q\right)e^{j\omega t} \tag{2.10}$$

Replacing $\underline{\ddot{W}}$, $\underline{\dot{W}}$ and $\underline{W}$ by their expressions in (2.8), assuming that the variation of $\omega$ is minor ($\dot{\omega} = 0$) and considering $F = 0$ (no-load condition) yield (2.11) and (2.12). The modelling and identification processes are performed without any load and $F$ is considered as a disturbance during closed loop operations.

$$m\ddot{W}_d + d_s\dot{W}_d + (c - m\omega^2)W_d - \omega\left(2m\dot{W}_q + d_sW_q\right) = NV_d \tag{2.11}$$

$$m\ddot{W}_q + d_s\dot{W}_q + (c - m\omega^2)W_q + \omega\left(2m\dot{W}_d + d_sW_d\right) = NV_q \tag{2.12}$$

These two equations describe the vibratory behaviour as a function of the voltage and the excitation frequency. In order to simplify the model and because we have a

degree of freedom for the choice of the d-q frame, we set $V_d = 0$. Hence, we decide to align the rotating reference frame on the voltage vector. This can be represented by the vector scheme of Figure 2-15, where the vectors $\underline{V}$ and $\underline{W}$ are drawn.

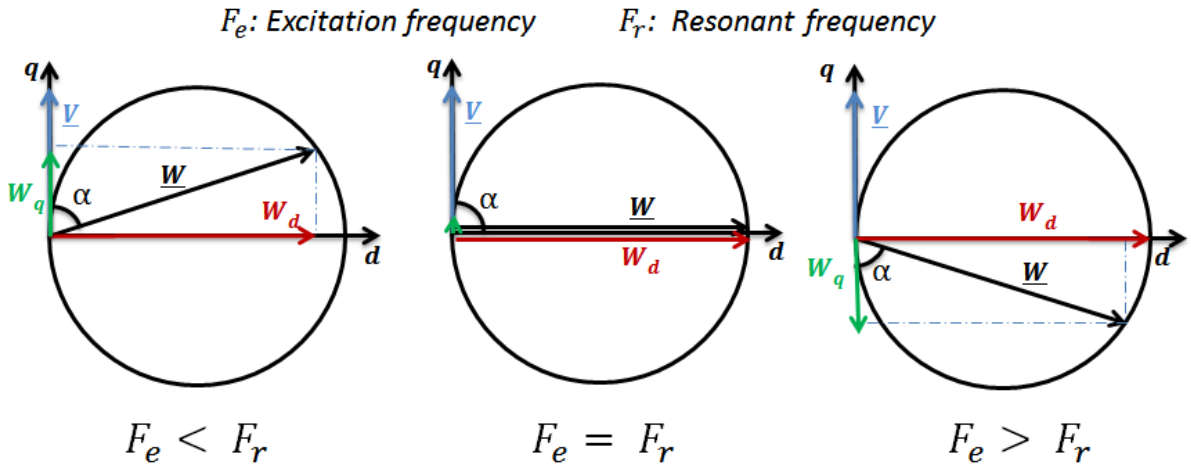


Figure 2-15: Vector representation of the vibration amplitude $W$ in d-q axis where q axis is aligned with the $\underline{V}$ reference vector.

It may be noted that this approach differs from the one described in (Pigache et al., 2006) because there, the axis $d$ was attached to $\underline{W}$ using a phase locked loop, leading to $W_q = 0$, and the voltage components $V_d$ and $V_q$ were constrained by the condition of a constant voltage amplitude $\left(\sqrt{{V_d}^2 + {V_q}^2} = cste\right)$. It will be shown later that our choice is more suitable to track the resonant frequency.

To provide the flexural vibration with nodal lines along the width of the plate illustrated in Figure 2-7 and to minimize the power consumption, the system must be excited at the resonant frequency. To do that, the vector $\underline{W}$ must be maximized by changing the excitation frequency so that the angle $\alpha$ between $\underline{W}$ and $\underline{V}$ is $\pi/2$. In that case, $W_q = 0$ leading to $W = W_d$. When $W_q$ is nonzero, we can detect that the system is not excited at the resonance and the excitation frequency must be adjusted to minimize $|W_q|$. It can be noted that to impose a desired level of the vector $\underline{W}$, the voltage can be adjusted, which leads to an increase or decrease of the diameter of the circle; but if the system is not operated at the resonance, the power consumption is not optimal. For that reason, the resonance tracking must be done in parallel with the control of $W$.

### 2.4.2 Equations at resonance

The synchronisation of the vector $\underline{V}$ on the axis q makes $V_d = 0$. Moreover, at resonance, we have ${\omega_0}^2 = \omega^2 = c/m$. For steady state conditions, the derivative terms of $W_q$ and $W_d$ are zero. Then, equations (2.11) and (2.12) give the equations (2.13) and (2.14):

$$\omega\, d_s\, W_q = 0 \tag{2.13}$$
$$\omega\, d_s\, W_d = N\, V_q \tag{2.14}$$

From the equation (2.13), we can conclude that the imaginary part of the vibration amplitude $W_q = 0$ and (2.14) gives a linear relation between $V_q$ and $W_d$. With this representation on d-q frame, we are able to determine easily whether we are exciting the system at the resonance or not by verifying if $W_q$ is null or not.

Besides, to track the resonant frequency, two parameters are adjustable: the voltage amplitude $V$ and the angular frequency $\omega$ ($\omega = 2\pi f$). Each of them has an influence on the real and imaginary part of vibration respectively $W_d$ and $W_q$, as the voltage is synchronized on the q axis. The diameter of the circle plotted on Figure 2-15 is a function of the voltage amplitude $V$: if the voltage increases the diameter increases also. The variation of the voltage frequency affects the angle between $\underline{W}$ and $\underline{V}$ which is $\pi/2$ at resonance. If this angle is less than $\pi/2$, the excitation frequency must be increased and if this angle is higher than $\pi/2$ the excitation frequency must be decreased in order to minimize the ratio $V/W$.

### 2.4.3 Transfer functions for the control

Since $\underline{V}$ is attached to the axis q, we write $V_d = 0$ and $V_q = V$. This condition gives rise to the equations (2.15) and (2.16):

$$m\dot{W}_d + d_s\dot{W}_d + (c - m\omega^2)W_d - \omega\left(2m\dot{W}_q + d_sW_q\right) = 0 \tag{2.15}$$
$$m\dot{W}_q + d_s\dot{W}_q + (c - m\omega^2)W_q + \omega\left(2m\dot{W}_d + d_sW_d\right) = NV \tag{2.16}$$

From these equations, two working conditions can be studied: firstly in the vicinity of the resonance, secondly, for variations of the supply frequency.

#### 2.4.3.1 Modelling of the vibration amplitude in the vicinity of the resonance

In the vicinity of the resonance $W_q = 0$, and the equation (2.16) can be written as follows:

$$\omega_0\left(2m\dot{W}_d + d_sW_d\right) = NV \tag{2.17}$$

The resonant angular frequency $\omega_0$ depends on c and m:

$$\omega_0 = \sqrt{\frac{c}{m}} \tag{2.18}$$

Applying Laplace transformation, we find a first order transfer function tween $W_d$ and $V$:

$$\frac{W_d(p)}{V(p)} = \frac{K_1}{1 + \tau_1\, p} \tag{2.19}$$

with $K_1 = N/d_s\omega_0$ and $\tau_1 = 2m/d_s$.

Hence, in the rotating reference frame, the evolution of the vibration amplitude follows a first order equation whose time constant equals $\tau_1$ and static gain is $K_1$.

#### 2.4.3.2System behaviour to frequency changes

In this section, we assume that $W_d$ is perfectly controlled and constant. Hence, the derivatives terms of $W_d$ which are $\dot{W}_d$ and $\ddot{W}_d$ will be null and equation (2.15) becomes:

$$(c - m\omega^2)W_d - \omega\left(2m\dot{W}_q + d_s W_q\right) = 0 \tag{2.20}$$

In this equation, $\omega$ and $W_q$ are variables, leading to a differential equation with non-constant parameters. For the purpose of simplification, we propose a linearization of the equation. Indeed, considering that $\omega = \omega_0 + \Delta\omega$, we can write:

$$c - m\omega^2 = c\left(1 - \left(1 + \frac{\Delta\omega}{\omega_0}\right)^2\right) \tag{2.21}$$

The first order Taylor approximation can be employed because the variation between the excitation frequency $\omega$ and the resonant frequency $\omega_0$ is very small, and $\Delta\omega \approx 0$; thus, we can write:

$$\left(1 + \frac{\Delta\omega}{\omega_0}\right)^2 \approx 1 + 2\frac{\Delta\omega}{\omega_0} \tag{2.22}$$

By replacing (2.21) and (2.22) in (2.20), we have:

$$c - m\omega^2 \approx -2m\omega_0\Delta\omega \tag{2.23}$$

Same considerations lead us to approximate $\omega$ to $\omega_0$, and with (2.22), and (2.20), we obtain the equation (2.24):

$$-2m\Delta\omega W_d = 2m\dot{W}_q + d_s W_q \tag{2.24}$$

Leading to:

$$\frac{\left(\frac{W_q(p)}{W_d}\right)}{\Delta\omega(p)} = \frac{K_2}{1 + \tau_2\, p} \tag{2.25}$$

with $K_2 = -2m/ds$ and $\tau_2 = 2m/ds$.

Two important remarks can be elicited from these transfer functions:

- $\tau_1 = \tau_2$: the two transfer functions (2.19) and (2.25) have the same time constant.
- This transfer function shows that changes in the supply frequency of the tactile stimulator result in the change of the ratio $W_q/W_d$, according to a first order equation.

In the next section, the method of parameter's identification and the control of the output of these models will be investigated.

## 2.5 Identification of the model parameters

In this section, the two transfer functions previously detailed are identified by applying a step variation of the input and measuring the output in time domain. The experimental set-up necessary for the identification is described.

### 2.5.1 Experimental setup description

The tactile stimulator presented in II)A) is used in the identification process. It is connected to a PC through the serial communication port in read and write mode (Figure 2-11). The read mode allows us to display in real time different parameters with 1 kHz sampling frequency, like the instantaneous vibration amplitude, the voltage amplitude and the excitation frequency. The write mode is used to send the amplitude references to the system. The DSP is powered by an USB port.

It may be noted that to identify the two transfer functions, we have to fulfil specific conditions: work in the accurate d-q frame, at the resonance for the first relation between $W_d$ and $\underline{V}$, and for the second relation between $W_d/W_q$ and $\Delta\omega$, we have to suppose that $\underline{W}$ is regulated. More precisely, to achieve these conditions, we can say that it is necessary to tune the supply frequency so as to assume a 90° angle between $\underline{V}$ and $\underline{W}$, and to tune the $\underline{V}$ amplitude in order to obtain the accurate $\underline{W}$ amplitude. The practical way to operate these conditions is described in Appendix A2.

The control method consists in controlling $W_d$ to a reference value and $W_q$ must be controlled to be zero by adjusting the angle $\alpha$ to be $\pi/2$ between $\underline{V}$ and $\underline{W}$ to excite the system at the resonant frequency.The structure can be simplified in order to deduce the block diagrams of Figure 2-16 from which the PI regulators may be tuned.

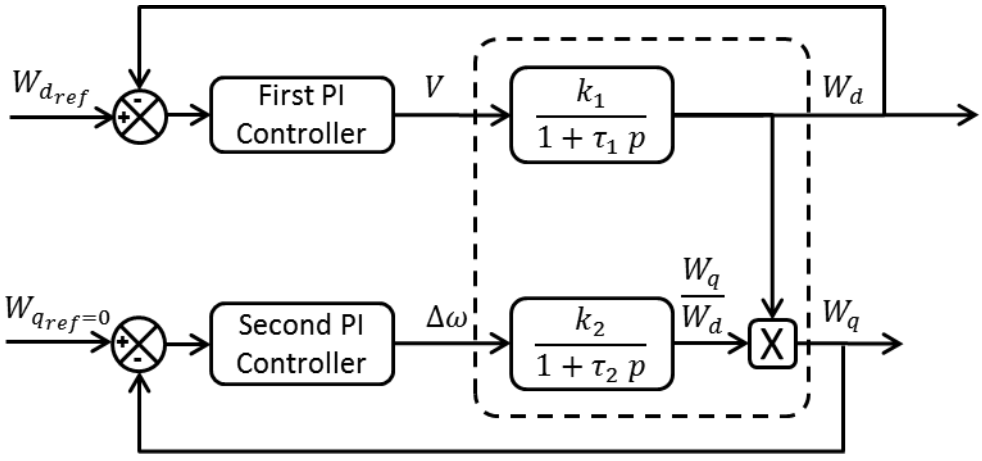


Figure 2-16: Control loops able to impose $W$ and to operate the system at the resonance.

### 2.5.2 Identification approach

#### 2.5.2.1 Identification of the transfer function between $W_d$ and $V$

The first point is to identify the static gain $K_1$ of the transfer function (2.20). For that aim, successive values of the voltage from 50V to 400V peak to peak are applied to the piezoceramics at the resonant frequency, and the vibration amplitude is measured. The choice of this range of voltage is explained by the desired range of the vibration amplitude [0.5...2.5 µm]. This relation between the supply voltage and the vibration amplitude is linear in the useful range for this application. Figure 2-17 shows the slope of curve which is $W_d/V = K_1$.

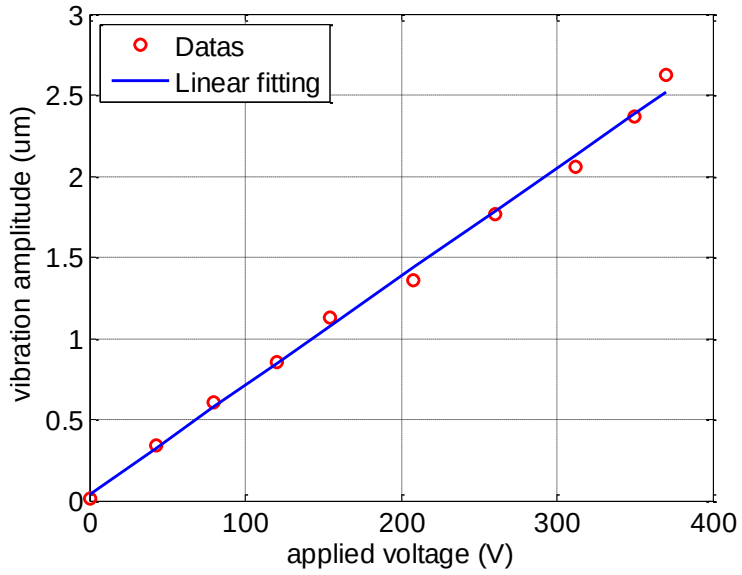


Figure 2-17: The linear relation between the supply voltage (peak to peak) and the vibration amplitude at the resonance.

We also recorded the response of the system at each step of variation of $V$. Despite the different voltage levels, it may be noticed that a first order behaviour was obtained as predicted by the modelling. From these characteristics, we used the least-squares method (ARX (Ljung, 1998)**)** for the identification of $K_1$ and $\tau_1$ from (2.19) because it gives good results at low order. An example of the identified first order model is illustrated in Figure 2-18.

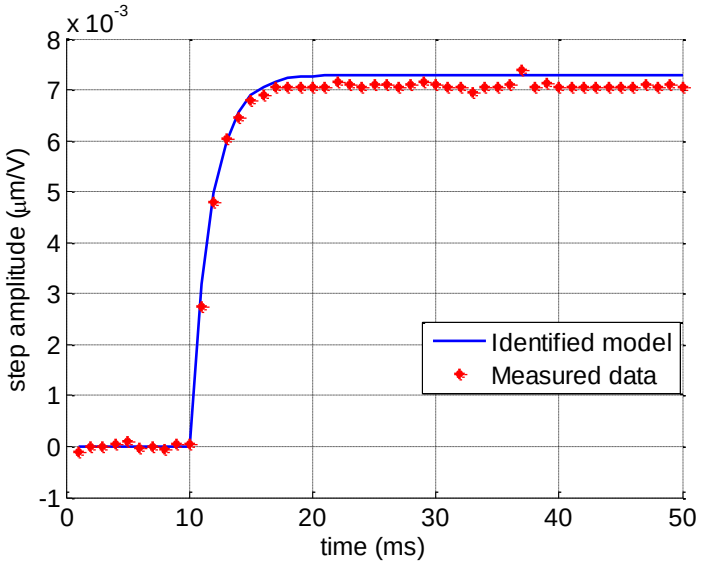


Figure 2-18: An example of one of the identified first order model, the voltage amplitude is 154 $V$ peak to peak, giving $K_1 = 7295\ (pm/V)$ and $\tau_1 = 1.74\ ms$.

The identification results for each trial are presented in Table 2-1.

Table 2-1: Parameters of the identified transfer functions

| | | | | | | | | | Mean |
|---|---|---|---|---|---|---|---|---|---|
| Voltage amplitude | 80 | 120 | 154 | 208 | 260 | 312 | 350 | 370 | |
| $K_1$ (pm/V) | 7611 | 7108 | 7295 | 6547 | 6795 | 6620 | 6764 | 7103 | 6980 |
| $\tau_1$ (ms) | 1.97 | 1.85 | 1.74 | 1.71 | 1.81 | 1.94 | 1.97 | 2.07 | 1.88 |

The variations of $\tau_1$ as a function of the voltage applied are plotted in Figure 2-19.

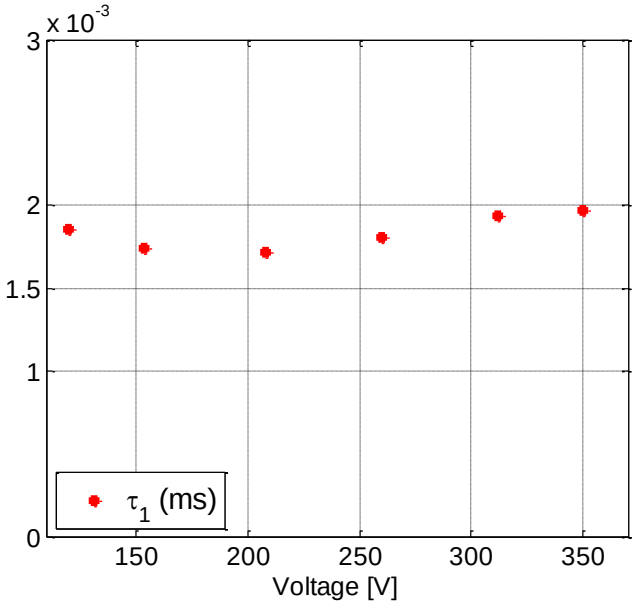


Figure 2-19: Evolution of $\tau_1$ as a function of the applied voltage

The deviations of $\tau_1$ (± 6 %) and $K_1$ (± 5 %) are found to be sufficiently small to consider that they are constant for all voltage conditions.

### 2.5.2.2 Identification of the transfer function between $W_q/W_d$ and $\Delta\omega$

The identification of this second transfer function needs some experimental conditions, already explained in the modelling. In particular, for using linearization, we must ensure that:

- The system is excited in the vicinity of the resonance in order to fulfil the assumption leading to (2.23).
- The real part of the vibration amplitude $W_d$ is constant. To ensure this assumption, a closed loop control of the vibration amplitude is performed. This control is detailed in section 2.6.

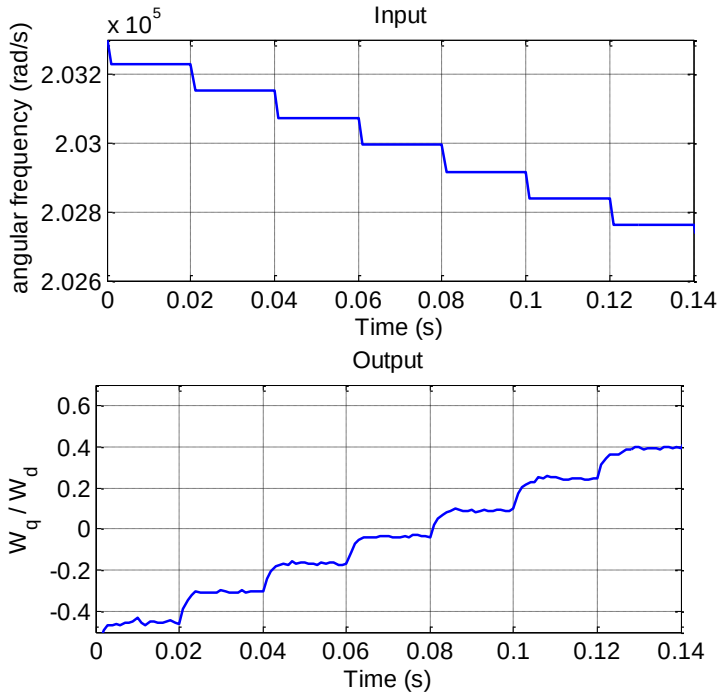


Figure 2-20: Response of $W_q/W_d$ following decreasing steps of the angular frequency

The transfer function (2.25) between $W_q/W_d$ and $\Delta\omega$ is identified by applying steps of $\omega$ as input, and measuring $W_q/W_d$ as output.

Figure 2-20 represents the evolution of the quantity $W_q(p)/W_d$ as a function of time, when variations of the frequency are applied. Every 20 ms, a decreasing step of $\Delta\omega = -77\ rad/s$ of angular frequency is applied. At the same time, $W_d$ is maintained constant. Figure 2-21 illustrates the relative error of the controlled $W_d$ in response to decreasing steps of the angular frequency to check that it is maintained constant.

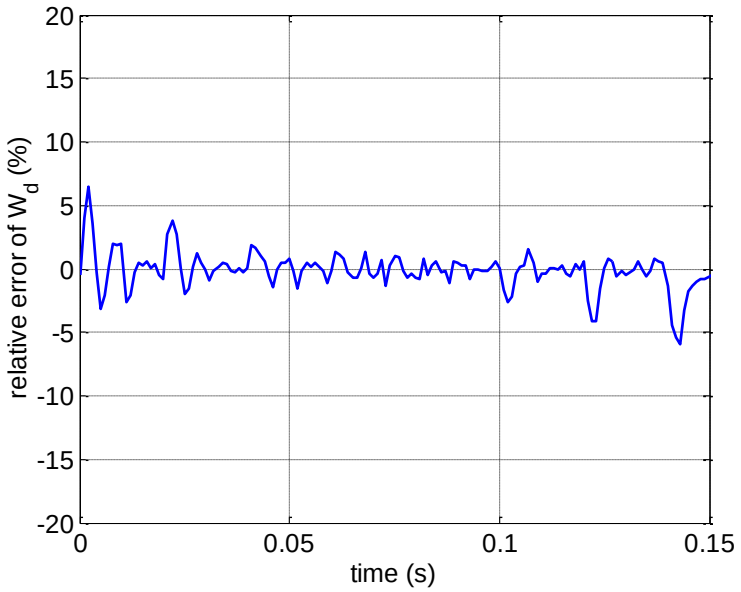


Figure 2-21: Relative error of the controlled $W_d$ in response to steps of angular frequency ($W_{dref}$ is 2 µm).

In response to decreasing steps of the angular frequency $\omega$ from $\omega_1$ to $\omega_2$ around resonance, the quantity $W_q(p)/W_d$ increases following a first order behaviour. The identification of the transfer function presented in (2.25) gives the parameters $K_2$ and $\tau_2$ for each step. The two extremes and the medium experimental identification results are presented in the Table 2-2.

Table 2-2: Parameters of the identified transfer functions

| | | | | Mean |
|---|---|---|---|---|
| $\omega_1$(rad/s) | 203229 | 202995 | 202839 | |
| $\omega_2$(rad/s) | 203151 | 202917 | 202761 | |
| $K_2(10^{-3})$ | 1.9727 | 1.6876 | 1.8564 | $K_2 = 1.812$ |
| $\tau_2$(ms) | 1.5360 | 1.6504 | 1.8608 | $\tau_2 = 1.624$ |

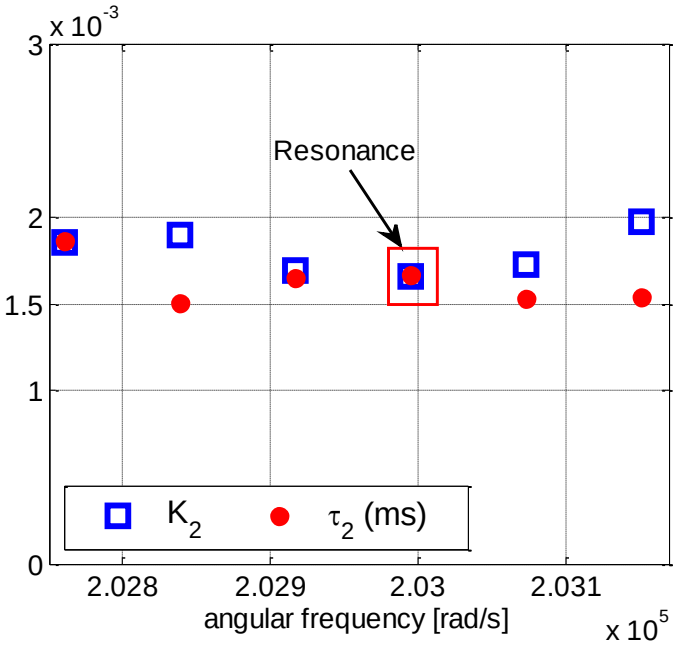


Figure 2-22: Evolution of $\tau_2$, $K_2$ as a function of the angular frequency

Moreover, we have plotted some values of $K_2$ and $\tau_2$ as a function of the angular frequency in the vicinity of the resonant frequency Figure 2-22. It can be stated that at the exact resonant angular frequency ($\omega = 202995$ rad/s), this ratio between $K_2$ and $\tau_2$ is equal to 1 as expected by (2.25).

Finally, the parameters of the function between $W_q(p)/W_d$ and $\Delta\omega$ are $K_2 = 1.812\ 10^{-3}$ and $\tau_2 = 1.624$ ms.

The most important feature of the identification is that we validate by real measurement the validity of the model and approximations. We find that the two transfer functions have a similar constant time (respectively $\tau_1 = 1.88$ ms and $\tau_2 = 1.62$ ms). Moreover, the transfer function giving $W_q(p)/W_d$ as a function of $\Delta\omega$ has the static gain equal to its time constant. In the next section, a real time implementation of the two controllers will be achieved and thanks to an experimental measurement, a comparison between the closed loop control against the open loop one will be presented.

## 2.6 Control of the vibration amplitude

### 2.6.1 Tuning of the controller coefficients

The parameters of the controller are calculated through the identified transfer function. The two transfer functions are of first order type. A classical proportional integral controller is sufficient due to its low transfer function order; it can reduce the response time without any static error. In the following part, the method for the parameters calculation is presented.

The structure of the controller is defined in (2.26) which contains two variable parameters $K_p$ and $K_i$:

$$PI_{controller} = K_p + \frac{K_i}{p} \tag{2.26}$$

The classical closed loop control for a first order system $H(p)$ is represented in Figure 2-23:

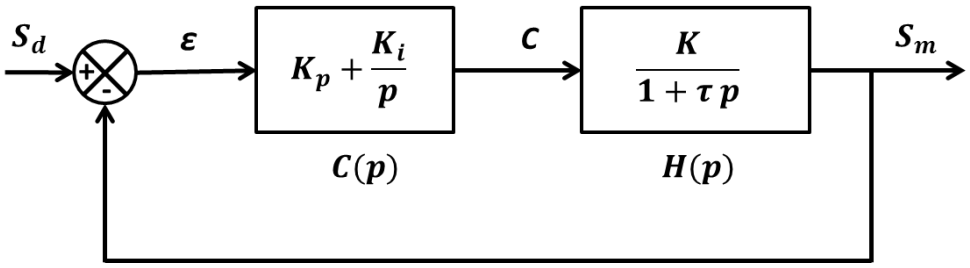


Figure 2-23 Classical closed loop control for a first order transfer function using PI controller

With $S_d$ is the reference, $S_m$ is the measured output, $\varepsilon$ is the error between $S_d$ and $S_m$ and $C$ is the output of the controller. The characteristic equation of the closed-loop system shown in Figure 2-23 is given by:

$$\frac{S_m}{S_d} = \frac{C(p)H(p)}{1 + C(p)H(p)} \tag{2.27}$$

with

$$C(p)H(p) = \left(\frac{KK_i}{1+\tau\, p}\right)\left(\frac{1 + \frac{K_p}{K_i}p}{p}\right) \tag{2.28}$$

We assume that $k_p/k_i = \tau$ to compensate the pole of the transfer function.

By equating the characteristic equation in closed loop with this assumption, we find a first order system between $S_m$ and $S_d$ given by:

$$\frac{S_m}{S_d} = \frac{1}{1 + \tau_f\, p} \tag{2.29}$$

With $\tau_f = 1/K.K_i$ is the desired time constant in closed-loop. The parameters of the controller can be calculated from $\tau_f$, and the parameters of the transfer function in open loop ($K$ and $\tau$): for instance, the desired response time $t_{r\,5\%}$ can be imposed. For a first order function, it is equal to 3 $\tau_f$ which leads to the equations of the controller parameters:

$$\begin{cases} K_p = \dfrac{3\,\tau}{K t_{r\,5\%}} \\ K_i = \dfrac{K_p}{\tau} \end{cases} \tag{2.30}$$

This method will be used to tune the controllers for the two transfer functions developed in the section 2.4.

### 2.6.2 Discretization of the controllers

In order to implement the digital PI controller in the DSP, the discretisation step is required. The standard equation of the PI controller is expressed as follows:

$$C(t) = K_p\, e(t) + K_i \int_0^t e(\tau) d\tau \tag{2.31}$$

where $e(t)$ is the difference between the desired output $S_d$ and the measured output $S_m$, $C(t)$ is the controller output, The two controller parameters are $K_p$ (the proportional term) and $K_i$ (integral parameter).

Using Z-transform of the equation (2.31):

$$C(z) = \left[K_p + \frac{K_i}{1 - z^{-1}}\right] E(z) \tag{2.32}$$

Rearranging gives

$$C(z) = \left[\frac{\left(K_p + K_i\right) + \left(-K_p\right)z^{-1}}{1 - z^{-1}}\right] E(z) \tag{2.33}$$

$$C(z) - z^{-1}C(z) = \left[\left(K_p + K_i\right) + \left(-K_p\right)z^{-1}\right] E(z) \tag{2.34}$$

The equation (2.34) can be converted to recurring equation as:

$$c[k] = c[k-1] + \left(K_p + K_i\right)e[k] + \left(-K_p\right)e[k-1] \tag{2.35}$$

The digital controller is then implemented in the DSP in C language and saturation is also added to limit the controller output.

### 2.6.3 Results for the two control loops

The two controllers were implemented in the DSP with a sampling frequency of 1 kHz. We remind that the control scheme is shown on the Figure 2-16. The response time of the two controllers was chosen by calculating the controller's parameters in order to accelerate the response time of the vibration amplitude to reach about 2 ms, otherwise it is roughly 5 ms in open loop. This response time is chosen to approach the bandwidth of the finger perception which is about 400 Hz. By applying different sinusoidal signals with variable frequencies, the bandwidth of the system, corresponding to 3 dB of amplitude ratio, was measured in open and closed loop, giving an increase of its value from 80 Hz to 160 Hz from open to closed loop configuration. We

notice also that, due to the sampling frequency of 1 kHz, above 120 Hz the sinusoidal signal starts to be distorted if we assume that eight points are sufficient to generate a sine signal.

In this part, the implemented control strategy will be validated into two levels: dynamic and robustness. The dynamic behaviour of the system in response to a step input of vibration aims at validating the response time reduction by operating the closed loop configuration. The robustness of the vibratory behaviour will be validated by the variation of the external temperature and the normal force applied by the fingertip. The first series of experiments shows the response in open and closed loops of the vibration amplitude at the resonance and without any finger force applied (Figure 2-24).

The reference value for $W_q$ is zero, whereas the reference value for $W_d$ is 2 µm. By observing the response of $W_d$, we can conclude that the use of the closed loop configuration has an influence on the response time by decreasing it from 5 to 2 ms by tuning the controller parameters. This response time reduction may make the vibration more sensitive to the fingertip. The response of $W_q$ is almost zero both in close or open loop which is explained by the absence of external disturbance factors in this case. By repeating this experiment 30 times, the standard deviation of the step response was about 1.3 % at the desired vibration amplitude of 2 µm.

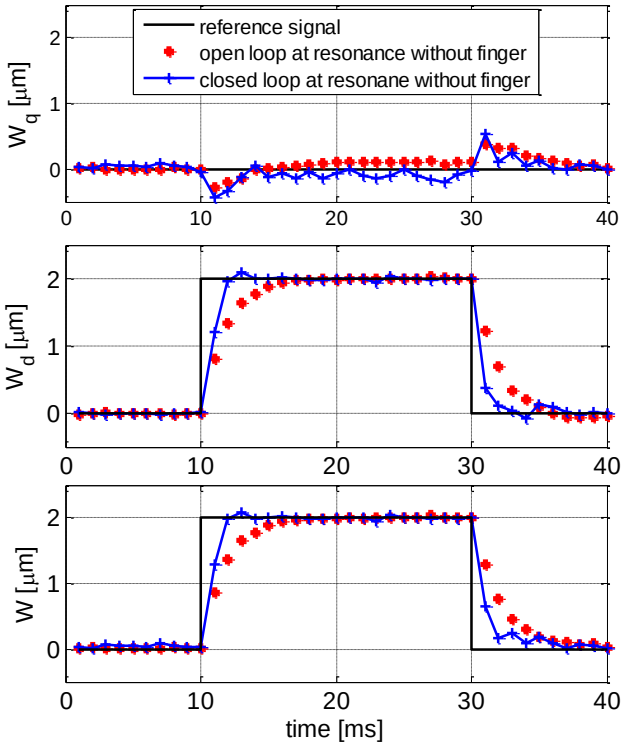


Figure 2-24: Response of the system in open and closed loops when exciting the system at resonance and without any finger force. Figures (a), (b) and (c) represent respectively the evolution of $W_q$, $W_d$ and $W$ which is the module of $W_d$ and $W_q$.

The second series of experiments aims at evaluating the robustness of the controllers against temperature variation. The idea is to power the ceramics at the same excitation voltage as in the first experiment, at an initial frequency which would correspond to the resonant frequency at 33°C ($\omega_0 = 202450\ rad/s$) while the real temperature during this experiment is about 24°C ($\omega_0 = 202995\ rad/s$). We consider this large possibility of the temperature variation from 33°C to 24°C in order to validate the robustness of the controller. If the controller works well with a minimum response time with this extreme condition, we will conclude that the system control strategy will work better when the temperature variation is smaller. Therefore, the control strategy will be validated.

In open loop, we observe Figure 2-25 that $W_q$ becomes nonzero and $W_d$ decreases from the desired vibration amplitude $W = 2\ \mu m$ to $1.6\ \mu m$. On the other hand, the closed loop control strategy ensures robustness against temperature variation with a low response time $\approx 2\ ms$ and no more static error (Figure 2-25). If we wanted to reach the same vibrating amplitude in open loop with this error on the temperature, we should provide a higher voltage supply.

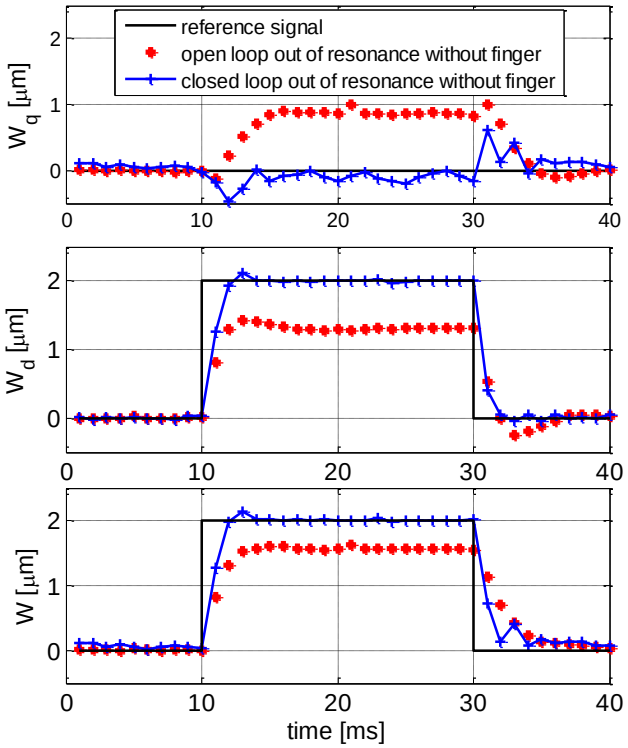


Figure 2-25 Response of the system in open and closed loop control when exciting the system as if it was at 33°C whereas the actual temperature is 24°C and without any finger force. Figures (a), (b) and (c) represent respectively the evolution of $W_q$, $W_d$ and $W$ which is the module of $W_d$ and $W_q$.

In the closed loop control, $W_q$ is nearly zero which proves that the excitation frequency of the system has converged quickly towards the resonant frequency (Figure 2-26). At the instant 11 ms, the frequency controller is switched on and converges to the resonant frequency of the temperature 24° C which is 32300 kHz (Figure 2-14). In red (the dotted line), for open loop condition, the excitation frequency is still fixed to the resonant frequency of 33°C.

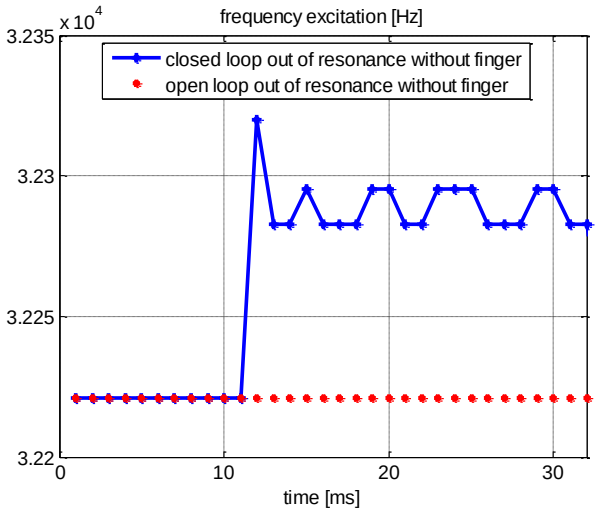


Figure 2-26: Frequency excitation behaviour in open loop and closed loop control when the system is excited out of resonance.

In order to assess the system performance against the two disturbing factors at the same time (finger force and temperature variation), a third experiment has been performed. The experimental conditions are similar to the previous experiment one (excite the system at the 33°C resonant frequency whereas the current temperature is 24°C), but this time, the finger is sliding on the active surface, while applying a force of about 2 N, which is quite a high force value for touching in exploration conditions. The finger has to move laterally back and forth on the tactile plate to feel stimulation; the measured normal finger force is displayed on a screen in front of the subject to help him/her maintaining it constant. These two conditions of temperature variation and finger force presence are performed to evaluate the robustness of the control law in the extreme disturbance conditions. While the open loop control is sensitive to the disturbing factors, the closed loop maintains the vibration constant in a short response time.

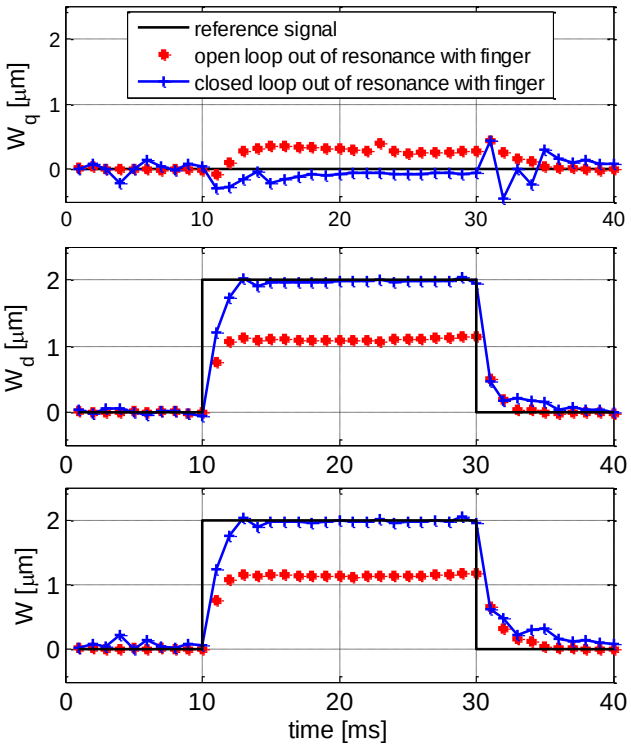


Figure 2-27 : Response of the system in open and closed loop control when exciting the system as if it was at 33°C whereas the actual temperature is 24°C and with approximately a 2 N normal finger force. Figures (a),(b) and (c) represent respectively the evolution of $W_q$, $W_d$ and $W$ which is the module of $W_d$ and $W_q$.

Now, the goal consists in validating the robustness of the controller against a variable level of the normal force when the finger is sliding on the plate. The result of the experimental measurement illustrated in Figure 2-28 indicates that the closed loop control is able to guarantee a stable level of $W$ whatever the normal force is (<2.5 N). It is shown that in closed loop, the applied signal to the piezoceramics reacts to ensure a stable level of $W = 2\ \mu m$ inversely to the open loop control.

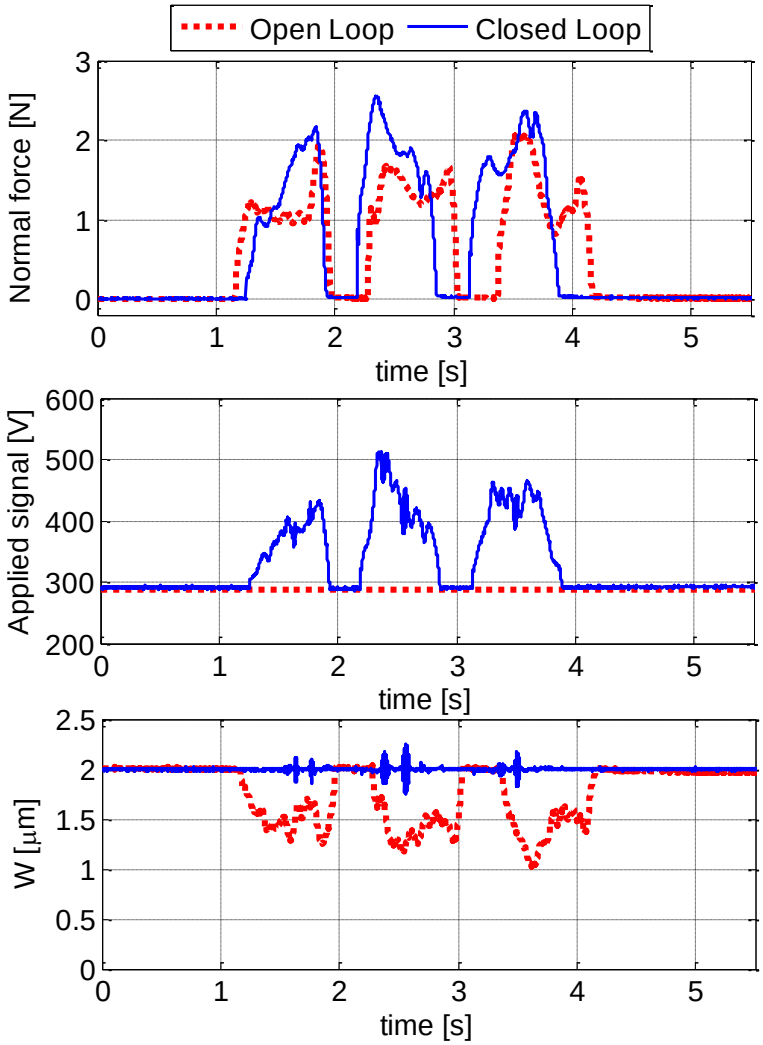


Figure 2-28: A comparison between the open and closed loop control when the finger is sliding on the plate excited at 2 µm (peak to peak). As response to the normal force applied by the finger is between 0 and 2.5 N, it can be shown that the applied voltage signal to the piezoceramics reacts to ensure a stable level of vibration *W* with the closed loop control.

### 2.6.4 Psychophysical validation

The previous paragraphs have shown that the closed loop control improved the robustness and the dynamic of the wave amplitude. But we have to check whether these improvements are useful on the point of view of touch feeling or not. To perform this task, an experiment has been carried out with ten volunteers aged between 22 and 38. All volunteers wore closed headphones to mask the audible noise which may be produced by the abrupt change of the excitation signal. The subjects had to explore laterally the surface of the stimulator with their finger. They were asked to maintain a constant force of about 0.5 N and the normal force is displayed on a computer screen to help the subject stay in control. The external temperature was about 24°C. The vibration amplitude has been changed from 0 to 2 µm peak to peak according to the finger position. The spatial period of the applied square signal was 5 mm in order to give the illusion of touching gratings. Two stimuli were put to

test in a random order, open-loop control and closed-loop control. Volunteers were asked to say which of the two stimuli gave the highest sensation intensity of gratings. The same experience has been repeated five times for each volunteer.

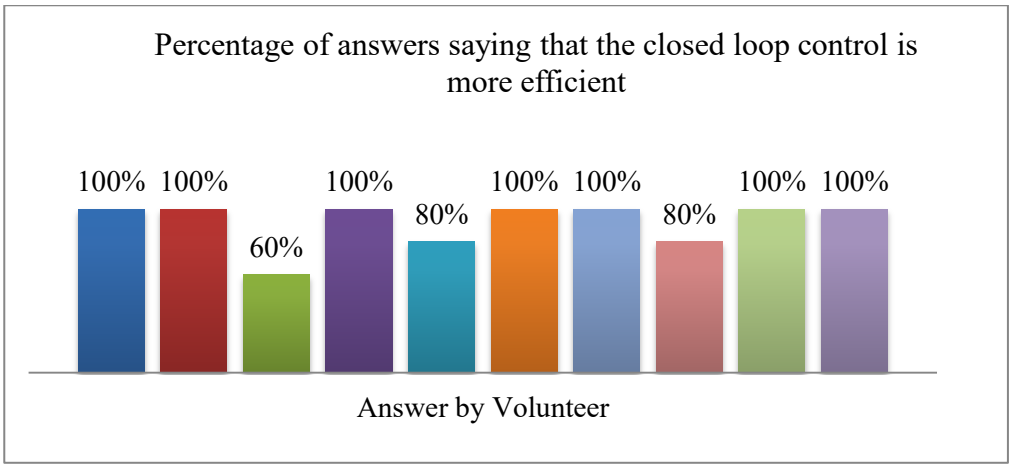


Figure 2-29: The percentage of answers per subject telling that the closed loop control configuration is more accurate than the open loop one to simulate gratings.

The result of this psychophysical test gives 46 out of 50 (92%) answers telling that closed loop control is more sensitive for perceiving the gratings than the open loop one. This result confirms also that the lower response time increases the capability of the device to simulate gratings.

## 2.7 Conclusion

In this chapter, we presented a state of the art of the existing tactile stimulation devices based on the ultrasonic vibrations, and developed in the L2EP Lab. Much progress has been made in the development and the improvement of the devices. From the first tactile feedback device, improvements have been done on the tactile plate characteristics on the piezoceramic sensors' implementation on the position measurement by using different sensing methods leading both to the reduction of the device bulkiness and the increase in the finger detection precision. Different sizes are also studied from a small haptic knob of 4 cm of diameter, a rectangular plate of (83 mm × 49 mm) to a large device size of (198 cm * 134 mm). In our work, we used the large device version and we began by analyzing its robustness against external disturbances. After that, we proposed a new approach to control the wave amplitude of the vibration created for tactile stimulation. For that aim, a new modelling has been developed analytically in a rotating reference frame. By aligning the rotating frame on the voltage, we obtained two first order type equations, for the control of the vibration amplitude and for the tracking of the resonant frequency which has been also validated experimentally in the useful range of work. The identification has been performed and two simultaneous closed loop controls of the vibration amplitude and of the frequency have been implemented. The closed loop results showed a high robustness of the new control strategy against the disturbing factors. The objective was to make the effect of the tactile feedback insensitive to external disturbances such as the fingertip force and the temperature variation. The closed loop control was proven to be more sensitive through a psychophysical experiment conducted on ten subjects; 92% of answers validated our approach. To go further, the next chapter will deal with the relation between the modulated friction measured by a tribometer and the human perception in order to analyse which parameter has a significant influence on the tactile perception.

# Chapter 3

# Friction and perception

# 3 Friction and perception

In the previous chapter, the control strategy of the tactile stimulator was developed and implemented. The objective to make the effect of the tactile feedback insensitive to external disturbances such as the fingertip force and the temperature variation was achieved and validated using a psychophysical test. This important step investigates the relation between the vibration amplitude and the perception and optimizes, at the same time, the power consumption of the tactile device. The topic of the present chapter concerns the relation between perception and friction in the tactile stimulation process based on the tactile stimulator. As described in the previous chapters, this device is able to modulate the friction between the finger and the plate. The science of friction is called tribology which will be integrated between the vibration and the perception in order to investigate more the perception of simulated surface by the user's finger. The following Figure 3.1 describes the relation between vibration amplitude and perception undertaken thought the friction reduction analysis.

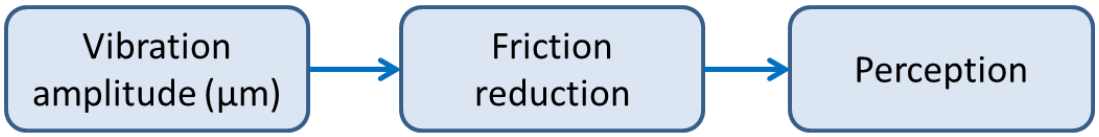


Figure 3.1: The friction investigation process undertaken from vibration to perception

The overall aim of this study is to simulate the sense of touch of real textures using an ultrasonic friction modulation device. In order to achieve this aim, the determination of the criterion to be controlled by the tactile stimulator is very important. This criterion should be clearly defined to approach to the tactile perception of the user's finger. For that reason, the relation between the tribological criteria and the perception of the simulated surface is a landmark for the reproduction of the touch sense. Since no former research has conducted a specific study to figure out which criterion is the most important to detect a friction difference, it was necessary, for us, to carry ourselves a study on tactile sense to answer the following question: To which tribological parameter the human finger is most sensitive? For this aim we studied different parameters in terms of human perception using tribological and psychophysical investigations.

Two experiments were conducted for more than 20 subjects. The aim of the first experiment is to determine the perception threshold for friction, that is, the smallest vibration amplitude of the plate detected by the subjects. On the other hand, the goal of the second experiment is to determine the criterion having the greatest influence on the perceived discrimination of friction by relating psychophysics to tribological measurement between the finger and the active surface of the stimulator (Ben

Messaoud et al., 2016a). Four tribological criteria were proposed to the subjects to be compared: the difference or the ratio between the coefficient of friction and the friction force either with or without any vibration of the plate. According to the statistical analysis, it was found that the best criterion is the ratio between the coefficients of friction with and without vibration of the plate, called the friction contrast. Consequently, the dependence of the friction contrast on the initial COF between the subjects' fingers and the plate was also analysed and related to the stimulus detection. In addition, the dependence of this friction criterion on the sliding velocity is to be highlighted.

## 3.1 Relation between friction and perception

### 3.1.1 State of the art

In tactile perception, the tribological behaviour between the finger and the surface represents an important factor in identifying and perceiving the surface texture. Researchers have investigated the evaluation of the friction between finger and surfaces to better understand the factors influencing the perception. Some factors have an influence on the friction between the surface and the finger. Some factors can be skin features (hydrolipid film, finger properties), environmental features such as temperature and humidity which can modify the finger characteristics, and sliding conditions like normal load and velocity as well as counterpart features (material, roughness or texture of the surface).

Moderate moisture increases the friction of the skin as discussed in (Hendriks and Franklin, 2009; Tomlinson et al., 2011b). Conversely, in wet skin conditions, the film of water formed can act as a lubricant in mixed or hydrodynamic regimes (Derler et al., 2009; Pasumarty et al., 2011; Tomlinson et al., 2011b).

The relationship between finger mechanical properties and friction behaviour is rarely studied. Nevertheless, fingertip impedance or stiffness in the shearing direction, that is, in relation to touch, has been measured in (Nakazawa et al., 2000; Wang and Hayward, 2007; Wiertlewski and Hayward, 2012). The result proves that when the contact force increases, the deformation of the finger pad become smaller (Pawluk and Howe, 1999). In addition, the shearing stiffness increases also and the strain rate of the fingertip in lateral direction decreases. The influence of the stiffness in normal direction of fingers on the friction behaviour has been studied with silicone artificial fingers: the coefficient of friction (COF) is higher for a softer silicone (Han et al., 1996) This result is in contradiction with the recent study of (Cornuault et al., 2015), where the finger stiffness is linked to the hydrolipid film. In fact, the finger stiffness, i.e. the elastic modulus, has been showed to increase with the lipids/water ratio and decrease with the water amount on the finger skin. Moreover, the COF has a contrary evolution with the finger stiffness.

The evolution of the COF between the finger and a counterpart decreases with the increase of the normal load. The COF follows the commonly used law from (Bowden and Young, 1951): $\mu \propto {F_n}^{n-1}$, where $F_n$ is the normal force and $n$ a coefficient between two-thirds and one. The COF between the finger and a counterpart seems to increase for very low sliding velocities (from 0.1 to 10 mm/s) (Tang et al., 2008) and decreases for higher velocities (up to 1.5 m/s) (Derler and Rotaru, 2013) in the case of smooth surfaces for both wet and dry fingers (Pasumarty et al., 2011).

The influence of the rubbing surface features on finger friction has been extensively studied (Derler and Gerhardt, 2011). Depending on the roughness of the counterpart in contact with the finger, the friction regime can be dominated by adhesion for smooth surfaces or by deformation of the fingertip for rough surfaces. Thus, in dry friction, for surface roughness with $R_a$ (the arithmetic average of asperities height's absolute values) in the range of 0.03–11.5 μm (Hendriks and Franklin, 2009), (Derler and Gerhardt, 2011; Skedung et al., 2011, 2009) $R_z$ (the average distance between the highest peak and lowest valley) in the range of 0.05–45 μm (Derler et al., 2009), or $R_q$ (the root mean square of asperities height) in the range of 0.004–2μm (Masen, 2011), the COF decreases with increasing roughness, because of a decrease of the tangential force owed to adhesion (Derler et al., 2009). For $R_q$ up to 90 μm, the COF increases with increasing roughness (Tomlinson et al., 2011a), because of an increase in skin deformation (Tomlinson et al., 2013). However, in the case of wet friction, that is, hydrodynamic lubrication, a low $R_a$ has the opposite effect, because it reduces the friction (Derler et al., 2009). For a gentle surface roughness in comparison with fingerprints, the evolution is dependent on the topography of the surface (shape, height of asperities, and distance between asperities) (van Kuilenburg et al., 2012). The fingertip point of contact when interacting with an object or when exploring a surface has been studied because of its importance to determine the haptic perception (Delhaye et al., 2014).

Material in contact with the finger influences the friction. The COF between the finger and the smooth surface of a homogeneous material can be classified in decreasing order: soft polymers such as rubber, hard polymers (except polytetrafluoroethylene – PTFE) (Gee et al., 2005), and metals and PTFE (Hendriks and Franklin, 2009). Glass can give a lower or higher coefficient of friction than hard polymers (Adams et al., 2013; Bergmann Tiest, 2010; Smith and Scott, 1996) and metals, probably depending on its state of cleanliness.

The influence of friction between the finger and a surface on the perceived friction, or slipperiness, has been less studied. One probable reason is the difficulty of changing the friction without changing the surface roughness or the material (Adams et al., 2013; Gee et al., 2005). Therefore, other surface characteristics are changed, not only the friction properties. A convenient solution for modifying the friction between the finger and a surface is to use a tactile stimulator to stretch the skin (Bark

et al., 2009) of the fingertip or to modify the friction of a tactile plate used as a touch pad (Biet et al., 2008). The effect of skin stretching, simulating friction, on the perception of friction has been highlighted by using a force feedback arm and contact location display apparatus (Sylvester and Provancher, 2007). One of the most important solutions is to use a tactile stimulator, which gives the opportunity to change the friction between the surface and the finger without changing the roughness of the material. The tactile stimulator used in this study allows us to quickly obtain a variable and repeatable coefficient of friction and can be used to simulate real textile fabrics (Bueno et al., 2015).

As described in the previous chapters, the tactile stimulator used in the present study is based on friction modulation because of the possibility of instantaneously changing the contact conditions between the finger and the plate by acting like a lubricant. This kind of device can be also very interesting for the study of the influence of friction on the perceived friction and/or friction threshold (Biet et al., 2008). In (Samur et al., 2009), authors use a similar device based on ultrasonic friction modulation device to determine the just noticeable difference (JND) of friction. A psychophysical experiment coupled a tribological measurement was carried out with just one subject. The result shows that a change of around 20% in the coefficient of friction can be perceived by the human finger.

### 3.1.2 Which friction parameters influence the perception?

The central issue surrounding the tactile perception and therefore the simulation of textures with the tactile stimulator is “Which is the friction most influencing parameter on the human finger perception?”. Answering this question may help us to identify and use more the tactile stimulation device with the objective of controlling the parameter which influences more the finger perception. As described below, the generation of ultrasonic vibrations under the finger when touching the surface lubricates the contact. Many parameters can characterize this contact lubrication in a tribological point of view: the reduction of the coefficient of friction, the reduction of the friction force, the ratio between the reduced and the initial coefficient of friction/force or the difference between the reduced and the initial coefficient of friction/force.

The present chapter presents an analysis of the friction between the index finger and the surface of the stimulator excited by different signals related to the human perception. The main goal of analysing the relation between human-perceived friction and friction characteristics is to improve the simulation of the texture touch sensation using a programmable tactile device (Bueno et al., 2015). First, the perceived threshold for friction, that is, the smallest detected vibration amplitude (VA), is determined from a panel of more than 20 subjects. Second, this threshold is used to evaluate the relation between the tribological response and the psychophysical evaluation. A statistical analysis will be undertaken to assess this

relation in order to determine the criterion correlated to the perceived friction discrimination. Moreover, the influence of the subject friction response and the sliding velocity on the perception will be studied.

## 3.2 Tactile perception's threshold

In this section, the aim is to determine the tactile perception's threshold as a function of the vibration amplitude (VA). The goal is to find the smaller detectable stimulus by operating psychophysical experiment.

### 3.2.1 Experimental protocol

Figure 3.2: Experimental set-up of used to determine the tactile perception's threshold

The objective of the present experiment is to determine the perceived friction threshold as a function of the VA of the tactile stimulator. This parameter is required to determine the range of useful and detectable VAs. The exploration distance of 40 mm is delimited by two marks on the plate of the stimulator and a metronome is used to guide users to guarantee a constant pulsation of 30 beats/min corresponding to an average velocity of 20 mm/s. The duration of the experiment depends on the subject, but it is generally less than 10 minutes, to limit tactile perception fatigue. The perceived friction threshold is evaluated by determining the smallest difference in friction perceived by each subject. The protocol used is the following: the right part of the plate is not excited (VA = 0 µm), indicating that the friction is not modulated (initial friction), whereas the left part is excited at different VAs, reducing the friction. The starting excited VA proposed is 2 µm, the maximum practical value, and this amplitude is reduced by a step of 0.2 µm. When 0 µm is reached, the vibration is increased by the same step until 2 µm is reached in the left part. At each step, the subject is asked whether he or she feels a tactile difference between the right and the

left parts of the stimulator or a transition in the middle of the plate. No tribological measurements are taken in this experiment.

The experiment was carried out on 25 subjects, 13 males and 12 females, aged between 24 and 64; the mean age was 41 years. All subjects were right-handed except one. The subjects were students and staff randomly chosen from the university department. None suffered from physiological or cognitive deficits that might alter their tactile perception or judgment. Each psychophysical experiment is carried out using a specific protocol: after washing and drying his or her hands, the volunteer sits down in front of the experimental setup and then uses the forefinger of his or her dominant hand. The finger sliding direction is the medial radial direction from right to left and left to right. The subject acts on the normal load by pressing his or her finger on the tested surface with a load of about 0.5 N.

### 3.2.2 Results

As described in the previous section, the right part of the stimulator's plate is not excited and presents the maximum friction, whereas the left part is excited with a VA which decreases from the maximum value (2 µm) to zero and then increases from 0 to 2 µm. Figure 3.3 illustrates the percentage of the perceived friction difference as a function of the VA of the tactile stimulator for men and women and the mean value of all the measurements. In Figure 3.4, the tactile discrimination is based on the subject's age group: from 24 to 42 years (12 subjects) and from 44 to 64 years (13 subjects). The result indicates gender does not influence the 50% tactile threshold (Figure 3.3) and this threshold increases with age (Figure 3.4).

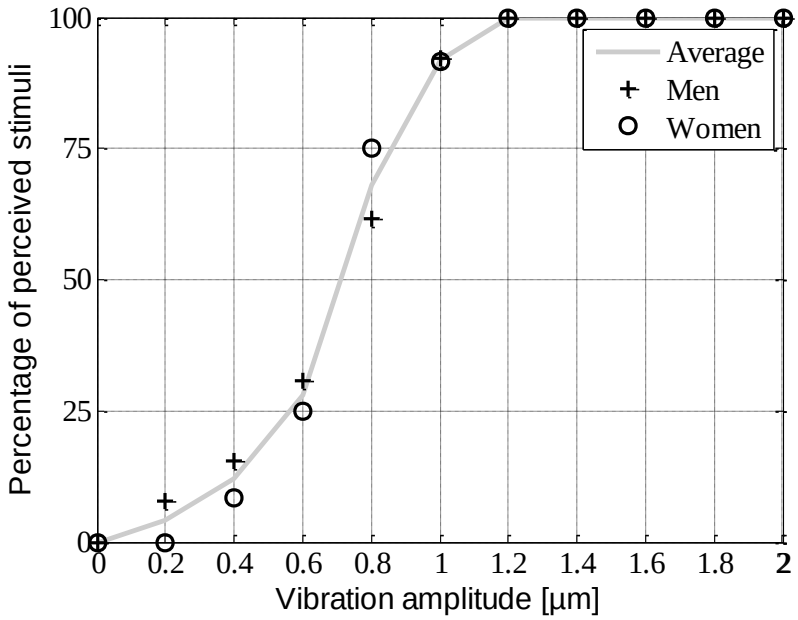


Figure 3.3: Percentage of the perceived stimuli as a function of the VA in microns; the averages of men's and women's responses are plotted respectively as crosses and circles. The average of all users is drawn by a grey continuous curve.

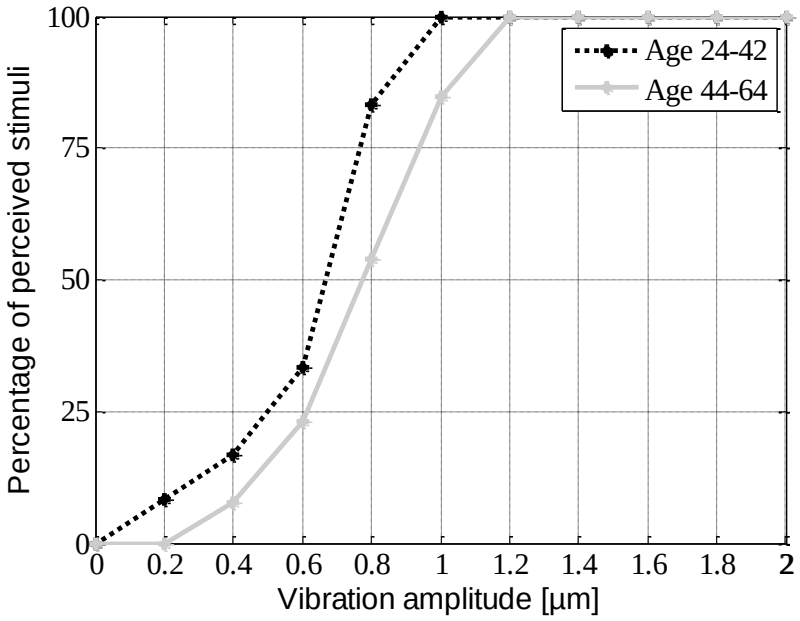


Figure 3.4: Percentage of the perceived stimuli as a function of the VA in microns; the average of subjects between the ages from 24 to 42 years is drawn by a dotted black curve, while the grey continuous curve represents the average of the subjects from 44 to 64 years.

Fifty per cent of the youngest group (aged between 24 and 42 years) can perceive a difference in the VA between 0 (non-excited stimulator) and 0.65 µm (the excited side of the stimulator), while the corresponding excited VA is almost 0.8 µm for the oldest group. Moreover, 75% of the youngest age group can perceive a difference of 0.77 µm compared to 50% of the older age group. This influence of age and the lack of influence of gender on the tactile perception is confirmed in the literature; see for example (Reuter et al., 2011) for the dependence of the tactile perception on age and (Woodward, 1993) for the increase in the tactile threshold with age and not with sex.

## 3.3 Friction discrimination criterion

In this section, the friction between the finger and the surface of the stimulator excited by different VA is analysed in a tribological and psychophysical point of view. The main goal of investigating the relation between human perceived friction and friction characteristics is to improve the simulation of the texture touch sensation using the programmable tactile stimulator.

### 3.3.1 Experimental protocol and tribological criteria

The second experiment was carried out on 21 subjects, 12 males and 9 females aged between 23 and 57; the mean age was 41 years, and only one was left-handed. In order to have a coherent measurement for all users, it is required to standardize the measurement conditions such as sliding velocity and normal applied force. For this aim, a specific tactile tribometer has been developed at the Textile Physics and

Mechanics Laboratory (LPMT) for the measurement between the stimulator and the volunteer's finger. It is a reciprocating tribometer, as illustrated in Figure 3.5.

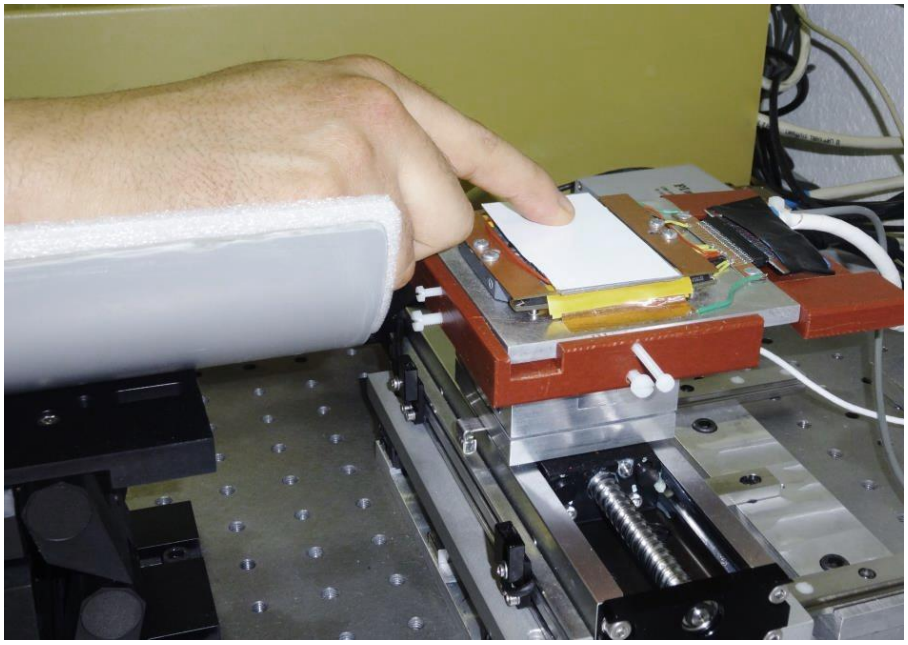

Figure 3.5: Photography of the finger touching the surface of the stimulator affixed on the tactile tribometer.

It is composed of a linear stage (VT75 100 DC HLS, controlled by a one-channel Mercury servo-controller C863, Physik Instruments Gmbh & Co. KG, Karlsruhe, Germany), onto which the sample is affixed, this linear stage is used to guarantee a constant speed of the user hand. The data acquisition is performed by a Pulse data recorder (Brüel & Kjaer, Mennecy, France). The normal and lateral forces are obtained from a three-axis load cell (model 3A60-20N, Interface Inc., Scottsdale, Arizona), onto which the tactile stimulator is affixed and which provides the components of the force exerted by the finger on the cell along three orthogonal axes (the vertical axis is denoted as z, the axes in the horizontal plane are named as x and y) (Figure 3.5). The load cell is placed on the linear stage and can be translated along the x axis. To ensure a correct position of the finger relative to the sample and for the comfort of the subject, an adjustable gutter is designed to support the subject's arm.

During the friction test, the exploration task is semi-passive; the subject should only maintain his or her finger in the original position while the surface is moved beneath with a controllable velocity. The sliding distance is set at 40 mm. The subjects were asked to maintain a constant force of about 0.5 N and a gauge on a computer screen shows the applied load to help the subject stay in control.

To evaluate the relationship between the perception and the tribological behaviour between the finger and the tactile stimulator modifying only the friction, the results obtained from the previous psychophysical experiment have been used.

Two vibrations amplitudes (Vas) were chosen: 0.7 μm, which corresponds to the threshold perceived by 50% of the subjects, and a lower value of VA of 0.4 μm, which was detected by around 10% of the subjects. This choice was made to divide people into two categories depending on their ability to discriminate the difference in tactile stimulation in order to determine the most important parameter influencing the friction perception. The protocol is to propose six stimulations to the fingers of the subjects for each sliding velocity, fast (20 mm/s) and slow (5 mm/s), in a random way: two stimulations without any vibration of the plate (the transition from one part of the stimulator to the other is from 0 to 0 μm), and therefore without any difference between the two parts of the tactile stimulator; two simulations with the left or the right part excited with a VA of 0.4 μm (the transition from one part of the stimulator to the other is from 0 to 0.4 μm or from 0.4 to 0 μm); and two stimulations with the left or the right part excited with a VA of 0.7 μm (transition from 0 to 0.7 μm or from 0.7 to 0 μm).

For each stimulation, the subject has to indicate whether he or she feels a transition or a difference between the right and the left part of the stimulator. Any subject answering “yes, I feel a difference” more than twice in four tests when no stimulus is present is automatically eliminated and his/her measures are not considered in the data processing. The normal and friction forces are recorded during the experiment.

To find the correlation between friction criteria and perception, the boxplot representation of the different criteria is chosen because of its concept of breaking data into four parts to create a display based on statistical measurements. This representation gives an instantaneous picture of the shape of data variation. All boxplots are designed according to (McGill et al., 1978), which means that the length of the whiskers is limited to 1.5*IQR (interquartile range). The point not included between the whiskers is called an outlier. The middle 50% of the data is contained in the box limited by the lower and upper quartiles while the bold line within the box represents the median. All statistical analysis in this study was performed with Matlab software.

The lateral force (along the x-axis) and the normal force (along the z-axis) are recorded using a tribometer when the subjects slide their fingers on the two parts of the plate. The instantaneous coefficient of friction μ is then computed. An example of sliding the finger of one subject is given in Figure 3.6.

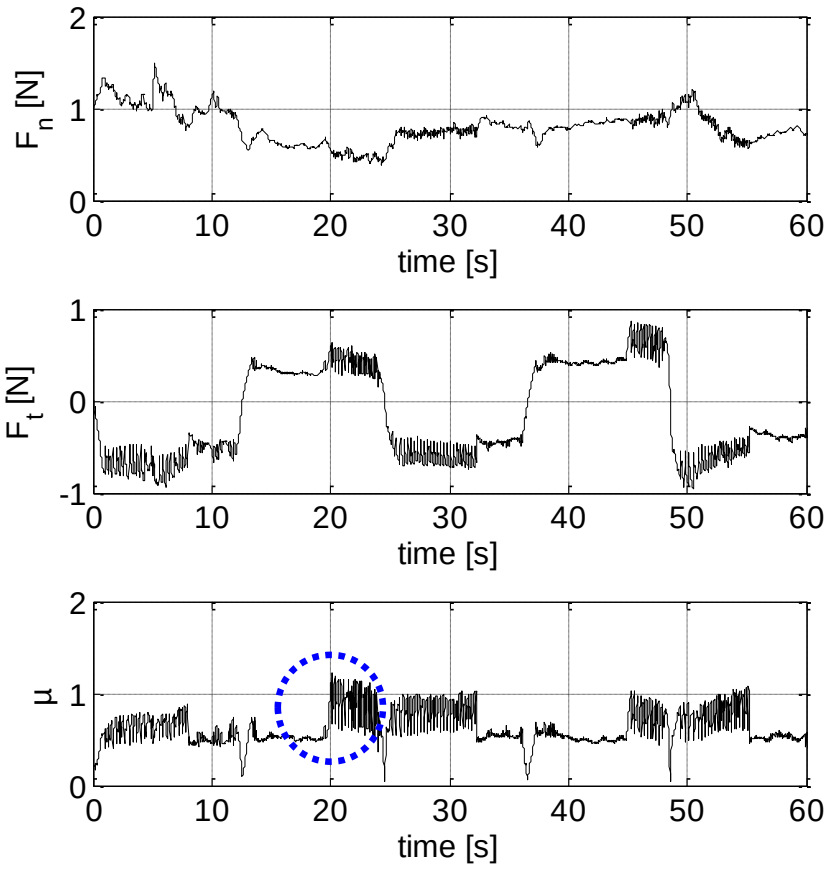


Figure 3.6: Normal force, friction force, and coefficient of friction of a subject sliding his or her finger on the tactile stimulator. Example of a female aged 46 years. The VA was 0.7 μm and the sliding velocity was 5 mm/s.

Figure 3.7 illustrates a magnified view of the coefficient of friction when the vibration changes from the active to the inactive state. In this area, the finger is sliding in one direction and the velocity of the oscillating table is constant. The coefficient of friction between the finger and the surface of the stimulator without vibration is defined as $\mu_0$. It represents the average of the dynamic coefficient of friction, which represents the maximum COF that is possible to obtain between the subject's finger and the tactile stimulator. The oscillation of $\mu_0$ is due to the stick-slip phenomenon when the finger is sliding under the plate; its intensity is variable and depends on the user's finger and the velocity. The parameter $\mu_1$ is the average of the reduced coefficient of friction for a VA of 0.4 or 0.7 μm.

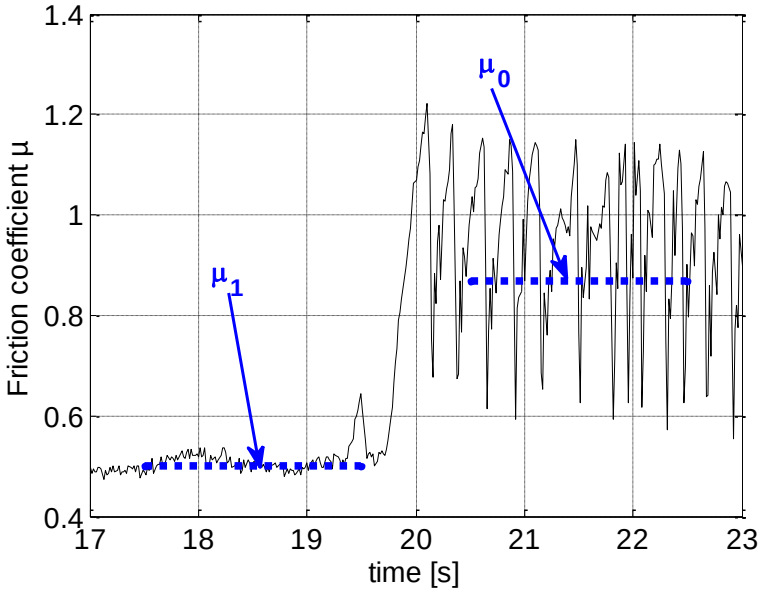


Figure 3.7: Magnified view of the coefficient of friction when the finger is sliding between an excited and non-excited parts.

Four tribological criteria have been analysed and related to the human finger perception. The first one is $\Delta F_t$, which represents the difference in friction force between the excited and the unexcited parts of the plate. This criterion is defined as:

$$\Delta F_t = F_{t0} - F_{t1} \tag{3.1}$$

where

$F_{t0}$ is the friction force without vibration, and $F_{t1}$ is the friction force when vibration is switched on.

The second parameter that will be analysed is the difference in the coefficient of friction $\Delta\mu$; this parameter is defined as:

$$\Delta\mu = \mu_0 - \mu_1 \tag{3.2}$$

where

$\mu_0$ is the coefficient of friction without vibration.

$\mu_1$ is the reduced coefficient of friction.

The third parameter represents the normalized friction force and can be called the Friction Force Contrast ($FFC$). This parameter is defined by the following formula:

$$FFC = \frac{F_{t0} - F_{t1}}{F_{t0}} \tag{3.3}$$

The last parameter is called friction contrast (Cornuault et al., 2015); it represents the normalization of the second criterion by dividing it by the initial coefficient of friction $\mu_0$.

$$FC = \frac{\mu_0 - \mu_1}{\mu_0} \tag{3.4}$$

The friction contrast is below 1 when the friction is reduced, which means that $\mu_1$ is always less than $\mu_0$. This parameter also represents the subtraction of 1 from the ratio between the two coefficient of frictions $\mu_1$ and $\mu_0$.

$$FC = 1 - \frac{\mu_1}{\mu_0} \tag{3.5}$$

The two last parameters, $FFC$ and $FC$, are comparable is terms of dimensions and a relation between them can be found by replacing the coefficient of friction by the ratio between the friction force $F_t$ and the normal force $F_n$, respectively, with the index being 0 when there is no vibration and 1 when the active plate is vibrating:

$$FC = \frac{F_{t0} - \frac{F_{n0}}{F_{n1}} F_{t1}}{F_{t0}} \tag{3.6}$$

If the normal force is constant ($F_{n0} = F_{n1}$), when alternating between the excited and unexcited parts of the plate, the friction contrast will be equal to the friction force contrast. This assumption means that the air gap produced by the tactile stimulation acts only on the lateral force, and this assumption is approximately verified by experimental measurements.

### 3.3.2 Results

Figure 3.8 to Figure 3.11 illustrate the boxplot representation of the perception of friction variation relative to the four measured friction criteria, respectively $\Delta F_t$, $\Delta\mu$, $FFC$, and $FC$, and for both sliding velocities 5 and 20 mm/s. For each figure, the differentiation is made between the excited vibrations VA of 0.7 µm (a) and 0.4 µm (b). For each case of VA, 84 measures corresponding to the four cases of the experiment are considered (4x21 subjects): a detected tactile stimulation (i.e. detection result is indicated “Yes”) is represented on the right part of the graph while an undetected tactile stimulation (i.e. detection result is indicated “No”) is represented on the left part.

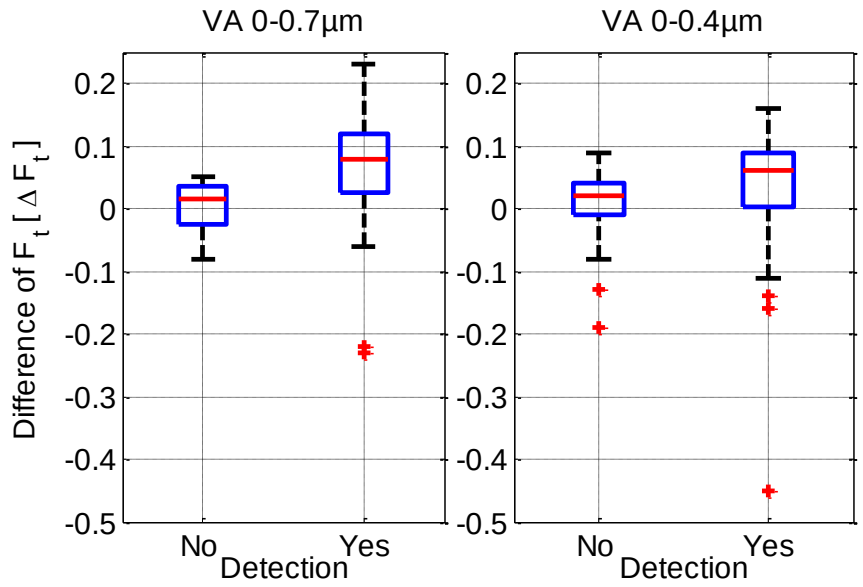


(a) (b)

Figure 3.8: Boxplots of the $\Delta F_t$ as a function of the tactile detection for the transition between 0–0.7 µm (a) and 0–0.4 µm (b) for both sliding velocities.

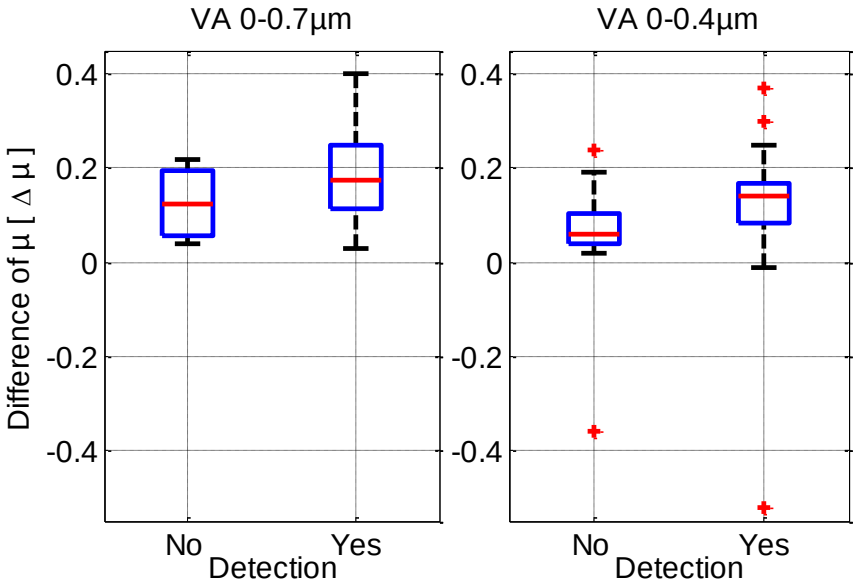


(a) (b)

Figure 3.9: Boxplots of the Δµ as a function of the tactile detection for the transition between 0–0.7 µm (a) and 0–0.4 µm (b) for both sliding velocities.

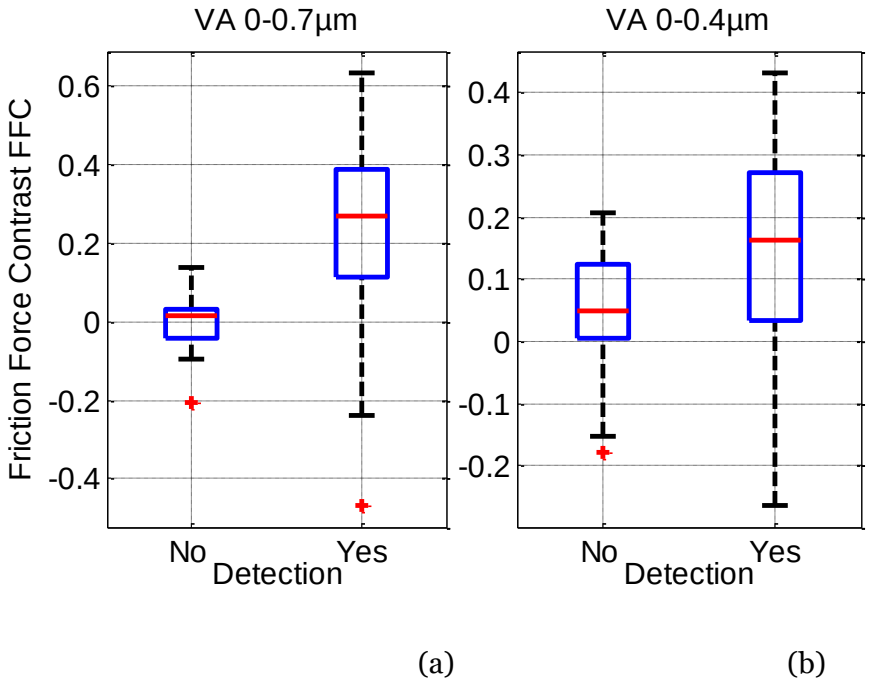


Figure 3.10: Boxplots of the friction force contrast $FFC$ as a function of the tactile detection for the transition between 0–0.7 µm (a) and 0–0.4 µm (b) for both sliding velocities.

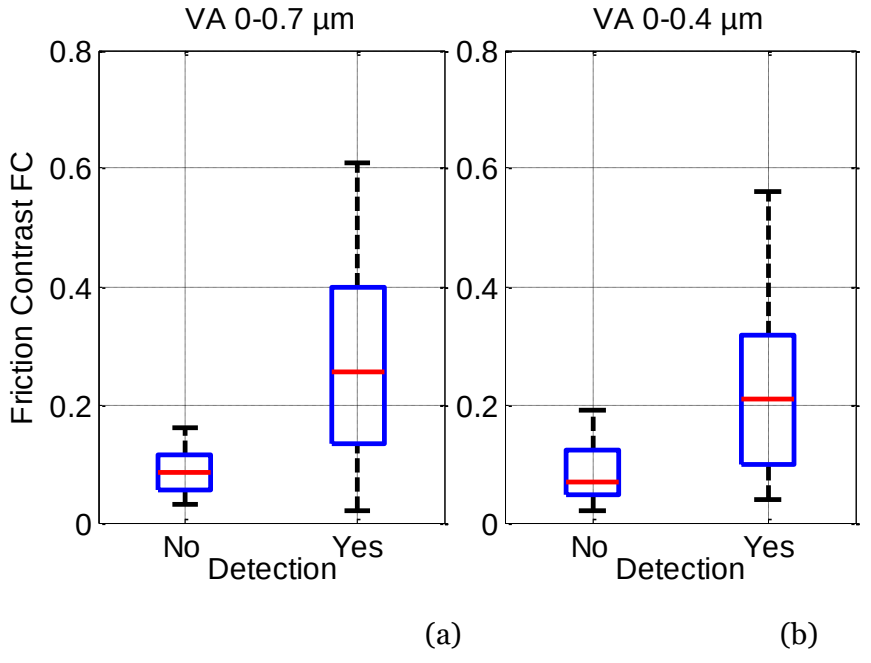


Figure 3.11: Boxplots of the friction contrast $FC$ as a function of the tactile detection for the transition between 0–0.7 µm (a) and 0–0.4 µm (b) for both sliding velocities.

### 3.3.3 Criterion choice

From the representation of the four criteria relative to perception, it can be seen that the $FC$ is the most discriminating parameter when comparing the tactile perception. As shown in Figure 3.8, Figure 3.9, Figure 3.10 and Figure 3.11, when comparing the lower and upper quartiles of the $FC$ criterion, the detectable and undetectable stimulations can be distinguished for the two VAs of 0–0.7 µm in (a) and 0–0.4 µm in (b), which means that the common part between the two detection cases is the smaller compared to the other criteria. The upper and the lower quarters are less well distinguished when evaluating $\Delta F_t$, Δµ, or $FFC$. It is also remarkable that all three criteria, $\Delta F_t$, Δµ, and $FFC$, have some outliers plotted by dots which make the distinction between the detection cases impossible because they are negative, indicating that the value of the criterion without vibration is lower than that with vibration. By comparing the two criteria $FFC$ and $FC$ because they have the same dimension, $FFC$ has a negative values which is explained by the fact that some subjects increase their normal force when they felt the transition between the non-excited and the excited parts which make the evolution of the friction force increasing rather than decreasing. We can conclude that the criterion focusing just on the friction force cannot characterize the tactile stimulation. Moreover, $FC$ has always positive values because it is based on the coefficient of friction, i.e. the lateral and normal force are considered here, which means that when the plate is excited by vibration, the friction is always reduced and $\mu_1$ is always equal or lower than $\mu_0$. These results show that the ultrasonic friction-modulation devices act on the coefficient of friction, not only the friction force.

### 3.3.4 Influence of the maximal friction on the friction criterion and on the perception

The results obtained from Experiment 2 revealed that the coefficient of friction without any vibration (VA = 0 µm) $\mu_0$ varies from 0.2 to 2.2 for all the subjects. Therefore, the present section will study if the contrast in friction is linked to the coefficient of friction $\mu_0$ of the subject.

For each of the two chosen vibration amplitudes, 84 measures were considered, which represents four different excitations for 21 subjects. By plotting the $FC$ as a function of the coefficient of friction $\mu_0$, it can be observed that, when the coefficient of friction $\mu_0$ increases, the friction contrast decreases for the two vibration amplitudes of 0.7 µm (Figure 3.12) and 0.4 µm (Figure 3.13). The curves illustrate a fitting of the measured raw data represented by points. The fitting function form is $a \cdot x^b$ with $a = 0.21$ and $b = -0.63$ in the first figure and $a = 0.15$ and $b = -0.60$ for the second figure. Based on these curves, it can be noticed that the subject who has a low initial coefficient of friction $\mu_0$ has a high friction contrast. These results are coherent with (Cornuault et al., 2015).

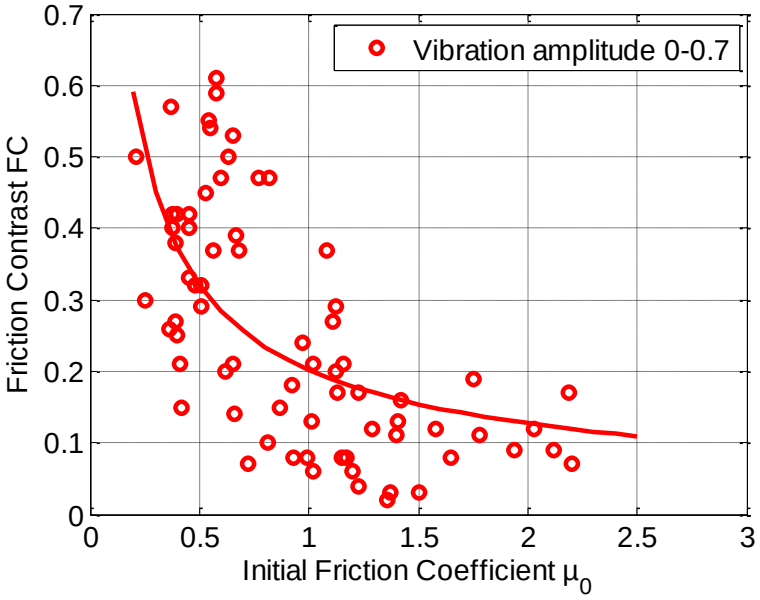


Figure 3.12: Friction contrast obtained from the experiment with a VA from 0 to 0.7 µm as a function of the initial coefficient of friction $\mu_o$ (VA = 0 µm) for both sliding velocities.

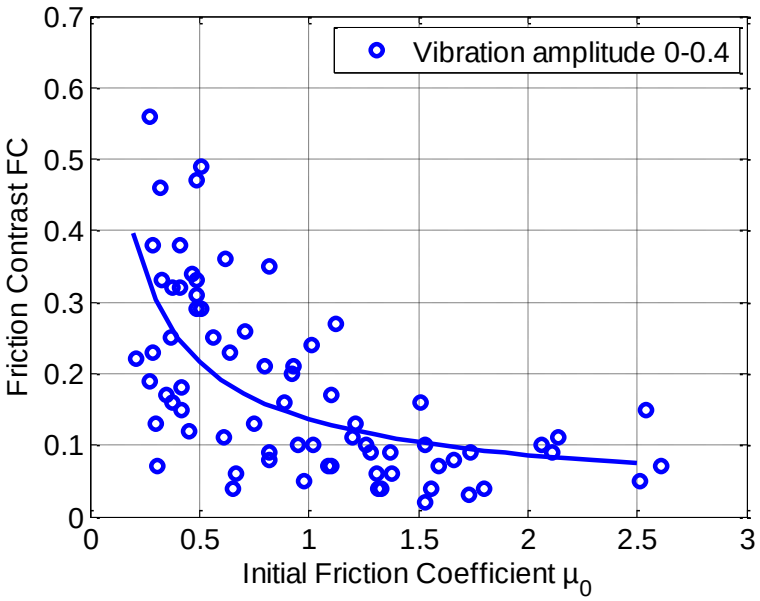


Figure 3.13: Friction contrast as a function of the initial coefficient of friction of the experiment with a VA from 0 to 0.4 µm for both sliding velocities.

From Figure 3.11, we can also observe that when the $FC$ exceeds 0.19, which corresponds to the maximum value of the undetectable case, the stimulus will be detectable by all of the participants. This result confirms, with a human panel of more than 20 subjects, the work of (Samur et al., 2009), which was done with a single subject who found that the just noticeable difference (JND) in friction is about 18%, which corresponds to a friction contrast ($FC$) equal to 0.18.

From the results describe above there is a correlation on one hand between the perception and the Friction Contrast and on the other hand between the Friction Contrast and the coefficient of friction without any vibration, called $\mu_0$. It is interesting to relate the coefficient of friction $\mu_0$ to the subject's stimulus detection in order to determine the influence of this parameter on perception. The histogram of the data distribution of $\mu_0$ for all the subjects and for both cases of measurements with the VAs of 0.7 and 0.4 µm, is shown in Figure 3.14. The detected stimulus is plotted in white colour with black continuous boundary line, while the undetected stimulus is represented by a grey dashed boundary line.

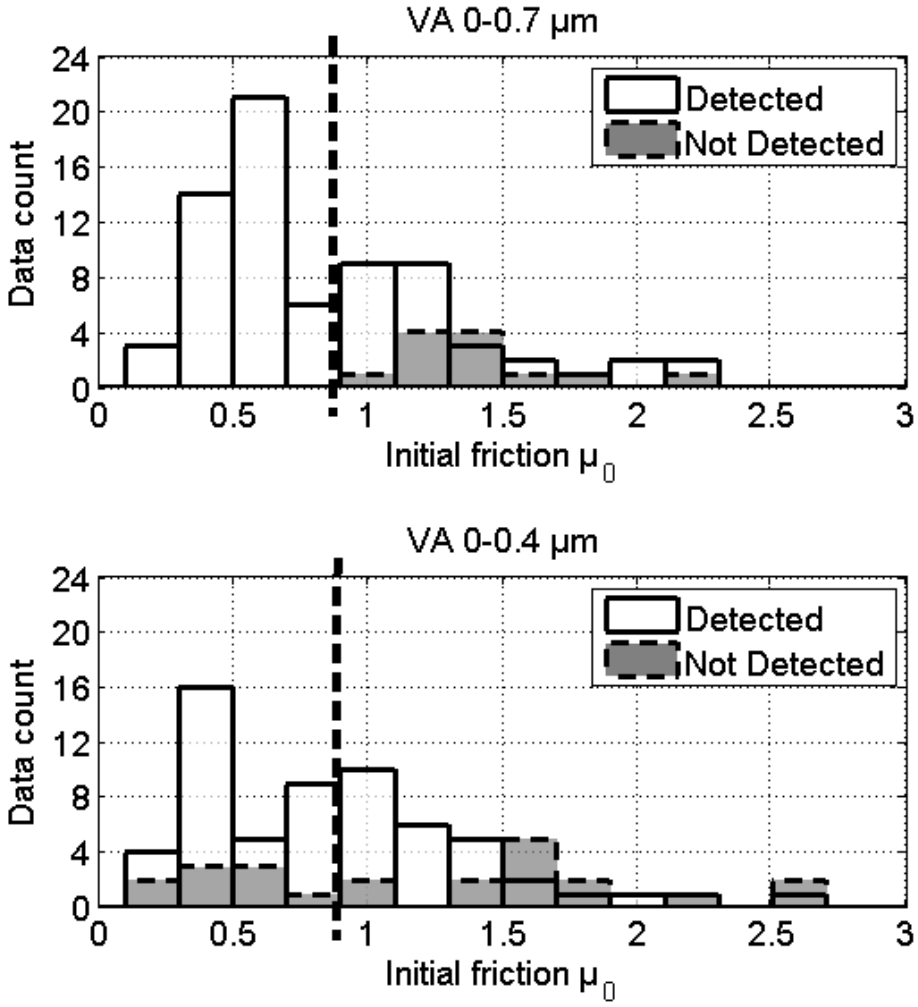


Figure 3.14: Histogram of the initial COF for the two VAs.

The number of plotted data is 84 for each VA. By choosing the value of $\mu_0$ nearest to the median to ensure the same number of separated parts, this value was found to be equal to 0.85. To analyse the data above and below the median value of $\mu_0$, Table 3-1 illustrates the relation between the detection and $\mu_0$ depending on the two VAs.

Table 3-1: Relation between the detection and the coefficient of friction $\mu_0$ for the two cases of experiments with different VAs.

| | | $\mu_0 < 0.85$ | | $\mu_0 > 0.85$ | |
|---|---|---|---|---|---|
| Detection | | No | Yes | No | Yes |
| VA 0–0.7 | Number | 0 | 42 | 12 | 30 |
| | Percentage | 0 % | 100 % | 28 % | 72 % |
| VA 0–0.4 | Number | 9 | 32 | 14 | 29 |
| | Percentage | 22 % | 78% | 33% | 67 % |

From this table, the discussion about the VA of 0–0.7 µm showed that if $\mu_0$ is lower than 0.85, all stimuli are detectable by all the subjects, but if $\mu_0$ is higher than this value, 28% of the subjects do cannot detect the stimuli. Regarding the second VA of 0–0.4 µm, the percentage of undetectable stimuli is about 22% when $\mu_0$ is lower than 0.85, but this percentage increases to 33% when $\mu_0$ is above 0.85. This result indicates that the percentage of participants not detecting stimuli increases with the coefficient of friction between their finger and the surface without excitation $\mu_0$.

This result is very important for the tactile stimulation experiment because it can explain the difference in perception between subjects. Moreover, the procedure for adapting the perception to the subject can be the following: after identifying the parameter $\mu_0$ for a subject, solutions can be found to take into account the subject finger properties and to adjust the VA depending on the subject. Figure 3.14 shows that, for a VA of 0.7 µm, if $\mu_0$ is lower to 0.85, the stimulus is always detected.

### 3.3.5 Influence of the sliding velocity

In this section, the focus will move towards the dependence of the friction contrast $FC$ on the sliding velocity. Figure 3.15 illustrates the mean value of the friction contrast $FC$ of all subjects as a function of the sliding velocity (continuous line for 5 mm/s and dashed line for 20 mm/s) and the transition of the VA from 0 to 0.7 or 0.4 µm. It can be noticed that $FC$ is higher when the velocity is lower (5 mm/s) whatever VA is from 0 to 0.7 or 0.4 µm. For example, when the VA is from 0 to 0.7 µm, the friction contrast is 28% higher at 5 mm/s than at 20 mm/s. When, the VA is from 0 to 0.4 µm, the effect of the velocity is also present and the difference in $FC$ between the two sliding velocities is 16%.

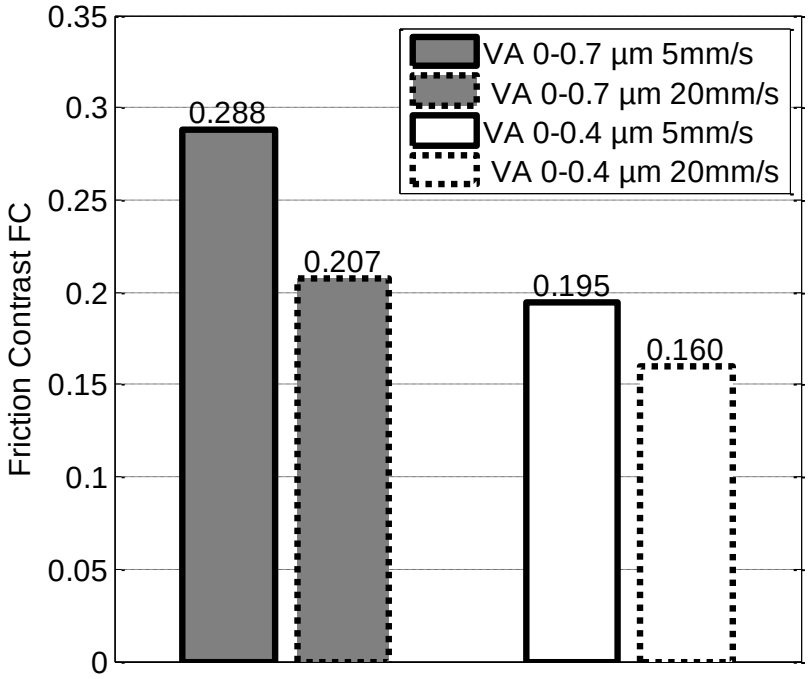


Figure 3.15: Variation of FC depending on the sliding velocity and on the transition of VA from 0 to 0.7 µm in grey colour and 0 to 0.4 µm in white colour.

From the results above, the influence of the sliding velocity on the friction contrast has been shown but the impact on the perception has to be studied. Table 3-2 illustrates the relation between the detection and the sliding velocity for the two VAs. For VA from 0 to 0.7 µm, the sliding velocity has no influence on the detection of the friction change, whereas for VA from 0 to 0.4 µm, the detection is slightly better with a low sliding velocity (78% of detected stimuli with 5 mm/s instead of 67% with 20 mm/s). These results show sliding velocity has a greater influence on the friction contrast than on the friction discrimination. Nevertheless, it can be considered to be in good conditions to perceive fine changes in friction it is better to touch with a low sliding velocity.

Table 3-2: Relation between the detection and the finger sliding velocity for the two cases of experiments with different VAs.

| | | Velocity 5 mm/s | | Velocity 20 mm/s | |
|---|---|---|---|---|---|
| Detection | | No | Yes | No | Yes |
| VA 0–0.7 | Number | 6 | 36 | 6 | 36 |
| | Percentage | 14 % | 86 % | 14 % | 86 % |
| VA 0–0.4 | Number | 9 | 33 | 14 | 28 |
| | Percentage | 21 % | 79% | 33% | 67 % |

## 3.4 Conclusion

In this chapter, the focus was put on the friction between the finger and the surface of the tactile stimulator excited by different VAs. In the first experiment, the friction threshold was determined as a function of the VA. The influence of the age on the tactile threshold was highlighted but the influence of gender was not observed.

In the second experiment, two VA cases were used to evaluate the relation between the tribological behaviour and the friction perceived discrimination: 0 to 0.4 µm and 0 to 0.7 µm. Statistical analysis derived from more than 20 volunteers was undertaken to assess this relation in order to determine the criterion affecting the perception of finger friction. This experience leads to the conclusion that the friction contrast criterion ($FC = 1 - \mu_1/\mu_0$) based on the ratio between the reduced and the initial coefficient of friction is the most discriminated criterion when comparing the detected and undetected tactile stimuli. The dependence of the friction contrast criterion on the initial coefficient of friction ($\mu_0$) between the subjects' fingers and the plate was also analysed and related to the stimulus detection. In fact, when $\mu_0$ increases, the friction contrast decreases, and therefore the friction discrimination also decreases. When the VA changes from 0 to 0.7 µm, a subject with an initial coefficient of friction lower than 0.85 could detect the transition of vibration with $FC$ more than 0.2. The dependence of this friction contrast criterion on the sliding velocity is also highlighted. In fact, a low sliding velocity of 5 mm/s gives a higher friction contrast than a sliding velocity of 20 mm/s leading to better friction discrimination.

The identification of the most influencing criterion on the tactile perception is the first and important step to improve the tactile stimulation. The *FC* criterion requires the determination of the coefficient of friction between the user's finger and the surface. The classic solution to measure the friction consists in putting the tactile device over a tribometer. This solution is complicated because it needs a real time communication between the measurement tools and the tactile device and a complex experimental set-up. Thus, it is not comfortable and cannot be moved from one place to the other which makes the tactile device non-portable. In the next chapter, a new design of the tactile device will be presented allowing a real time measurement of the friction.

# Chapter 4

# Design and evaluation of a smart tactile stimulator: SmartTac

# 4 Design and evaluation of a smart tactile stimulator: SmartTac

## 4.1 Why a smart device?

In the second chapter, a closed loop control was operated on the tactile feedback plate to eliminate the effect of the external disturbances on the vibration amplitude, in particular the effect of the normal applied force and the influence of the external temperature changes. The implemented closed loop control has ensured a stable level of vibration which was validated using psychophysical experiment. In the previous chapter, the tribological field between the vibration and the perception has been investigated to better understand the physical principle of tactile feeling and to develop the tactile stimulation process. It has been proven, using statistical analysis, that the friction contrast, which depends on the friction reduction, is the most affecting criterion for the perception of simulated surfaces. For this reason, studying the effect of the friction reduction which depends on the user's finger is highly important to take into account the link between tribology and perception. .

If we want to investigate the tribological behaviour of the interaction between the plate and the user's finger, it is mandatory to use an external system to measure the friction parameters. As it was used before, the coefficient of friction is defined using the Coulomb's law as the ratio between the lateral force and the normal force. Usually, a tribometer is utilized to measure these forces. The idea of the present chapter is to integrate the friction measurement in the tactile device in order first to analyse the friction characteristics even during the tactile stimulation process, and second, to be able to control directly the coefficient of friction which defines the friction contrast for each user. Moreover, the device must keep its small size to be transportable, and it must be robust against external disturbances and the finger user characteristics.

## 4.2 Design of the SmartTac

### 4.2.1 Device particularity

The SmartTac is a developed version of the Stimtac stimulator and the large version of Stimtac developed in the second chapter; it is actuated by piezoelectric ceramics to make a plate vibrating at one of its ultrasonic resonant frequency. Eight piezoceramics (four in each extremity) are glued under the active surface of the aluminium plate; the stimulator is sized 76×41×1.2 $mm^3$ (Figure 4-1a). The "SmartTac" is a smart tactile stimulator because it integrates new sensors allowing a real time measurement of the lateral force between the fingertip and the vibrating plate during the exploration process.

So, the common points between the large Stimtac and the SmartTac are the use of the same principle of operation which is the ultrasonic vibration, the control of the vibration amplitude by regulating the voltage and tracking the resonance frequency. The differences between the two devices are the small size of the new stimulator, because it will be used for the simulation of samples of fabrics, and the use of a mechanical structure under the plate to enable the measurement in real time of the coefficient of friction between the finger and the plate.

This additional mechanical structure is placed under the vibrating tactile plate and can support the sensors. The challenge of this structure is that it must be attached to the active vibrating tactile plate, placed under it, and in the same time, slightly elastic to enable the measurement of the lateral forces using force sensors. In order to measure this force, two strain gauge sensors (S1) and (S2) (FSS1500 from Honeywell) are used, located in this deformable mechanical structure as indicated on Figure 4-1b. S1 and S2 measure respectively the forces in x and y directions. After calibration, the tangential force applied on the plate is obtained. The mechanical structure is composed by a support frame (A), tightened by two screws to the top and the bottom of the tactile plate, and elastically connected to a central part (C) attached by two more screws to a solid aluminium base (D). This elasticity is allowed thanks to six deformable slats (B) between (A) and (C) when the finger is sliding. The normal force applied by the finger is measured from four other strain gauges located at the vibration nodes (S3-S6). The coefficient of friction (COF) can be easily deduced thanks to Coulomb's law on each sampling period. To sum up, the "SmartTac" is the unique device which combines a stimulator based on the friction reduction and a tribometer.

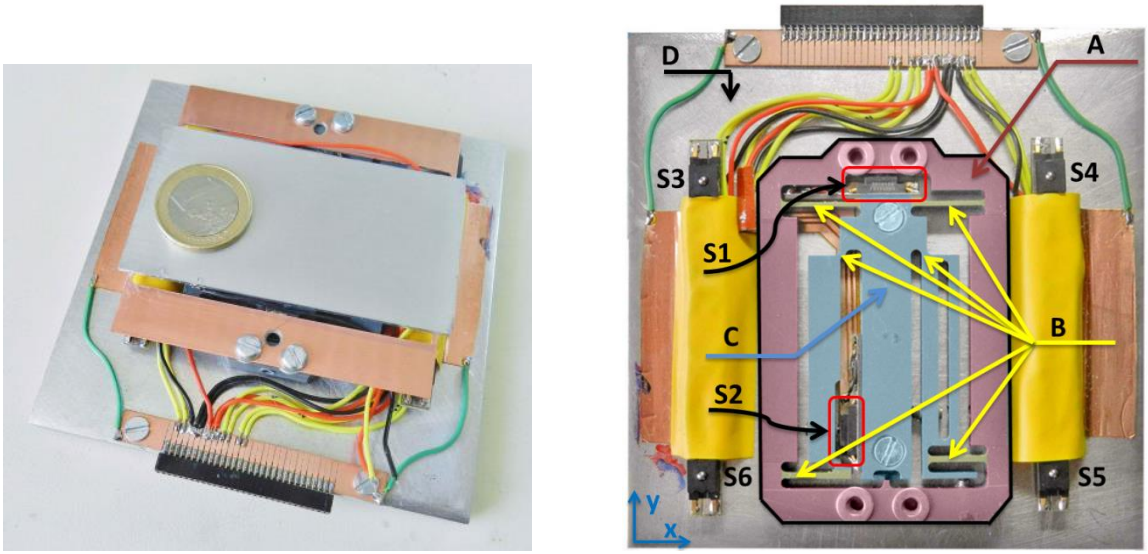


(a) (b)

Figure 4-1: a): Photo of the SMARTTAC, b): Fabricated mechanical structure placed under the active vibrating plate, able to measure, using two force sensors, the lateral force applied by the fingertip when it explores the active surface of "SmartTac"

### 4.2.2 Vibration amplitude control

The vibration amplitude control strategy used for the SmartTac is similar to the one described in chapter 2. The aim of this paragraph is to give the results of the control and to assess both its necessity and its accuracy.

The vibration amplitude is controlled mainly to maintain a stable level of vibration against the external disturbances. As detailed in the second chapter, the system is modelled after providing reasonable approximations with two first order models in a d-q frame. Based on the identification of these transfer functions, two PI controllers have been calculated. The first controller adjusts the voltage in order to obtain a constant vibration amplitude (d axis), while the second controller is able to control the parameter $\Delta\omega$ to guarantee the excitation of the system at the resonance, which maximizes the ratio vibration/voltage (q axis). The controllers are implemented together at 1 kHz frequency real-time. The PI controller's parameters are chosen to ensure both dynamic performances and robustness. As an example here, we have chosen to illustrate the robustness of the control law against the temperature variation: as a mechanical system, the tactile stimulator is sensitive to temperature variations which induce a shift of the resonant frequency. A variation of the resonant frequency is a real problem in use if it is not taken into account. In fact, the active surface is no longer excited at the resonance and the reduction of the friction is not optimized. To check the robustness of our control law, the idea is to supply voltage at an initial frequency which corresponds to the resonant frequency at 30°C (43250 Hz), although the real temperature during this experiment is about 20°C (that means a 0.3% higher resonant frequency). The closed loop should lead to a tracking of the actual resonance (43390 Hz) in a minimum time and as a consequence, the desired vibration amplitude will be obtained with less excitation voltage. Figure 4-2 illustrates the fully controlled system behaviour with the two loops, in amplitude and angular frequency (red curve). The second result (green curve) corresponds to a second experiment for which the system is excited at the resonant frequency 43250 Hz (30°C whereas we work at 20°C), and only the vibration amplitude is controlled. The desired vibration amplitude for the two experiments was 1 µm peak to peak.

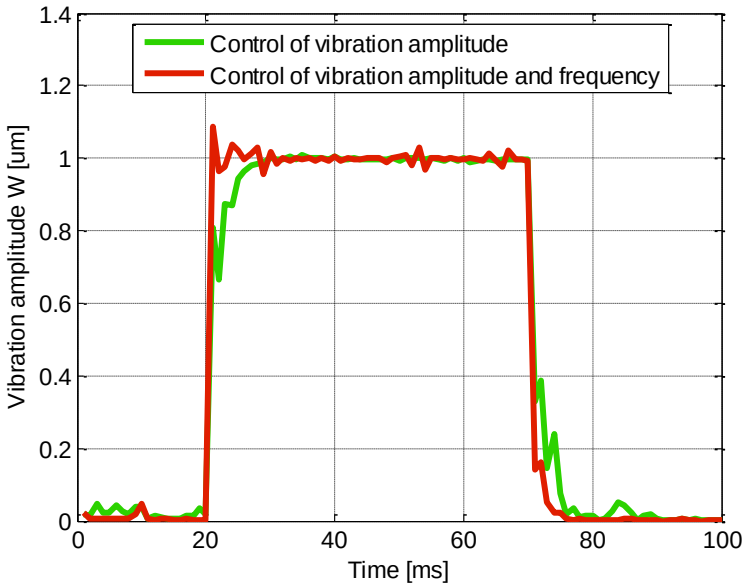


Figure 4-2: Experimental comparison between vibration amplitude response of the controlled system, and the response in the case of the double controlled system against temperature variation and vibration amplitude damping.

In steady state, it can be observed that in both experiments, the vibration amplitude is maintained constant (1 µm). But, in transients, we can observe a difference in the 5% response time of the system (5 ms in the vibration amplitude controlled system against 2 ms for the system controlled in vibration amplitude and frequency). To evaluate the importance of the double control in the energy consumption, Figure 4-3 shows the excitation voltage required to reach 1 µm of vibration amplitude PtP.

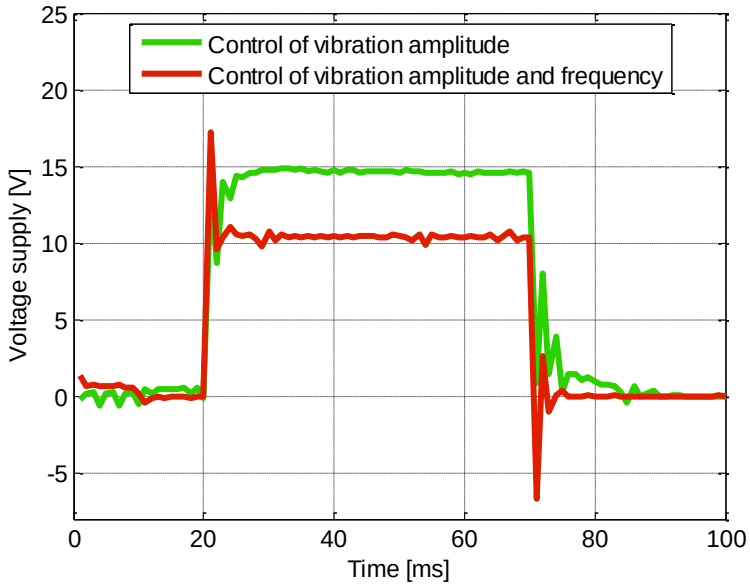


Figure 4-3: Experimental comparison between voltage of the controlled vibration amplitude system, and the response in the case of the double controlled system against temperature variation and vibration amplitude damping.

In this figure, we can verify the voltage supply is higher when the system is not operated at the resonance. The difference between the excitation voltages is about 30%, which indicates the importance of the two controllers when implemented in the tactile stimulator.

## 4.3 Friction control

### 4.3.1 Problematic

A tribological measurement of the coefficient of friction "COF" with 5 subjects (aged from 26 to 28, average of 27) for 5 controlled vibration amplitudes [0; 0.5; 1; 1.5; 2] µm has been performed using the SmartTac. The initial coefficient of friction, measured when the plate is not excited, has been measured for each user, thanks to the measurement of the lateral and of the normal forces. Then, the same operation has been performed for different values of vibration amplitude, leading to the knowledge of $\mu_1$, the reduced friction. It can be observed in Figure 4-4 that the percentage of the ratio between the reduced friction $\mu_1$ and the initial COF $\mu_0$ is highly variable, depending on each person and on the conditions of measurement (the finger moisture for example increases the friction (Pasumarty et al., 2011; Tomlinson et al., 2011b). The initial friction represents the friction between the finger of the user and the surface when the vibration is switched off whereas the reduced friction is the friction when the vibration is switched on at different levels from 0 to 2 µm with steps of 0.5 µm.

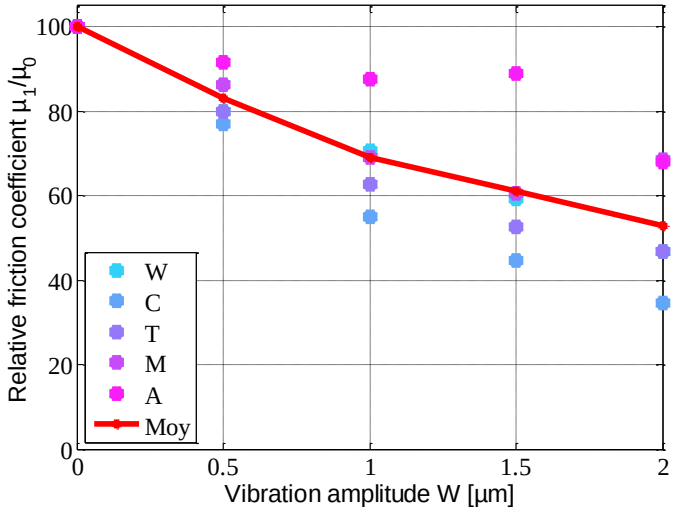


Figure 4-4: The ratio between the reduced friction $\mu_1$ and the initial friction $\mu_0$ in % depending on the vibration amplitude for five subjects plotted by colored points. The mean of measurements of all subjects is plotted by a continuous red curve.

Figure 4-4 highlights the disparity of the friction reduction between users, even for the same vibration amplitude. Yet, our aim is to propose a tactile stimulator able to render accurately texture feelings whatever the touch conditions or the user's finger characteristics. So, we propose a direct control of the COF in order to

standardise the friction reduction which may be provided by the tactile feedback device. Using this smart stimulator called SmartTac, it is possible to measure the lateral and the normal forces leading to a real time measurement of the instantaneous coefficient of friction $\mu = Ft/Fn$ between the finger and the surface of the plate. By knowing the actual friction under the finger, an adjustment of the vibration amplitude can be achieved to impose a desired friction in closed loop.

### 4.3.2 Control method

Because of the non-linearity between the vibration amplitude and the friction, a non-linear function which highly depends on the user as shown in Figure 4-4, it was not possible to implement a standard controller. So, we develop a controller based on data measurements. The sliding mode control is applied due its capability to operate with nonlinear systems (Shtessel et al., 2014). It is placed in a closed loop including the previous vibration amplitude control (see Figure 4-6). The controller acts on the vibration amplitude to control the coefficient of friction between the finger and the plate. The reference of the controller is calculated from the actual $\mu_1$ and the desired $\mu_{1_{ref}}$ coefficients of friction following:

$$E = 100 * \frac{\mu_1 - \mu_{1_{ref}}}{\mu_{1_{ref}}} \tag{4.1}$$

The controller task is to minimise the parameter $E$ to impose the instantaneous reference coefficient of friction $\mu_{1_{ref}}$. The variable delivered by the controller is the parameter $\Delta W$, it represents the value to add to the vibration amplitude $W$ to reach the friction reference. The developed controller operates following three cases; when $E \leq -25\%$, the controller's output is $-1$ µm, if this ratio is up to 25%, the controller output is 1 µm. the last case is when the ratio is between -25% and 25%; in this case, the controller evolves according to the equation $W = 0.04 * E$. The controller output is limited by a saturation set at ±1 µm to avoid a possible peak of vibration under the finger. The constant 0.04 multiplied by the parameter $E$ was chosen is order to find a compromise between the minimisation of the response time and the reduction of the chattering problem when the plate was controlled (Utkin and Lee, 2006). To sum up, the controller output is the following:

$$\Delta W(E) = \begin{cases} 1, & if \quad E \geq 25 \\ 0.04 * E, & if \quad -25 < E < 25 \\ -1, & if \quad E \leq -25 \end{cases} \tag{4.2}$$

The Figure 4-5 illustrates the controller output which is the vibration amplitude $W$ as a function of the friction ratio.

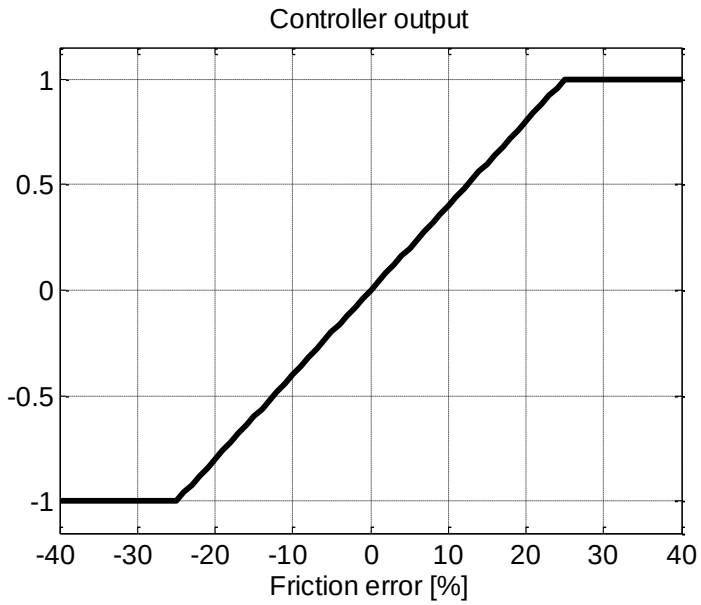


Figure 4-5: Controller output acting on the vibration amplitude depending on the friction error $E$

To sum up, the closed loop control structure is based on two nested loops. The first one consists in controlling the vibration amplitude $W$ using the controller $C_W$ which acts on the voltage applied to actuators and on the frequency. The second one is based on a direct control of the friction between the sliding finger and the plate. The controller $C_\mu$ generates the vibration amplitude $W_{ref}$ to ensure a desired coefficient of friction $\mu_{ref} = \mu$. Figure 4-6 illustrates the operated closed loop control structure.

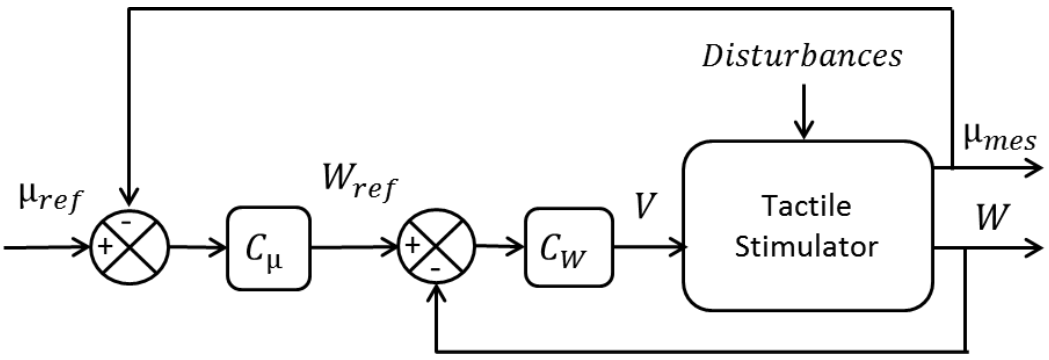


Figure 4-6: The proposed control structure aiming at controlling the friction coefficient $\mu_{ref}$

### 4.3.3 Results of the coefficient of friction control

The control loop acting on the vibration amplitude ensures the accuracy of the tactile stimulator itself on the point of view of physical variables, such as vibration amplitude or energy consumption. However, the user has to be taken into account also on a tribological aspect. In this section, the interest is to validate the friction

control strategy and its capability to impose a reference value of the coefficient of friction (COF) under the finger. The experiment consists in giving two references to the controller depending on the finger position.

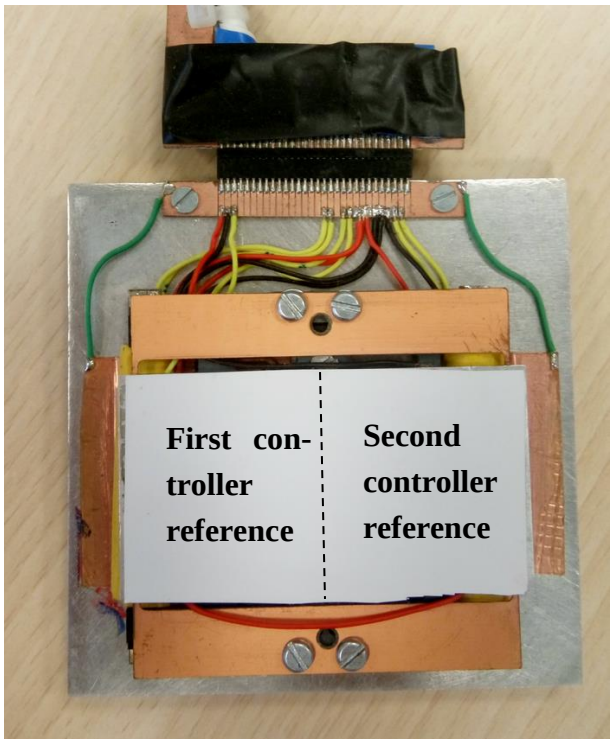


Figure 4-7: An illustration of the two references given to the friction controller depending on the user's finger position, the difference between the two parts in coefficient of friction is 0.1.

The difference between the two references in COF is imposed to be 0.1 in order to validate the controller dynamic behaviour. The references of the controller are given for each half part of the plate as illustrated in Figure 4-7.

Four subjects were participating to this experiment, they were chosen depending on their initial coefficient of friction in order to avoid the controller saturation.

The initial coefficient of friction for the four subjects, i.e. without any vibration, is respectively between: 0.3 and 0.4, 0.4 and 0.5, 0.5 and 0.6; and 0.6 and 0.7. The COF reference given to the controller depending on each subject is receptively: 0.2 to 0.3, 0.3 to 0.4, 0.4 to 0.5 and 0.5 to 0.6. With these values, we are sure to avoid the saturation of the control so the response time will be meaningful. Figure 4-8 illustrates the controlled coefficient of friction between a finger and the plate for each subject. The desired coefficient of friction is between the two values as explained in the foregoing depending on the finger position. For each subject, the experiment is repeated four times which are plotted with the average curve in Figure 4-8. This figure illustrates the experimental results for all the subjects, the x label represents the time in *ms* when the finger is sliding between the two parts of the plate. The

representation of the friction as a function of time is useful to show the time after which the response of friction reaches the desired value.

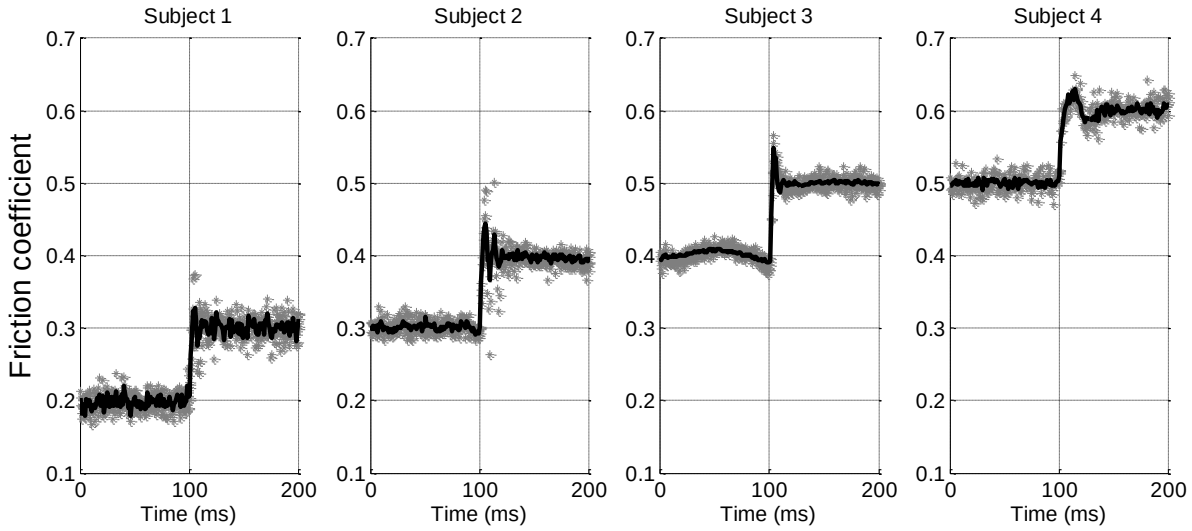


Figure 4-8: Closed loop control of the coefficient of friction as a function of time for the four subjects. The dotted curves illustrate at least four trials of touching the surface and the black continuous curve represents the average of all four measurements for each subject.

When comparing the mean curve of the controlled friction for the 4 subjects, we may conclude that the control strategy is valid in steady state to reach the desired final value of μ. In transient state, there is a small difference when comparing the controlled friction for subjects; Tab. 1 shows a comparison in the dynamic regime of the rise time and the overshoot for each subject. We find that the rise time is equal to $3.84 \pm 1.27\ ms$ and the overshoot of $37.5 \pm 10.2$ %.

Table 4-1: The difference between the rise time and the overshoot between the four subjects.

| | Subject 1 | Subject 2 | Subject 3 | Subject 4 | Mean |
|---|---|---|---|---|---|
| Rise time (ms) | 3.37 | 3.41 | 2.87 | 5.72 | 3.84 |
| Overshoot (%) | 27.6 | 44.4 | 48 | 30 | 37.5 |

Another experiment has been conducted to validate the robustness of the proposed control strategy. The reference of coefficient of friction has been set from 0.3 to 0.2 with steps of 0.05. The Figure 4-9 illustrates the evolution of the controlled coefficient of friction in response to the vibration amplitude $W$ while the finger force $F_n$ and the velocity of the finger were varying. Note that all these variables are sampled at the frequency of the control loop which is 1 kHz.

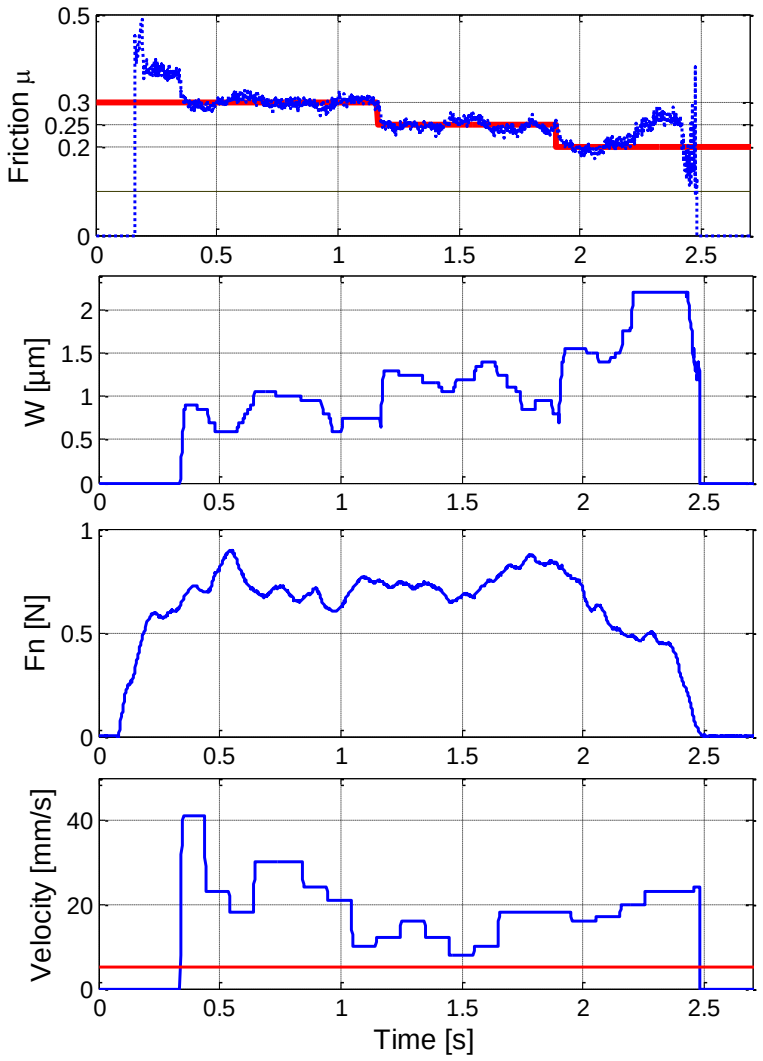


Figure 4-9: Robustness validation when controlling steps of the coefficient of friction control even if the normal force and the velocity are variable.

It may be observed from this experimental result that even if the normal force or the velocity change, which is usual in the natural exploration of the human finger, *W* reacts to maintain the friction at a desired value. We observe also that the controller output which is the vibration amplitude *W* begins to change when the velocity exceeds a given threshold defined at 5 mm/s to avoid the noise in the friction signal. From the instant 2.2 s, it can be shown that the friction was not maintained to 0.2 which is explained by the saturation of *W*.

To sum up, the dynamic and the robustness of the proposed control strategy were validated in the new tactile stimulator by giving different levels of the desired coefficient of frictions. It is interesting to note also that in the dynamic test, different levels were given to each user, the difference between the given references is explained by the difference between the users initial friction. For example, it was not possible to impose 0.3 as friction COF value to a user which had an initial friction about 0.8 because the saturation at 2.1 μm limits the device range of work. In this case, the friction COF will be limited by the maximum reduction that can be imposed

by the device when reaching the saturation. This limitation in $W$ is necessary to avoid the ungluing of the piezoelectric ceramics used as actuator to produce the ultrasonic vibrations.

### 4.3.4 Friction contrast control

As demonstrated in the previous chapter, controlling the friction contrast is more relevant than controlling other friction criterion. As the SmartTac is able to control the coefficient of friction μ, it is also possible to control the friction contrast because a linear relationship links the two parameters as illustrated in (4.3).

$$\mu = \mu_0(1 - FC) \tag{4.3}$$

To perform the control of the friction contrast, we must recalculate, from the $FC$ reference, the associated $\mu_{ref}$. The control strategy to control the friction contrast on the SmartTac is illustrated in Figure 4-10.

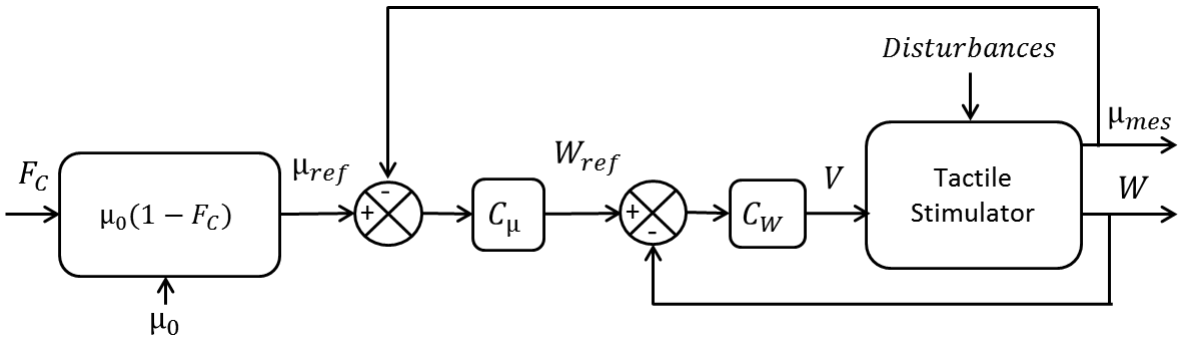


Figure 4-10: The operated control strategy to control the friction contrast between the fingers' users and the tactile plate. The reference $FC$ is a function of the initial coefficient of friction $\mu_0$ which is supposed to be constant.

To check the accuracy of the FC control, experimental trials have been performed following the structure depicted in Figure 4-10 and with one volunteer who is the author of this thesis. The experiment has been repeated over 50 times consecutive and a set of four significant curves have been extracted and presented in the figure where the normal force and the velocity are in the same range. Two references in $FC$ are given to the friction controller, the first one is $FC = 0$ and the second one is $FC = 0.2$. The first reference, $FC$ is zero, means that the reference in coefficient of friction μ is equal to $\mu_0$. The second reference means that the coefficient of friction μ is equal to 80% of the initial coefficient of friction. The difference between the direct control of μ and the control of the friction contrast is the need to determine $\mu_0$ the initial coefficient of friction between the finger's user and the plate without vibration. This parameter must be measured before beginning the tactile stimulation. Then, the $\mu_0$ must be injected in the equation (4.3) to impose the reference which gives the targeted value of $FC$. Each of the two $FC$ references 0 and 0.2 are imposed respectively at the right and the left sides of the plate. The volunteer must slide his

finger on the plate between the two parts, many parameters are recorded such as the $FC$, the output of the controller, $W$ expressed in µm, and the normal force applied. As mentioned previously, the initial coefficient of friction of the contact finger against plate must be measured previously. This parameter was evaluated as $\mu_0 = 0.55$ after at least ten friction tasks done by the volunteer.

The experimental results are illustrated in the Figure 4-11.

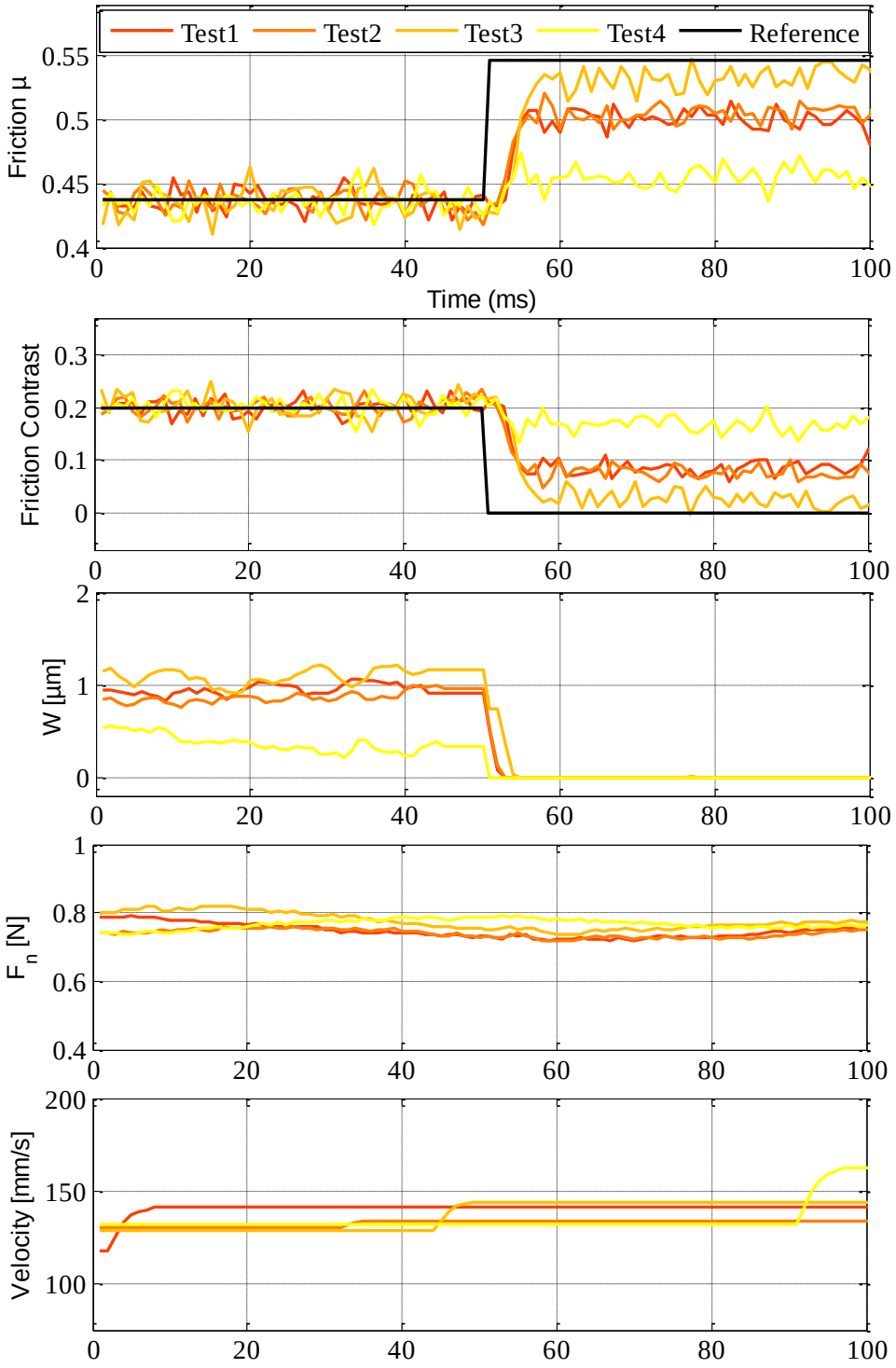


Figure 4-11: Experimental results of the friction contrast control, the curves are plotted as a function of time. The reference of the controller is $FC = 0.2$ when $t < 50\ ms$

and $FC = 0$ when $t > 50\ ms$, it is plotted in continuous black line. The controller output $W$, the normal force and the velocity are plotted respectively in (c), (d) and (e).

Figure 4-11 illustrates respectively the coefficient of friction, the friction contrast, the vibration amplitude response, which is the response of the controller, the normal force applied by the volunteer and the velocity of the finger. The sliding time was about 60 seconds and different cases of the friction contrast $FC$ are plotted in this figure. The four curves selected among all the trials we performed were chosen to be in the same range of the normal force and velocities in order to compare them. The reference of the $FC$ was 0.2 which means 20% of friction reduction as the $\mu_0$ was about 0.55; the right part of the plate was supposed to present $\mu_0 = 0.55$ and the left part was imposed to present $\mu$=0.44. It can be seen that in the left part of the plate, the coefficient of friction is well adjusted to $\mu$=0.44. We can see also that $FC = 0.2$ in the same part of the plate. However, it is not the accurate value of $FC$ because it is still calculated from the predetermined $\mu_0 = 0.55$. But, if we look at the right part of the curve, we can notice that the initial coefficient of friction is changed in spite of the constancy of the normal force and the velocity. If we use the actual value of $\mu_0$, then $FC$ wouldn't be equal to 0.2. The change of the initial coefficient of friction between the three measurements can be explained by the skin hydration or the moisture which increases the friction as discussed in (Gerhardt et al., 2008).

The non-stationarity of the initial coefficient of friction $\mu_0$, even between two near tests, is a real problem for the control of the friction contrast because if we suppose that this parameter is constant, the reference of the controller $W_{ref}$ is mistaken. To cope with this problem, we could use a hydrophobic film to avoid the moisture absorption of the touched film of the plate. The actual film we use is a PVC plastic which is hydrophilic (Marshall, 1990). It was chosen as a compromise between reducing the stick-slip effect of the finger and producing a maximum friction reduction. However, such a change would affect all the results of the previous chapter. The second solution is to reduce the moisture of the users' fingers because it is the most influencing parameter on the friction variation. So, we propose to use the talc powder to reduce this non-stationarity and to have almost a constant evolution of the initial coefficient of friction.

A tribological friction test was performed to compare the coefficient of friction variability with and without using talc powder. The experiment consists in sliding the finger one time from one edge to the opposite of the active surface of the stimulator at rest (without any voltage supply). The user, who is the author, slides his finger on the plate in one direction by trying to maintain its normal force and its velocity constant. Each plotted point represents the average value of the coefficient of friction, sliding velocity and normal force when the finger is sliding on the plate during one trial and it is represented as the average of each cycle. The sliding task is repeated more than

100 times to observe the variation of $\mu_0$ with and without the talc powder. The results of this friction test are illustrated in Figure 4-12.

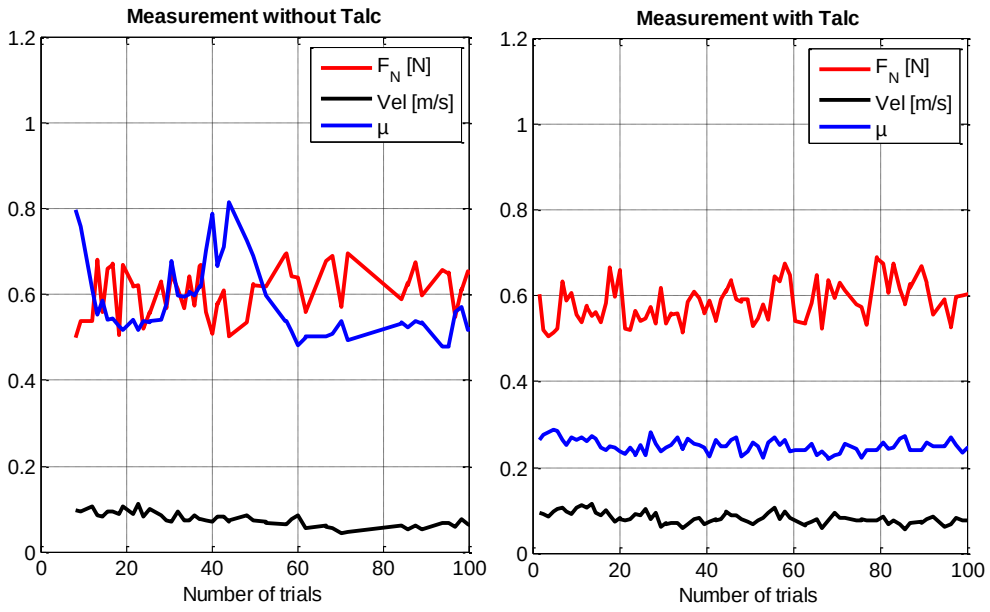


Figure 4-12: Result of the friction test with and without the talc powder on the finger. The normal force $F_N$ and the finger velocity were in the same range for the two tests, $0.5\ N \leq F_N \leq 0.7\ N$ and the velocity was about $Vel$ 80 mm/s. The coefficient of friction μ was variable without the Talc and almost constant even if reduced as expected- when using the talc powder.

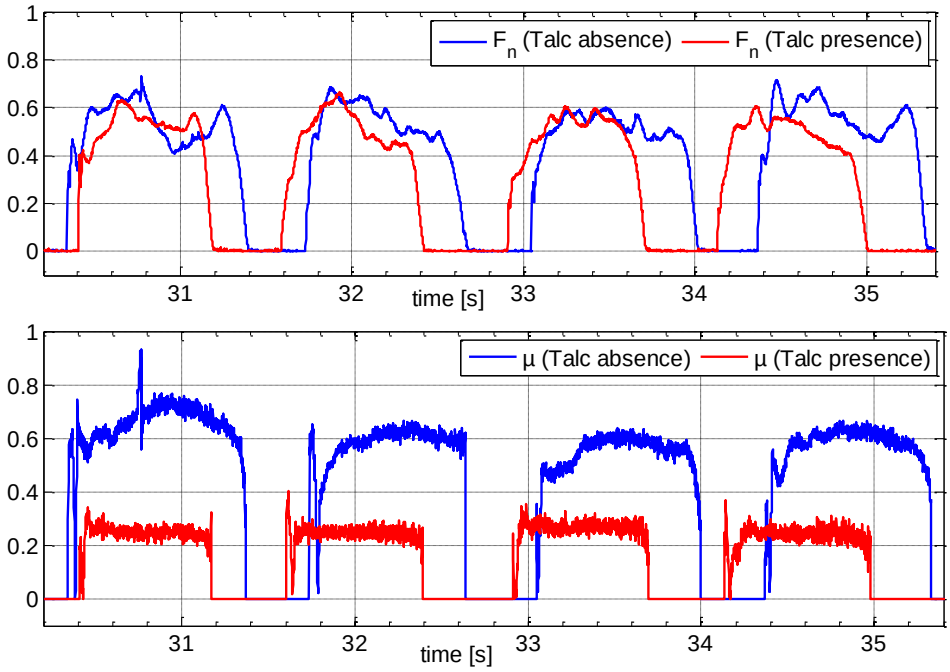


Figure 4-13: Evolution of the coefficient of friction μ with and without talc powder, the normal forces are in the same range. Four cycles of friction are selected to show the difference between the two cases.

The other parameters of the friction test which are the normal force and the velocity were in the same range, $0.5\ N \leq F_N \leq 0.7\ N$ and the velocity was about 80 mm/s. It can be noted that the variability of the coefficient of friction μ was reduced when using the talc powder. In the same time, the average value of μ was also reduced to more than 50% which can probably increase the perception as discussed in the previous chapter. By plotting the normal force and the coefficient of friction as a function of time, in Figure 4-13, it can be noted that when using the talc, the coefficient of friction is almost constant during each cycle and from one cycle to the other, which was not the case without talc. We can see that the presence of the talc can cope with the issue of non-stationarity of $\mu_0$. Netherless, the Figure 4-13 highlight the presence of noise on the μ curve with or without talc. This noise maybe an issue if we want to simulate very fine textures with evolution of μ in the range of this noise.

To go further in the analysis of the direct control of the friction, we can try to quantify this noise. Moreover, we will compare the direct control of the coefficient of friction to a constant reference μ=0.2 with the control of the vibration amplitude to 1 μm. The results of the two control strategies are illustrated in Figure 4-14:

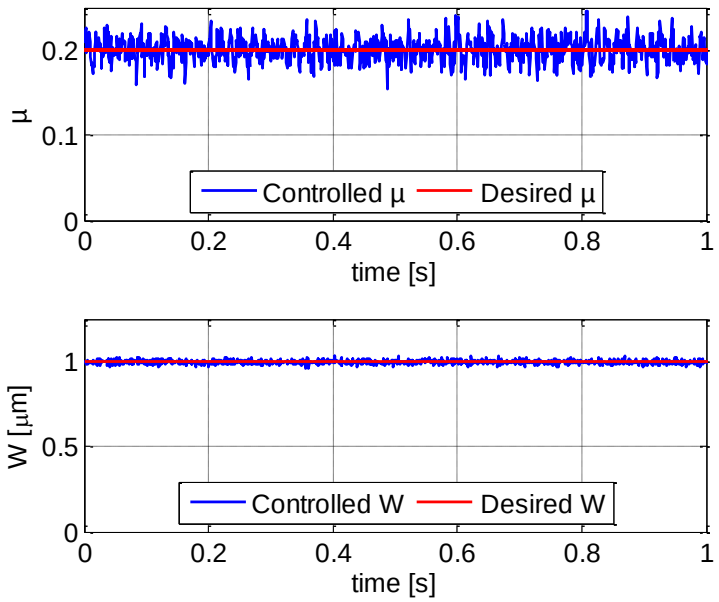


Figure 4-14: The controlled response of μ and $W$ for a constant desired reference.

In this figure, μ and $W$ are controlled to be closer to the desired values, but the noise of the μ control strategy is greater than the noise of the $W$ control strategy. To evaluate the error on the control, the mean absolute deviation of the two vectors defined by the equation (4.4) can be analysed.

$$Mad = \frac{1}{n}\sum_{i=1}^{n}|x_i - \overline{x}| \tag{4.4}$$

With $n$ is the number of considered points, $x_i$ is either the μ or the $W$ values, and $\overline{x}$ is either the mean value of μ or the mean value of $W$.

The result of the mean absolute deviation presented in percent gives $\pm 5.5\%$ for the control of μ and $\pm 0.9\%$ for the control of $W$. It may be noted that the $\pm 5.5\%$ of the noise is in the same order as the coefficient of friction evolution we want to control for the real fine texture simulation that it will be shown in chapter 5. For this reason, the direct method of the COF will need a further improvement to be operated in the simulation of this kind of surfaces. In the following chapter, we will use the control of $W$ to simulate these surfaces.

## 4.4 Conclusion

In this chapter, we proposed a new high fidelity smart tactile stimulator called "SmartTac". The developed control method of controlling the vibration amplitude and tracking the frequency proposed in the chapter 2, was also implemented in the SmartTac device. The capability of this tactile stimulator to control in real time the coefficient of friction was exposed, thanks to a particular sensor implementation in the stimulator. Actually, the SmartTac is tactile feedback plate with an embedded tribometer inside.

Tribological validation of the COF control was proved by repeated experiments with four subjects showing a stable and desired level of friction with a low response time of about 4 ms. After that, a first method to control the friction contrast has been shown and a limitation of using the SmartTac appears, which is the variability of the initial coefficient of friction. A solution to reduce this variability has been proposed based on using talc powder. Nevertheless, even when using talc powder, another issue appears with the direct control of the COF: due to the weakness of the control, a high level of noise arises on the final value of μ. So, a comparison between the two control methods, the control of the vibration amplitude and the control of the friction contrast, has been performed to evaluate the noise induced in the two methods. The results give a very low error for the control in $W$ against a non-negligible error for the control of $FC$ which makes this method not yet accurate when simulating fine textures.

# Chapter 5

# Real surface simulation

# 5 Real surface simulation

In the previous chapters, the design and the improvement of a tactile stimulator device have been performed in order to produce a tactile device able to simulate real surfaces. The SmartTac has proven its capacity of adaptation to the temperature change by tracking the resonance and to the user's finger force influences. Regardless of the finger characteristics, the stimulator is able to control the vibration amplitude $W$ or the coefficient of friction μ. The control method based on the vibration amplitude was selected to simulate textile fabrics. The purpose of this chapter is to evaluate the capability of the SmartTac to simulate the sensation of touching real fabrics.

Some previous works have evaluated techniques and algorithms to render real textures using tactile devices (Bau et al., 2010), (Winter and Perriard, 2013), (Giraud et al., 2010; Winfield et al., 2007). In (Kim et al., 2013), a tactile-rendering algorithm to simulate 3D geometric features on transparent touch screen surfaces is presented. The device is able to modulate the friction between the fingertip and the touch screen surface using the Electrovibration principle. A psychophysical model is established to relate the perceived friction force to the controlled voltage applied to the tactile device. The average friction perception between the users determined by the model is utilized to render the touch sensation of simulated textures. The reference signal to simulate tactile patterns comes from a transformation of the 3D image to grayscale, then to the applied voltage which has a linear relation between the grayscale and the applied voltage. The latter is related to the level of the electrovibration which permits the tactile stimulation.

In (Wiertlewski et al., 2011), an apparatus is made and used to simulate five naturalistic textures made out of PVC plastic. It is based on modulating the lateral force of the finger by deforming laterally the skin. This bidirectional apparatus is able to be operated both as a sensor and or an actuator. When it is used as a sensor, the real textures are placed on the measurement system and the finger position, the normal applied force, and the lateral force measured by the transducer are recorded. Then, the measured signal is filtered and implemented in the device to be operated by the actuator, to render the sensation of real textures.

In (Ilkhani et al., 2014, p. 496–504) an electrostatic tactile display is utilized to simulate three different materials classified depending on their roughness: cardboard, plastic, and wood. The three selected materials in this study have uniform roughness in all directions. An aluminium spherical tip with radius of 5 mm is employed to collect the contact acceleration data when the tooltip is sliding on the surfaces. The contact force is adjusted to 0.35 N and the velocity is about 74 mm/s to standardize the measurement condition for all samples. The data signals extracted

from the real materials are correlated to the voltage level of the electrovibration to produce the tactile stimulation. Several psychophysical experiments are carried out in order to evaluate the quality of the rendered real texture. The confusion matrices used to rate the texture similarity of each virtual texture with the real surfaces gives good results.

A related European project called HapTex (Magnenat-Thalmann et al., 2007) was performed in 2004-2007 to address the drape simulation of textile fabrics. The technique to produce the tactile stimulation is the actuation of a matrix of pins. Due to the limited pin density of about one per $mm^2$, it was not possible to simulate yarn roughness, hairiness and pile of fabrics.

The present study, which strengthens the collaboration between the two laboratories L2EP and LPMT, represents an attempt of texture rendering using an ultrasonic friction control device (the SmartTac) for three types of fabrics, chosen for their specificity: a velvet, a cotton twill and a polyester twill woven fabrics. The velvet is a woven pile fabric and has different tactile feeling depending on the direction of sliding. The cotton and the polyester twill fabrics are evenly distributed fabrics giving the same touch feeling in the two directions but their period of the textures are different; the type of material of these two fabrics is respectively natural and synthetic.

The aim of this chapter is to validate the capability of the device to accurately render fabrics touch feeling and to discriminate fabrics among each other. The chapter will be organized as follows. In the first section the method to render textures is described. The second section introduces the feature extraction of the fabrics friction characteristics. After that, psychophysical experiment results will be performed and analysed to compare the fabrics rendering methods. Finally, a conclusion summarizes and evaluates the main results.

## 5.1 Texture rendering method

As we are focusing on friction modulation devices, the simulation of fabrics will rely on the friction feature extraction we may perform from real fabrics. Then, the aim of the tactile device will be to make the device able to reproduce this characteristic and try to give the illusion of touching real fabrics. The principle of texture rendering is illustrated on the Figure 5-1.

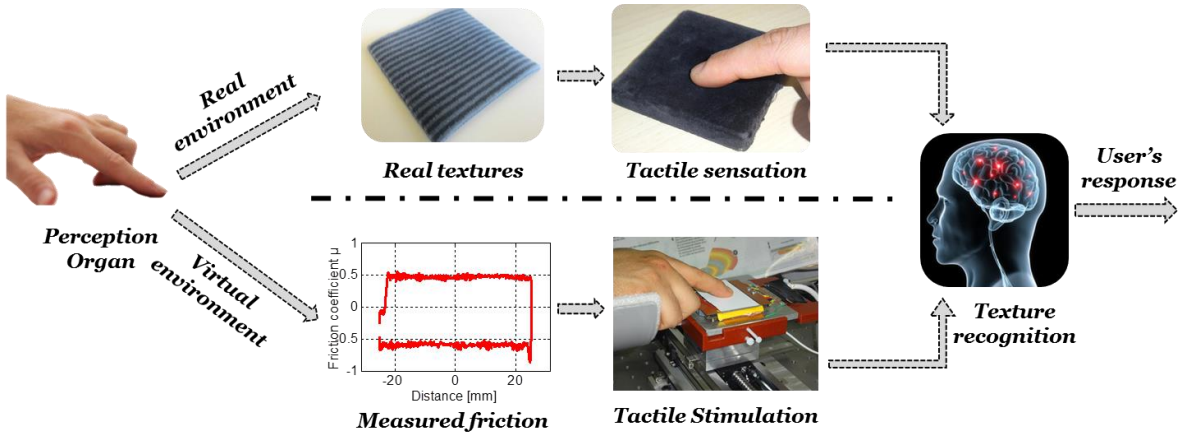


Figure 5-1: Texture rendering principle based on the reproduction of the friction characteristics of the fabrics. The measured signal is injected to the tactile device to produce the simulated tactile virtual surface.

The friction characteristics of the real fabrics surfaces should be defined to be measured and reproduced by the tactile device. As discussed in chapter 3, the friction contrast is the most influencing parameter on the human finger perception. For this reason, this variable will be used to characterize both the real and the simulated textures. The friction contrast is defined by the equation (5.1). It is a function of x which characterizes the finger position on the surface, with the assumption of uniformity in the y direction.

$$FC(x) = 1 - \frac{\mu(x)}{\mu_{max}} \tag{5.1}$$

The particularity of $FC$ comparing to the coefficient of friction μ, is that $FC$ is normalized which makes it significant, less sensitive to the own user's μ. It may be noted that it is not possible to recreate the measured COF because this parameter is not only a characteristic of the surface, but it depends on the whole tribological system and on the interaction between the user and the surface.

### 5.1.1 Friction contrast definitions

Consequently, the chosen controlled parameter is the friction contrast $FC$, that must characterise the texture surface, to be then reproduced by the SmartTac. In this study a set of three different fabrics is used and the aim is to simulate each fabric.

For this purpose, we define two different $FC$. The first one is called $FC_{F-F}$ which characterises the friction between the real fabrics and the finger or the artificial finger, that is a specific slider to imitate the finger mechanics. A discussion about the characteristics of the slider will be performed in the section 5.2.2. The second $FC$ noted $FC_{S-F}$ is the controlled parameter to be implemented in the tactile device and designates the reproduced friction contrast between the SmartTac and the user's finger. $FC_{F-F}$ is defined by:

$$FC_{F-F}(x) = 1 - \frac{\mu_{fabric}(x)}{\mu_{max(fabrics)}} \quad (5.2)$$

The $\mu_{fabric}$ is the coefficient of friction between the slider or the real finger and each real fabrics, $\mu_{max(fabrics)}$ is defined as the maximum value of the coefficient of friction between the slider or the real finger and the whole set of three fabrics, as shown in Figure 5-2. $FC_{S-F}$ is defined by the following equation:

$$FC_{S-F}(x) = 1 - \frac{\mu_{smarttac}(x)}{\mu_{\max(smarttac)}} \quad (5.3)$$

The parameter $\mu_{smarttac}(x)$ is defined as the desired coefficient of friction between the finger of the user and the SmartTac, $\mu_{\max(smarttac)}$ represents the initial coefficient of friction when the plate is not excited by ultrasonic vibration. This parameter may also be called as $\mu_0$ and it depends on the user's finger characteristics.

### 5.1.2 Fabrics-Finger friction contrast

The fabrics-finger friction contrast characterises the friction between the fabrics and the finger or the artificial finger. As defined in equation (5.2), to determine $FC_{F-F}$, two friction parameters must be determined; $\mu_{fabric}$ and $\mu_{\max(fabrics)}$. We define the parameter $\mu_{fabric}$ as the coefficient of friction between the finger or the artificial finger and the fabrics. This parameter depends on the slider position and can be plotted as a function of the displacement x. $\mu_{\max(fabrics)}$ represents the maximum coefficient of friction of all fabrics. Indeed, our aim is to simulate the three fabrics in order to evaluate the capability of discrimination of the tactile device, so the scale of coefficient of friction must be defined once for the three fabrics. $\mu_{\max(fabrics)}$ does not depend on the slider position. As $\mu_{fabrics}$ is always less or equal than $\mu_{\max(fabrics)}$, then $0 \leq FC_{F-F} \leq 1$. Figure 5-2 shows an example of the coefficient of friction profile ($\mu_{fabric}$) as a function of the finger position for the three different fabrics velvet fabric (VEL), cotton twill (SCOT) and polyester twill (SPET) woven fabrics. The positive and negative values of μ indicate both directions. The sliding distance is 40 mm and the velocity is constant (20 mm/s) thanks to the linear stage which moves the hand of the user as shown in the Chapter 3.

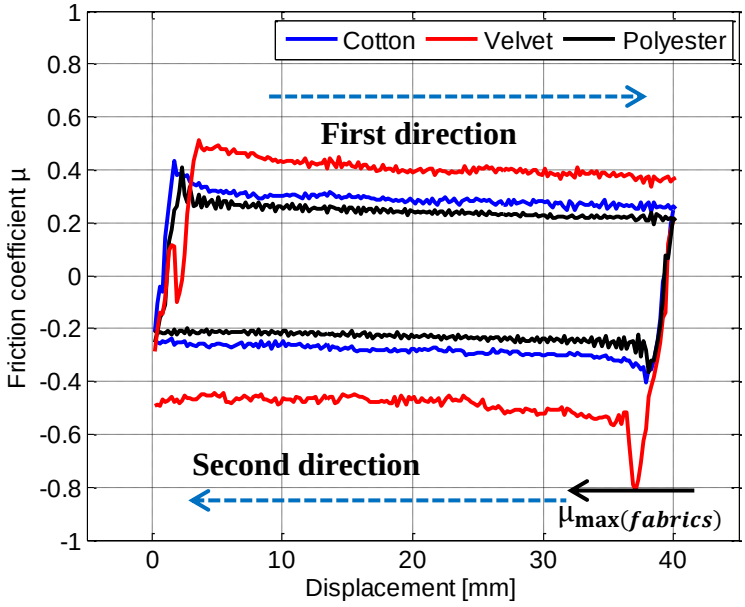


Figure 5-2: Example of the coefficient of friction profile $\mu_{fabrics}$ when the user' finger is sliding against the three different fabrics.

In this figure, the maximum coefficient of friction $\mu_{\max(fabrics)}$ is defined as the maximum value of the three fabrics and is about 0.81. The finger is sliding in the two directions of fabrics. The $FC_{F-F}$ can be extracted from this curve following its definition in (5.2), the Figure 5-10 illustrates the curve of the friction contrast extracted from the coefficient of friction profile.

### 5.1.3 SmartTac-Finger friction contrast

The $FC_{S-F}$ represents the reproduced friction contrast between the user's finger and the SmartTac and must correspond to the $FC_{F-F}$. In order to simulate accurately the texture, the first idea is to impose $FC_{S-F} = FC_{F-F}$. However, $FC_{S-F}$ must be adjusted to take into account the maximum friction reduction which may be provided by the device. The friction contrast induced by the SmartTac is limited to 1 which corresponds to $\mu_{smarttac} = 0$. However, this cannot be practically possible using the stimulator because the finger cannot reach a zero of friction value. In order to determine the capacity of the stimulator to reduce the friction, an experimental protocol was setup. Six volunteers (aged between 23-27 years) have participated in this experiment. They were asked to explore the surface of the tactile feedback plate by maintaining a normal force approximately around 0.5 N and an exploration velocity of about 20 mm/s. The right half of the plate was excited in order to perform a vibration amplitude varying from 0.5 to 2 µm by steps of 0.5 µm, whereas the left part was not excited. By plotting the measured $FC_{S-F}$ as a function of the vibration amplitude (VA), we found, as expected, an increase of $FC_{S-F}$ when VA increases. We can conclude that the developed device can reduce the friction to approximately 60% ($FC_{S-F} = 0.6$) when exciting it at 2 µm corresponding to the maximum vibration amplitude we can perform with SmartTac.

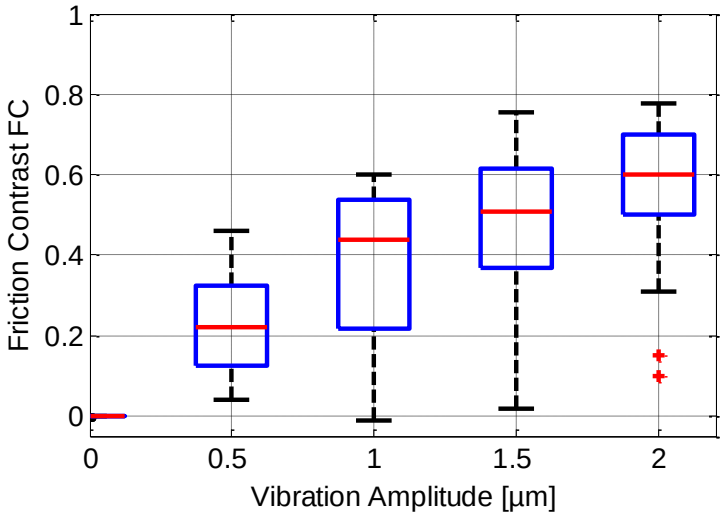


Figure 5-3: Friction contrast $FC_{S-F}$ as a function of the VA from 0 to 2 µm. The boxplot illustrates the difference between the six individuals participating in this tribological experiment (Ben Messaoud et al., 2015a).

In the Figure 5-3, we may note that there is an important variability of the friction reduction between users. To take this diversity into consideration, the relation between $FC_{S-F}$ and $FC_{F-F}$ must be found by determining the maximum possible level of $FC_{S-F}$ for each user. The maximum level of $FC_{S-F}$ must be correlated to the maximum value of $FC_{F-F}$ as illustrated in Figure 5-4. The slope of the curve determines the ratio between the two $FCs$. This relation between $FC_{S-F}$ and $FC_{F-F}$ depends on the user's finger.

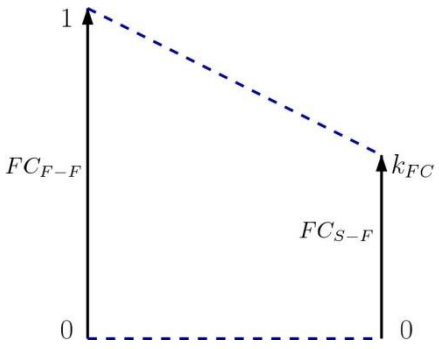


Figure 5-4: The ratio between $FC_{S-F}$ and $FC_{F-F}$ is the parameter $k_{FC}$ which must be determined for each user.

### 5.1.4 Texture rendering strategy

After identifying the criterion to be extracted from the surfaces, we want to simulate and input the variable to be applied to the stimulator. This section will be focused on the texture rendering strategies that can be employed to simulate real fabrics. In other words, our aim is to perform the best control structure able to reproduce the right $FC_{F-F}$. The strategies can be based on the direct method of texture reproduction or on an alternative method.

- The direct method is based on the relation between the two defined $FC$, and it takes the diversity of users into consideration using all the capacities of the SmartTac.
- The alternative method based on the control of the vibration amplitude, can be also operated. Yet, this method does not take the difference between individuals into consideration, but its response time is lower than the friction control method.

The direct method has two levels of control. The first level is the adaptation of the device to the finger normal force influence and to the resonance shift by maintaining $W$constant: this is the inner VA loop. The second level is the adaptation of the tactile stimulator to the user's finger characteristics when operating the closed loop control of the coefficient of friction. As the SmartTac can modify the coefficient of friction, it was required to add two blocs between the desired friction contrast ($FC_{F-F}$) and the desired coefficient of friction $\mu_{ref}$. The first bloc contains the adaptation constant ($k_{FC}$) to determine the $FC_{S-F}$, while the second bloc is operated to relate $FC_{S-F}$ to the control parameter of the SmartTac which is the $\mu_{ref}$. These two parameters are linked by the relation $\mu_{max}(1 - FC_{S-F})$ which depends on $\mu_{max}$ between the surface of the stimulator at rest and the user's finger, which needs a measurement of the initial coefficient of friction before doing the tactile stimulation. This maybe a weakness point for this approach, accounting for the results of chapter 4 where we highlight the non-stationarity of the COF. Figure 5-5 illustrates the bloc diagram of control.

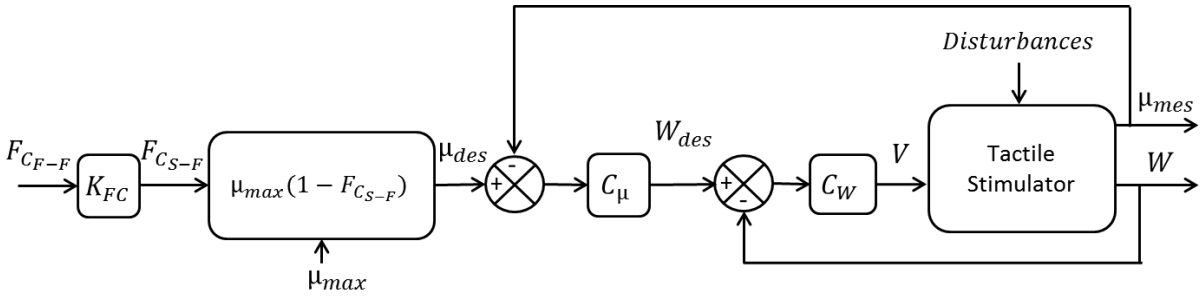


Figure 5-5: Bloc diagram of the control of the friction contrast $FC_{S-F}$ using the tactile device.

The alternative method is introduced to cope with the non-stationarity issue explained in chapter 3. Actually, this method will not use all the capacity of the SmartTac as it will not take into consideration the diversity of users. This method is based primarily on the direct control of the vibration amplitude $W$ using the internal loop which adjusts the voltage $V$ to impose $W$. The advantage of this strategy is that its response time to impose $W$ is small and almost constant comparing to the previous method (2 ms against to 4 ms). The bloc diagram of the $W$ control method is given in Figure 5-6.

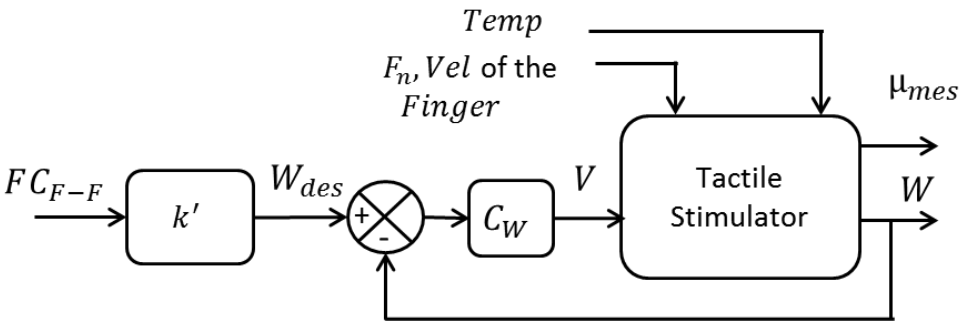


Figure 5-6: Bloc diagram of the vibration amplitude strategy to simulate fabrics.

In this control strategy, because it does not consider the finger friction behaviour, the signal measured from the fabrics to be simulated is directly related to the desired vibration amplitude which is the controller setpoint. Hence, a constant can be determined depending on the capacity of the stimulator to generate $W$. As the maximum amplitude that can be produced by the SmartTac is 2 μm and the other part, $FC_{F-F_{max}}$ cannot exceed 1, the constant $k'$ will be determined to be equal to 2.

$$W_{ref} = k' FC_{F-F} \tag{5.4}$$

### 5.1.5 Sum up of the control strategies

A comparison between the two strategies of control is illustrated in the Table 5-1:

Table 5-1: A comparison between the two control methods

| Control of μ | Control of W |
|---|---|
| + Acts on physical characteristics which is the friction directly.<br>+ Uses all the capacity of SmartTac in measurement and adaptation: normal force, temperature and finger friction force | – Acts on a variable that can give different sensations depending on the user.<br>– Adaptation only on the user's normal force and the temperature change. |
| – The response time is variable depending on the user between 3 and 5 ms.<br>– The initial COF can change during the experiment which makes false the setpoint of the controller.<br>– The control of μ suffers from noise | + The response time is almost constant and about 2 ms for all users.<br>+ The signal reference in $W$ is always constant and cannot be affected by any parameter.<br>+ The control of W suffers from less noise than the control of μ |

As discussed in the chapter 4, the problems on the direct friction control method, which are the non-stationarity of the initial coefficient of friction relative to time and the noise in this method, makes it non useful when simulating the real fine fabrics.

For these reasons, the second method of control focusing on the control of $W$ will be operated in the following to simulate the real fabrics. A further improvement of the direct method could probably make it operated in order to use all the capacity of the new tactile stimulator SmartTac.

## 5.2 Fabrics measurement

### 5.2.1 Characteristics of the fabrics

In order to evaluate the capabilities of the developed stimulator SmartTac, three different fabrics are chosen which are: velvet fabric, cotton and polyester twill woven fabrics. These fabrics have different characteristics which affect the user's touch perception. The velvet is a woven pile fabric in which the cut threads are evenly distributed. It provides different sensations depending on the finger movement direction, along or against its pile main direction. The two others fabrics have a periodical texture similar to grooves and give a similar sensation in the two directions of movement. The polyester twill woven fabric is smoother than the cotton twill woven fabric because the spatial period of grooves is smaller. Another difference between these two fabrics is that cotton has a standard hairiness contrary to the polyester which has no hairiness. A sample of the three fabrics is illustrated in Figure 5-7.

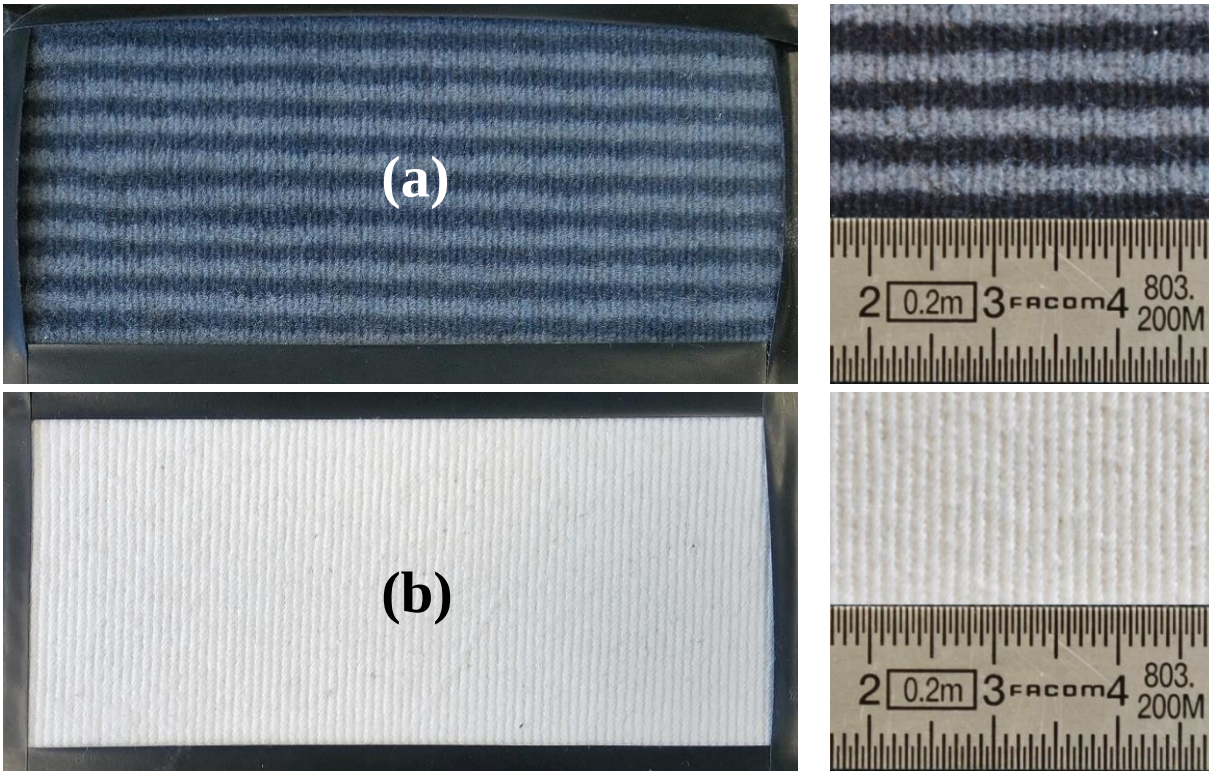

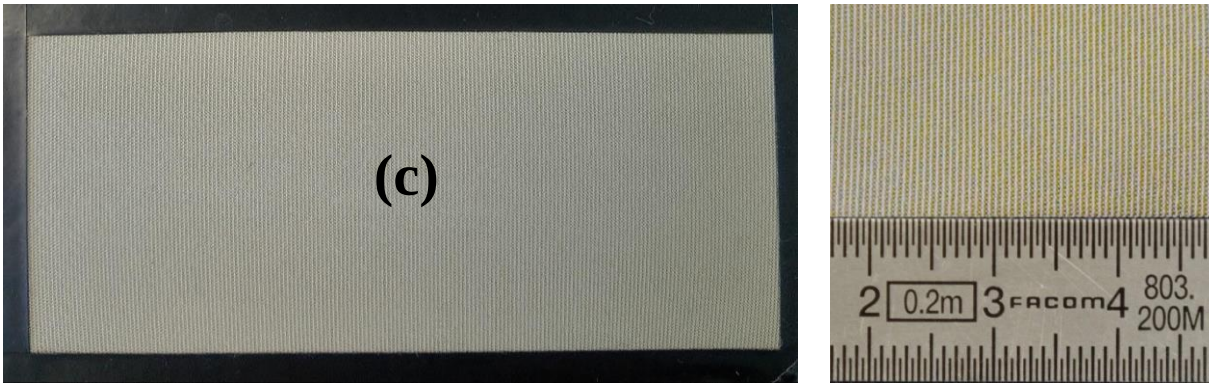


Figure 5-7: A sample of the three chosen fabrics for tactile simulation, a) velvet fabric, b) cotton twill and c) polyester twill woven fabrics with a zoom of each fabric on the right.

### 5.2.2 Friction measurement

To determine the variable $FC_{F-F}$, the friction between the fabrics and a human finger or a specific slider must be measured. In both cases, this signal must contain all the information related to the perception of the selected fabrics. At a first glance, the use of a human finger interaction measurement may be seen more significant to extract accurate features from the fabrics. However, it will be necessary to take into account the variability introduced by the different users. On the other hand, the use of a specific slider (or artificial finger) requires a wide study on the design of this slider, in order to fulfil the physical characteristics of a real finger interaction. The following paragraph shows the first step of fabrics characterization using both approaches.

#### 5.2.2.1 Fabrics characterization with a real and an artificial finger

Because the chosen strategy of command for SmartTac is the control of W, for each simulated fabric, the signal will be unique and will not be changed depending on the user's finger or the slider. Using the tactile tribometer detailed in the chapter 3, the coefficient of friction $\mu_{fabric}(x)$ between the users' finger and each of the three fabrics can be measured. It is compared with the friction signal obtained from an artificial finger under the same fabric. The artificial finger is composed by a silicone material covered by a textured film to imitate respectively the softness and the fingerprints of the real finger. The apparent contact area of the slider is about 1.5 cm², which is equivalent to the real finger surface when the pressure is 3 kPa (about 0.5N) (Breugnot, 2005). A comparison between different artificial fingers with different materials and a real finger in a tribological point of view has been investigated by (Camillieri and Buneo, 2015). This paper concludes that the artificial finger made of silicone and covered by the textured film is the nearest to the human finger when comparing to different slider materials, shape and texture. This frictional

behaviour of the slider must be compared to real (human) fingers when doing a friction test against textile fabrics.

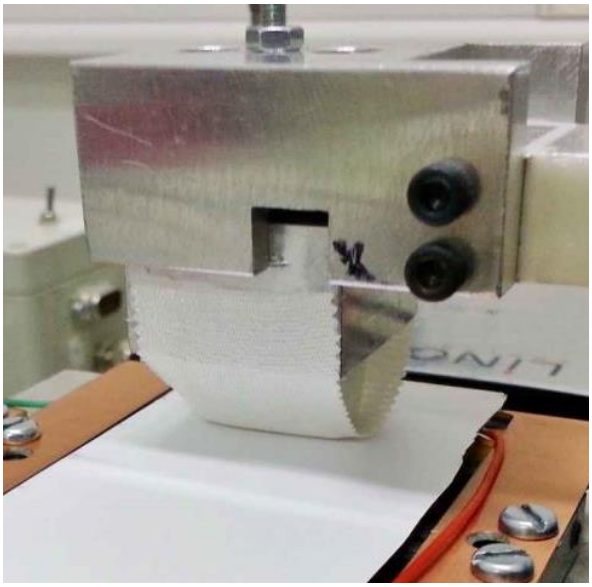

Figure 5-8: Photo of the artificial finger which imitates the finger friction characteristics when it is in contact with the surface of the tactile display.

The velocity is adjusted at 20 mm/s for the real and artificial fingers and the sliding distance is 40 mm for the real finger, 50 mm for the artificial finger. The normal applied force is about 0.5N for both fingers. Figure 5-9 illustrates the coefficient of friction measurement as a function of the displacement for four subjects' fingers and for the artificial finger, for the three investigated fabrics. When the coefficient of friction μ is positive, it represents the sliding in the direction from left to right and when μ is negative, the sliding direction is in the opposite direction (from right to left).

Subject 1: Female, 42 years

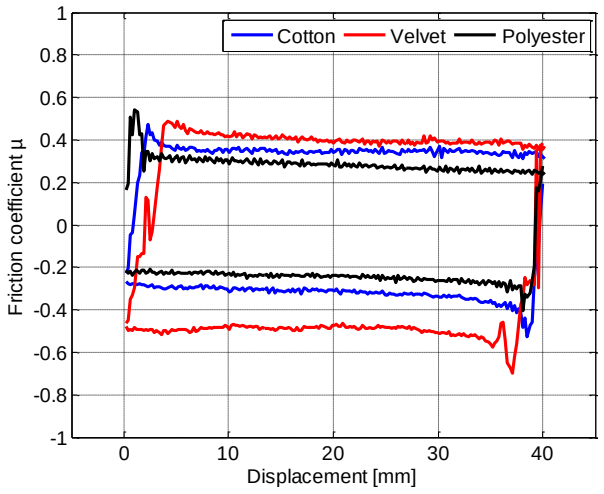


Subject 2: Female, 26 years

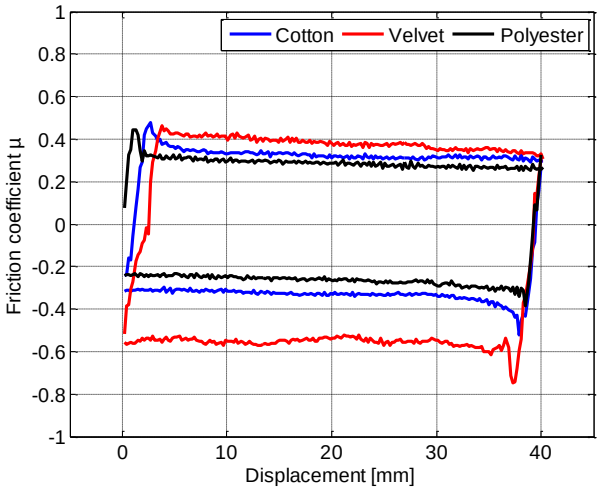

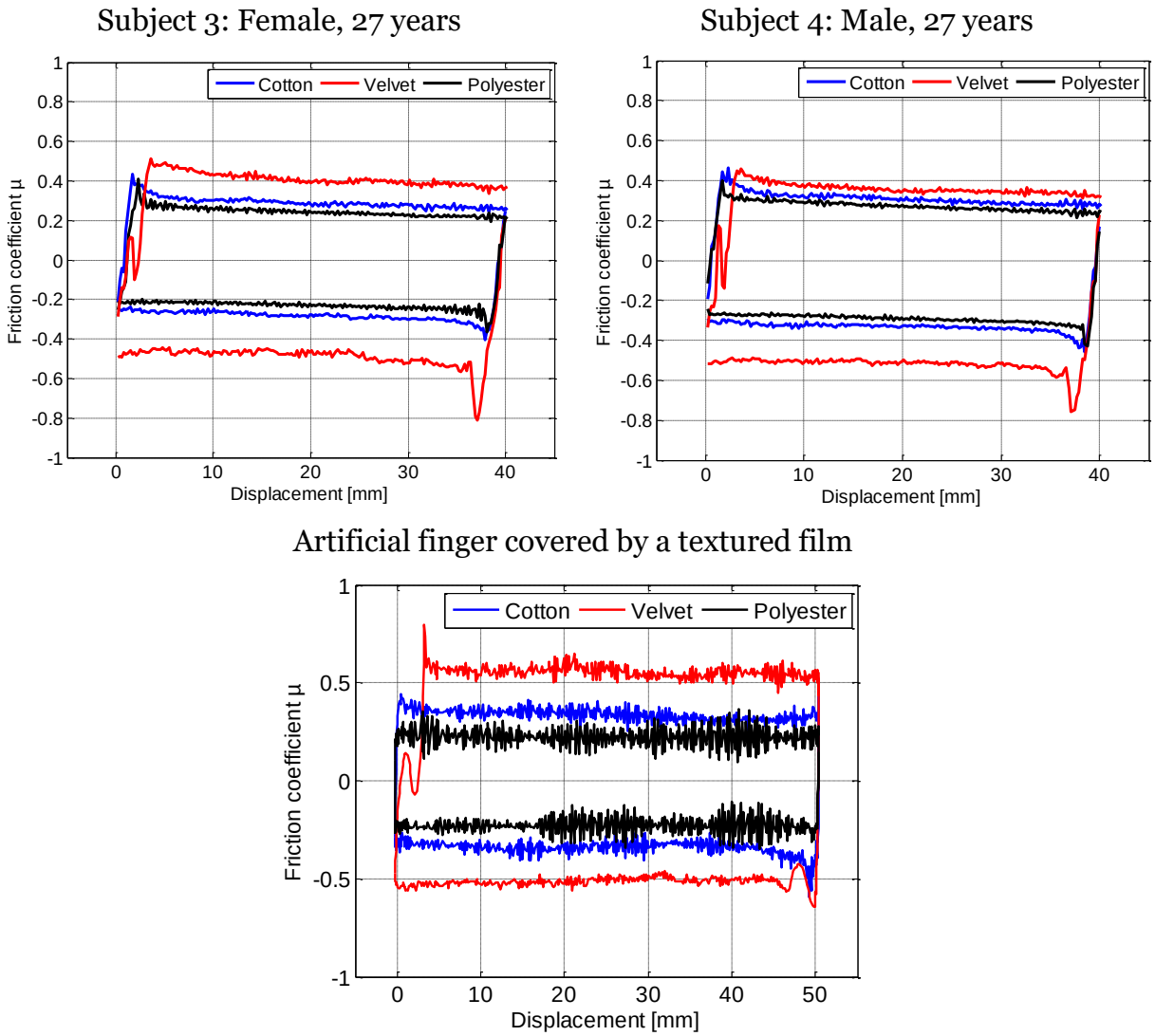


Figure 5-9: Coefficient of friction measurement profile as a function of the slider displacement for four subjects and the artificial finger.

It may be observed that the shape of the friction curve is almost similar for the subjects and the artificial finger. The evolution of this curve can be decomposed in different parts containing a constant and a transition zones between the two directions of motion. It can be shown also that the constant coefficient of friction (COF) between the three fabrics is different. Actually, from higher towards lower COF, we find that the velvet fabric against pile direction (from right to left), then we find the opposite direction of the velvet, along pile (from left to right), after that comes the measurement of the cotton twill woven fabric and finally the polyester twill fabric woven fabric. We may notice also that there is no difference when sliding in the two directions for the cotton and the polyester twill woven fabrics which is in correlation with tactile perception. Nevertheless, a difference may be noticed between the results given by the real and the artificial finger: the artificial finger gives a higher COF for the velvet along pile, a higher maximum value and presents more noisy curves. Another difference is also observed which is the transition time between the two directions, this time is briefer for the artificial finger comparing to the real finger. In fact, the joint stiffness of the artificial finger can be considered as infinite in

contrary with a real finger, therefore the lateral displacement of the oscillating table is equal to the artificial finger displacement but not to the real finger displacement. As discussed in the beginning of the chapter, the parameter $FC_{F-F}$ characterizes the fabric. As expressed in the equation (5.2), the extraction of $FC_{F-F}$ from the coefficient of friction is done by subtracting the absolute value of the ratio between the coefficient of friction and the maximum coefficient of friction from 1(Equation (5.2)). The following figure illustrates the $FC_{F-F}$ for the subjects and the artificial finger in the two directions for the three fabrics. The curves are plotted separately for each slider, the first and the second directions correspond respectively to the along and against pile direction for the velvet fabric, the same friction contrast behaviour is observed between the two directions for the cotton and the polyester twill woven fabrics.

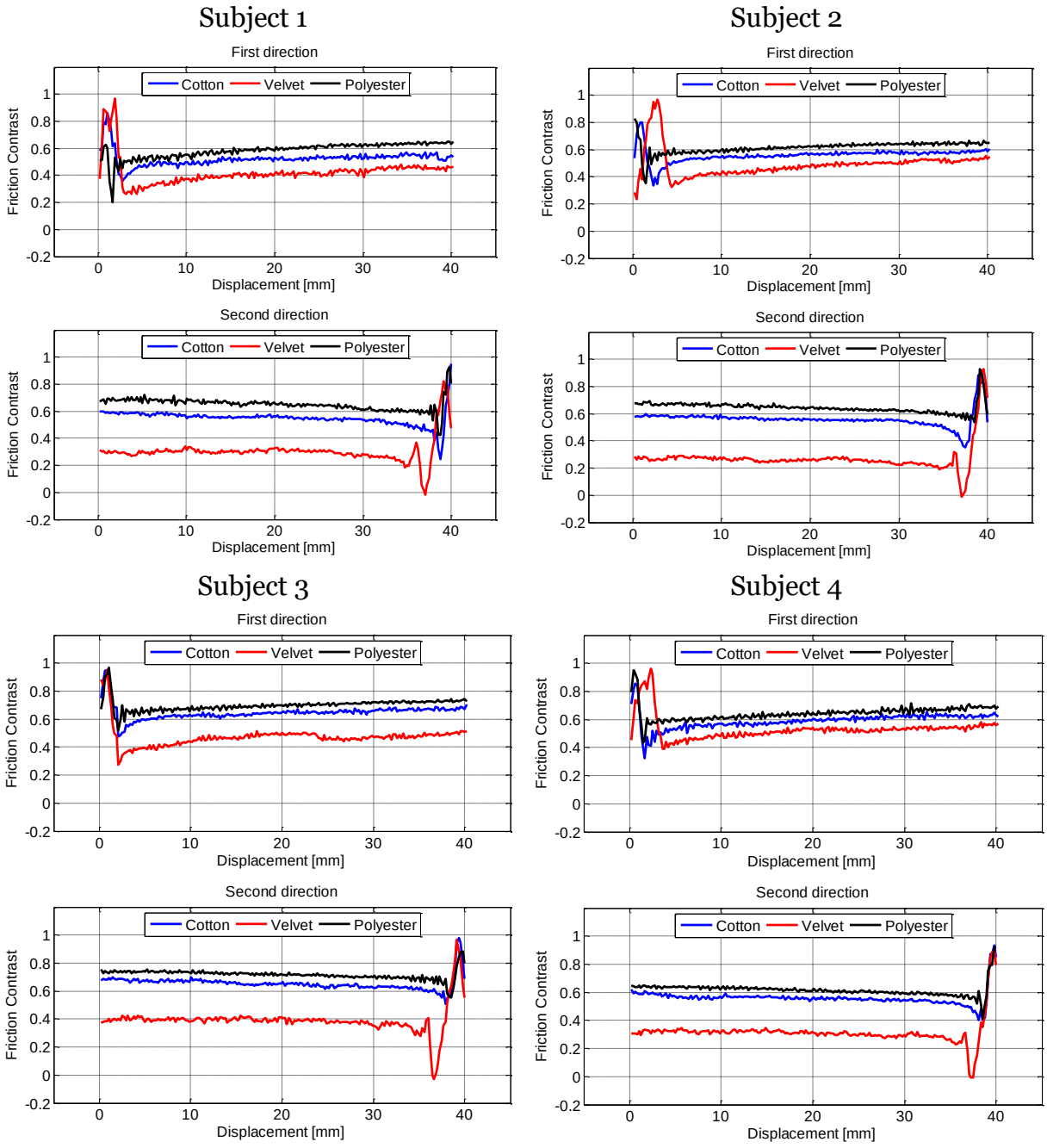

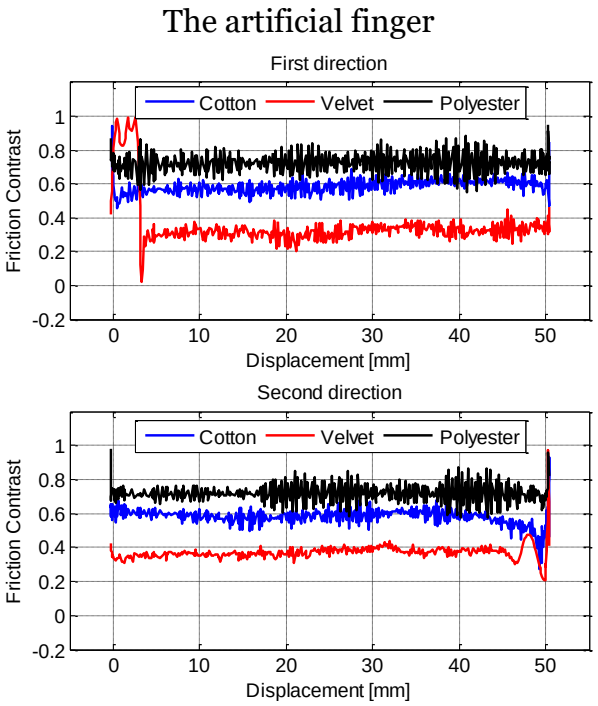


Figure 5-10: Friction contrast $FC_{F-F}$ a function of the displacement for the four subjects and the artificial finger. The two directions of displacement are plotted separately for each slider.

The shape of the $FC_{F-F}$ curve for the four subjects is almost the same. As for the curves obtained from the artificial finger, they still present a high level of noise and some differences compared to the ones from real fingers. The study with such an artificial finger should deserve to be gone deeper: the interest of using a probe is to avoid the long tests with users and to fulfil repeatability conditions. However, at this level, a deeper investigation should be performed on the quality of the artificial finger.

As a consequence, we chose to go on the study considering the real fingers' measurements. To cope with the dispersion of the results, we decided to take the average of the friction contrast signal measured for the four subjects.

In the case of velvet fabric, the curve is composed by a short time transition in the beginning of each direction (along and against pile), and then a constant evolution with a lower friction contrast in the along pile direction which is due to the smooth sensation perceived in this direction (Bueno et al., 2014). Regarding the polyester and the cotton twill woven fabrics, the evolution of the friction contrast can be estimated to a constant line which is the average value between the subjects. The average is calculated in the two directions because there is no difference between them. So, we found $FC_{F-F} = 0.65$ for the polyester twill and $FC_{F-F} = 0.58$ for the cotton twill woven fabric. The shape of the curves measured for the subjects is similar to the Figure 5-11.

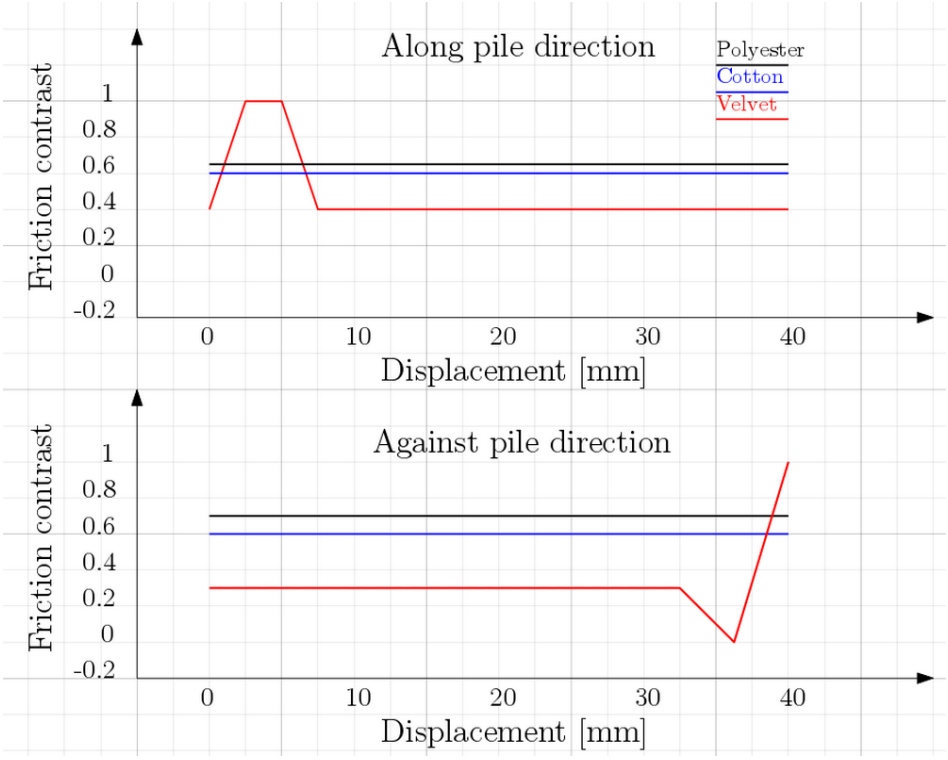


Figure 5-11: The repeatable evolution of the shape of the friction contrast behaviour.

The characteristics of Figure 5-11 may be considered as a robust basis for global texture simulation. However, these curves cannot accurately characterize the thin textures of the surfaces. The impossibility to measure the fine texture of the surfaces by sliding the users' fingers on the textile fabrics is probably due to the measurement system. A frequency domain analysis has been done on the $FC_{F-F}$ from the Figure 5-10 to identify the fine textures from the fabrics signals, this study concludes that the small deviation of the friction contrast curves present in the figure does not characterize the textures of the surfaces but it is just a noise. For that reason, we will have to consider an improvement of the measurement tool to extract the information involved in the fine details of the texture.

#### 5.2.2.2 Fabrics characterization with a special probe

To be able to extract the fine texture signal from the surfaces, we operate a sharp prismatic aluminium slider which has an apparent contact surface of 17x1 mm² (Figure 5-12) and do friction test against the three chosen textile fabrics.

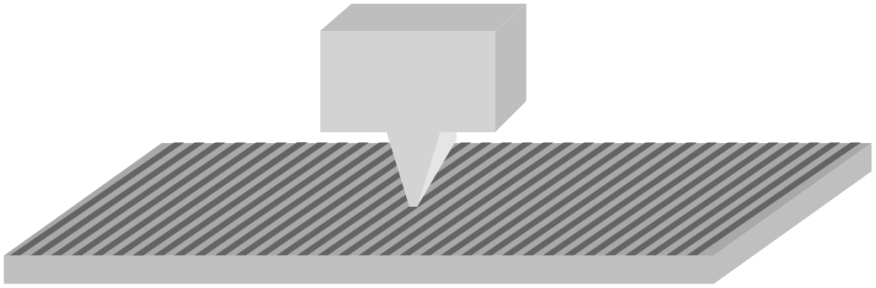

Figure 5-12: An illustration of the sharp prismatic aluminium slider operated in the friction measurement on a textured surface.

The velocity is adjusted at 20 mm/s and the normal force is adjusted at 0.2 N. The frequency spectrum of the measured coefficient of friction (COF) is plotted in the Figure 5-13. The steady state region was cropped out by truncating the initial transitory period of the recordings of each texture.

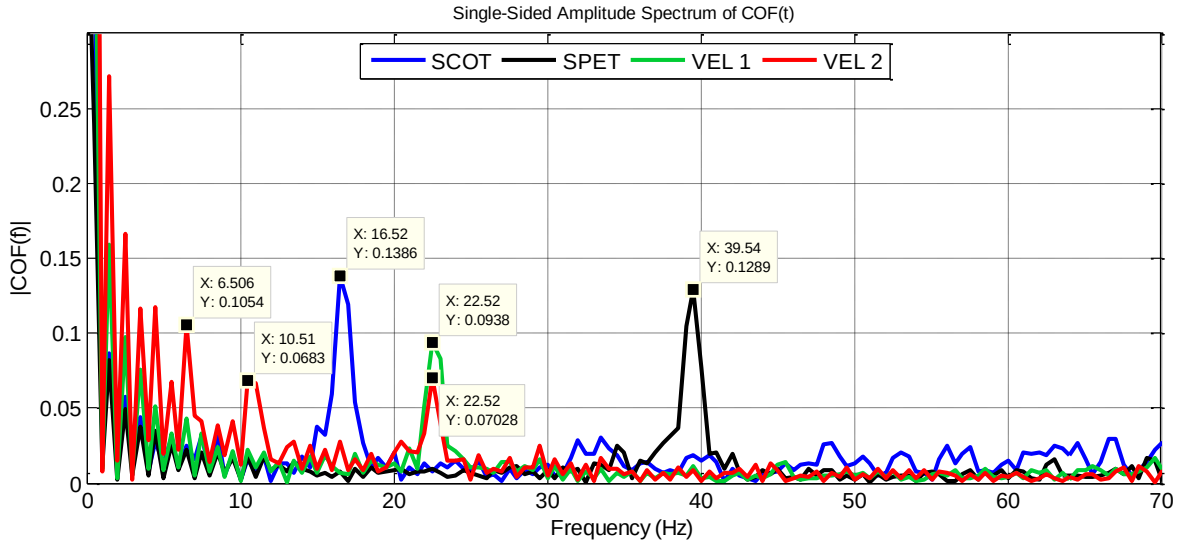


Figure 5-13: Frequency spectrum of the coefficient of friction with the pointed slider against the three textile surfaces, the black, blue, green and red curves illustrate respectively the polyester twill (SPET), the cotton twill (SCOT) and the velvet fabrics in its two directions, along (VEL1) and against piles (VEL2).

These measurements give the frequency for the texture of each textile fabrics. With the velocity 20 mm/s, we can link the temporal frequency to the spatial frequency. We calculate surface periods per 20 mm (Figure 5-7) and deduce the spatial frequency. The Table 5-2 illustrates the similarity between the measured frequencies using either the pointed slider or by determining by observation the spatial period of ribs (grooves) for the two twill woven fabrics and the spatial periods of the pile tuft for the velvet fabric.

Table 5-2: The similarity between the measured frequency obtained by measurement from the sharp prismatic slider and by observation of the spatial periods of the investigated textile fabrics

| Signal | SCOT | SPET | VEL1 | VEL2 |
|---|---|---|---|---|
| Frequency determined by the FFT spectrum (Hz) | 16.5 | 39.5 | 22.5 | 22.5, 10.5, 6.5 |
| Frequency determined the spatial period | 16 | 36 | 24 | 24 |
| Error of the frequency in % | 3% | 9% | 7% | 7% |

From Table 5-2, it can be noted that the polyester and the cotton twill have a unique frequency which corresponds to the number of ribs. Concerning the velvet fabric, two different evolutions can be extracted from the frequency spectrum depending on the motion direction: in the along pile direction, one frequency is found which corresponds to the number of pile yarns whereas for the against pile direction, by assuming as noise the frequencies less than 5 Hz, three frequencies can be extracted, 22.5, 10.5 and 6.5 Hz. The first frequency is in accordance with the number of yarns and the two other frequencies correspond to the fact of pushing the pile which are going up in this direction. Low frequencies below 5 Hz, due to heterogeneous pile have been previously observed in (Bueno et al., 1997). This difference is well recognized when touching the velvet as the individual feels the pile is homogeneous along its main direction and heterogeneous against its main direction.

#### 5.2.2.3 Complete tribological features extraction

Consequently, to perform the complete tribological features extraction, we propose a multilevel signal extraction divided into two parts: the first level is what we call the “shape” of the signal, defined as the average of the friction contrast of users. The second level is the determination of the specific frequencies of the textures extracted by the sharp prismatic probe measurements and eventually confirmed by spatial period measurement. Following this approach, a modified friction contrast is introduced:

$$FC_{F-F\,tot}(x) = FC_{F-F\,sha}(x)(1 + FC_{F-F\,tex}(x)) \tag{5.5}$$

With $FC_{tot}$ is the total friction contrast to be reproduced, $FC_{sha}$ is the friction contrast of the shape of the signal and $FC_{tex}$ is the friction contrast due to the texture, expressed as a sum of sinusoidal signals defined by an amplitude and a frequency.

$$FC_{F-F\,tex}(x) = A(i) * \sum_{i=1}^{i=N} \sin(2\,\pi\,f(i)\,x) \tag{5.6}$$

$N$ is the number of the relevant frequencies $f(i)$ in the spectrum (one for the cotton, polyester and the velvet along pile direction, and three for the velvet against pile direction). The only missing parameter to reconstitute the signal is the amplitude of the texture noted $A(i)$. This amplitude will be determined in percent in order to be adapted to the signal shape. A psychophysical experiment has been performed to determine the amplitude of each texture adapted for each individual.

## 5.3 Psychophysical validation

The goal of the psychophysical experiments is first to find the missing information in order to constitute the haptic fabrics texture which is the amplitude of $FC$ sinusoidal part of the texture, and second, to evaluate whether or not the $FC_{tot}$ defined in (5.5) describe correctly the real fabric surfaces. So the signal $FC_{tot}$ will be implemented in the SmartTac, and it will be translated into a wave amplitude $W$ reference, as explained in the section 5.1.5.

### 5.3.1 Thin texture determination

The first part of the psychophysical experiments aims at determining the accurate values of $A(i)$ parameters of the equation (5.6) for each investigated fabric. Eleven individuals have participated in this experiment, all right handed and between 22 and 28 years old. They gave their informed consent prior to the participation. The experiment consists in implementing $FC_{F-F\,tot}$ in the stimulator with $FC_{F-F\,sha}$ determined for each fabric by the results obtained in 5.2.2, whereas $FC_{F-F\,tex}$ has an adjusted variable level of the amplitude $A$. For the three surfaces successively, the volunteers are asked to touch the simulated surfaces and compare them with the real textures. They can increase or decrease the level of $A$ which has been already determined between 0% and 150% until they feel that the surfaces have similar touch sensation. A simple graphical interface programmed by Visual Basic software is used to change the level of $A$ and to move from a texture to another, and from a trial to the other. This experiment is repeated five times for each texture and in the two sliding directions for the velvet (along and against the pile). The average value of the results from five trials is calculated. In each trial, different initial values of $A$ are introduced to the subjects, which are [0, 25, 50, 75 and 100% of the maximum value]. The total duration of the study is approximately 10 minutes to avoid the tactile fatigue.

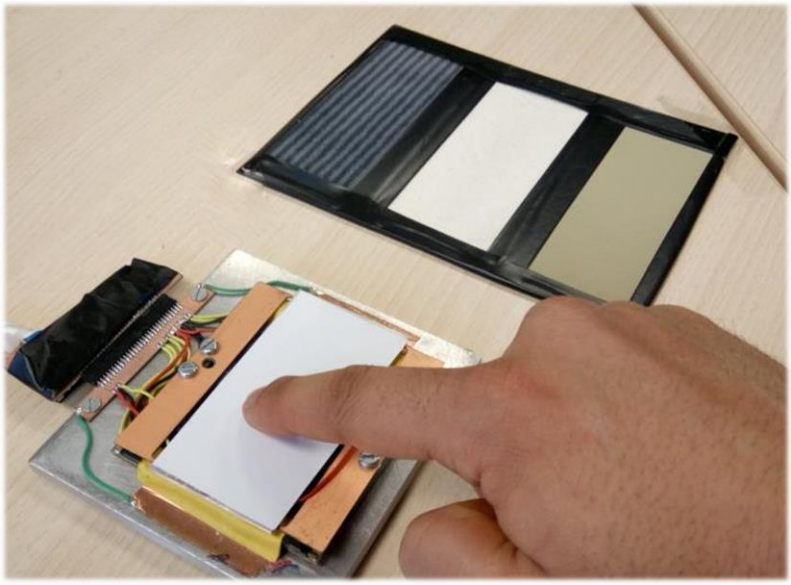

Figure 5-14: A volunteer during the experiment: he is touching the stimulator and can compare his feeling with the real textures on his right.

The results obtained show that even if the initial condition of *A* changes randomly, all the volunteers are able to find a repeatable amplitude value for each texture and direction.

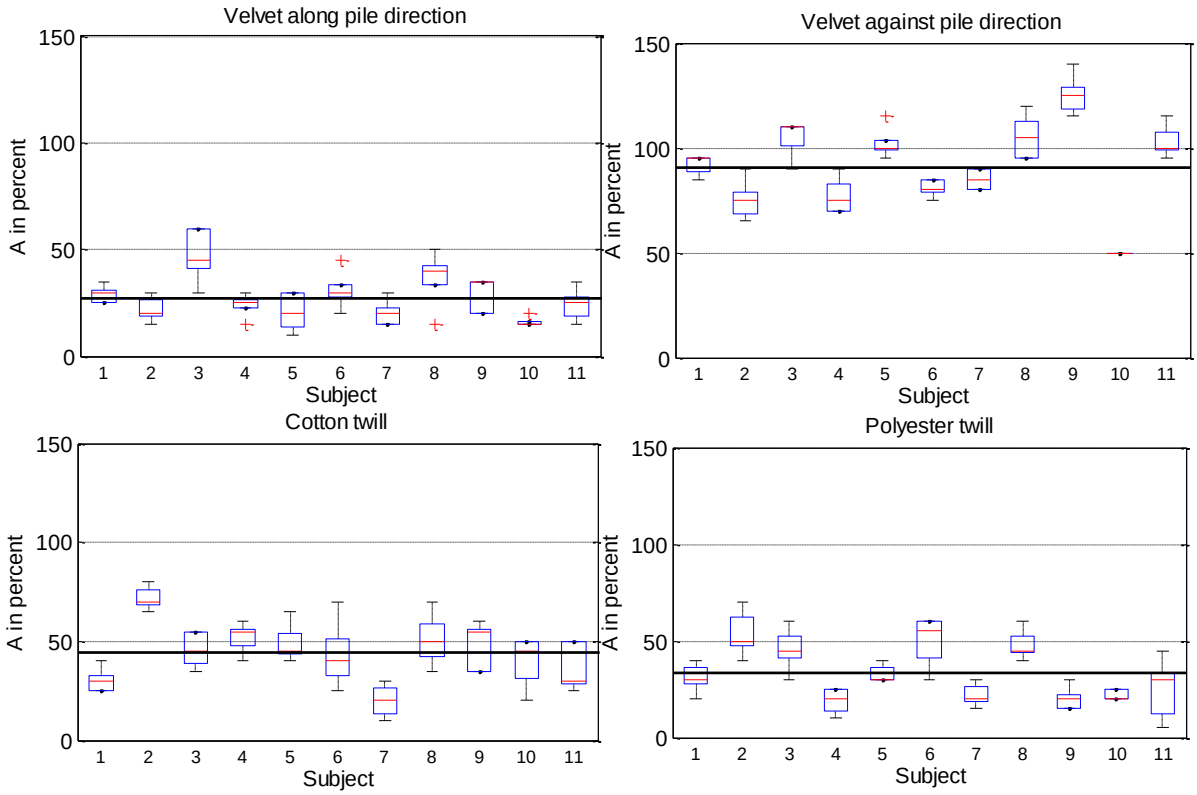


Figure 5-15: The boxplot of the final values of *A* (percentage of the amplitude of texture) for each texture and each direction for the velvet fabric and for each subject. For each boxplot, only the initial value of *A* is changed for each subject.

Figure 5-15 illustrates, with a boxplot representation, the convergence of $A$ for each texture and each direction. In addition, the convergence of each user to a level of $A$ is comparable with other users which enables us to define the average value of $A$ in order to characterize the fabric textures. It is also clear that a difference between the two directions of motion for the velvet is very distinguishable. The average value of $A$ along pile main direction, which is lower than the other direction, is 27%. Whereas the amplitude against pile direction is $A = 91\%$. As concerning the two other textures, the cotton and polyester twill woven fabrics, the average of $A$ is respectively 44% and 34%.

### 5.3.2 Validation of the simulated fabrics

The second part of the psychophysics experiments aims at evaluating the developed approach to simulate the textile fabrics. More precisely, this experiment aims at checking the capability of SmartTac to simulate different fabrics.

#### 5.3.2.1 Experimental protocol

21 volunteers participated in this experiment. They were 15 males and 6 females and aged between 22 and 57 years old with an average of 31 years old. Three of them were familiar with tactile devices, and the majority of them had no idea about the tactile stimulation and they touched the device for the first time. They were all right-handed except two. They all gave their informed consent and did not report any tactile deficit.

Each volunteer was asked to wash and dry his/her finger before starting the experiment. The volunteers undertook a training session during which they were taught how to touch the basic stimuli such as the unexcited stimulator, the maximum level of stimulation and gratings with different levels of frequencies but not the simulated surfaces. They were also asked to touch, with the index finger of their dominant hand, the three real fabric surfaces in two directions and feel the differences between them. Last they were asked to classify the surfaces according to their level of “smoothness-roughness” by assigning values from 0 to 100 (the smaller value corresponds to the “smoother” surface). It is obvious that the difference on a touch point of view between the different fabrics is not only the roughness, but the volunteers expressed their feeling with this descriptor.

The experimental protocol consists in simulating each surface 5 times to obtain 15 simulations for the three textile fabrics investigated. The simulated surfaces follow a random order so that the volunteers’ ability to discriminate may be evaluated. For each simulated surface, the volunteers are asked to tell which real fabric corresponds most to the stimulus. They can freely touch the real surfaces to try to identify the simulated one. The experimental protocol is almost similar to (Wiertlewski et al., 2011) but the difference is that in our experiment, the simulated surfaces were not presented to the volunteers before the experiment to avoid they memorize the touch

sensation of the simulated fabrics. Actually, the volunteers try the simulated surfaces for the first time during the experiment.

A graphical interface designed and programmed with the Visual Basic software was employed to facilitate the interaction between the user and the computer (Figure 5-16). The experimenter wrote the initials of each volunteer and clicked on the 'start' button to start the first simulated surface trial. The volunteer touched the simulated surface and compared it to the real surfaces to assign it to the surface that seemed to him/her the closest to reality. The 15 trials were carried out in the same way with a random order. In the end of the experiment, the volunteers' answers were saved in a separate file.

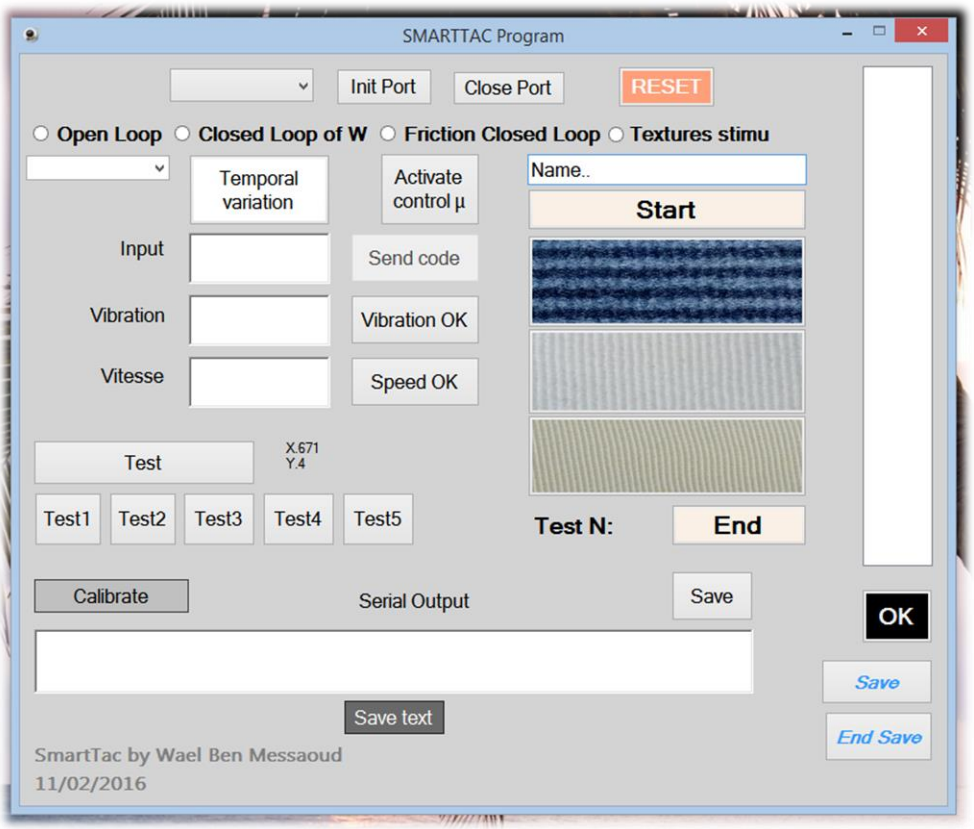


Figure 5-16: The developed graphical interface operated to do the psychophysical experiment.

### 5.3.2.2 Results and discussion

The training session on the touch of the real fabric surfaces before beginning the experiment gave several interesting results. First, the classification of the surfaces from the "smoothest" to the "roughest" one is: velvet fabric along pile direction (VEL1), polyester twill fabric (SPET), cotton twill woven (SCOT) and finally, velvet fabric against pile direction (VEL2). On the other hand, always from the training session of the real fabrics it may be noted that:

- All the volunteers detected the difference between the two pile directions of the velvet.
- When comparing the VEL1 and the SPET, the majority of the volunteers (15/21) detected that VEL1 is “smoother” than the SPET whereas a little minority (5/21) detected the opposite situation and just one volunteer felt that both surfaces were similar.
- 14/21 detected that the SCOT is “smoother” than the VEL2 and only one felt the same sensation between the fabrics. However, just 6/21 found the opposite. i.e. VEL2 is “smoother” than SCOT.

Now let us focus our attention on the second experiment. The overall results of the discrimination experiments can be represented by the confusion matrices illustrated in Figure 5-17. The answer rates are shown by a greyscale from no correspondence between the simulated and the real surfaces represented in white to the maximum correspondence represented in black colour.

It can be deduced that volunteers identified correctly the simulated surfaces. The average of the correct answers for the velvet is 81% with a standard deviation of 21%, 78% of correct answers for the cotton with 23% of standard deviation and 75% for the polyester with a 23% of standard deviation. From this figure, it can be noticed that a small confusion appears between the velvet and the polyester when the volunteers did not detect the difference in sensation between the two directions of motion because the touch perception of the polyester is almost similar to the along pile direction of the velvet. Another confusion is observed between the cotton and the polyester twill woven fabric, which can be explained by the misperception of the spatial period of each fabric.

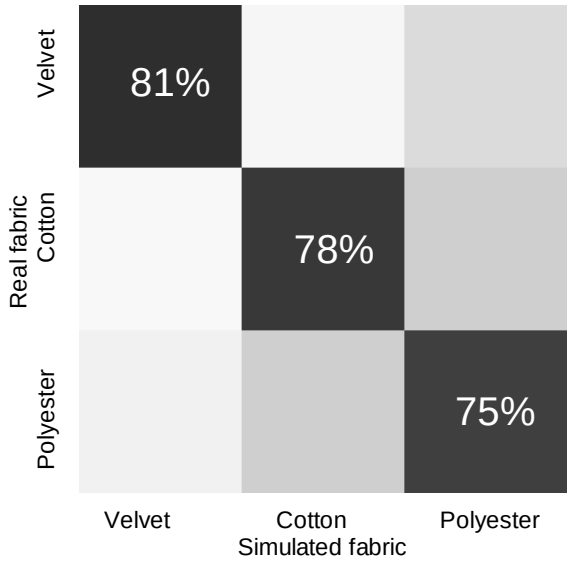


Figure 5-17: Confusion matrices relating the simulated surface to the real one. The greyscale represents the percentage of correct answers.

To see the results of the experiment in more details, Figure 5-18 illustrates the percentage of success for each subject.

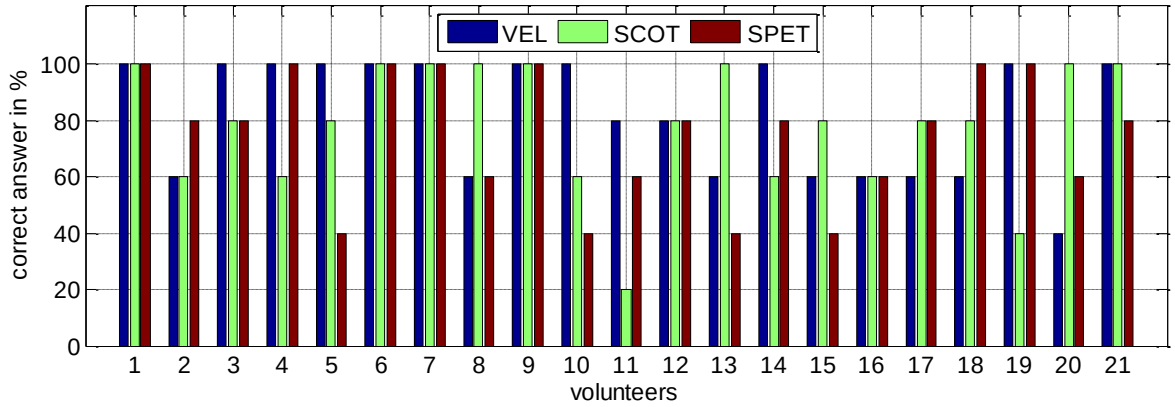


Figure 5-18: The percentage of the correct answers as a function of user for the three textile fabrics.

The percentage of the answers by user can be analysed by the Table 5-3:

Table 5-3: Success rate of the texture matching

| Success rate per subject | More than 3/5 (≥ 60%) | More than 4/5 (≥ 80%) | 5/5 (100%) |
|---|---|---|---|
| Velvet | 20/21 | 13/21 | 11/21 |
| Cotton twill | 19/21 | 14/21 | 8/21 |
| Polyester twill | 17/21 | 13/21 | 7/21 |

## 5.4 Conclusion

This study presents an experimental evaluation of the novel tactile stimulator called SmartTac used to simulate real textures such as fabrics and investigates the effect of the provided tactile stimuli on the users' perceptions. For that aim, we use the tribological parameter called friction contrast introduced in chapter 3. The use of the friction contrast instead of the coefficient of friction is explained by the less dependence of this parameter on the users' fingers. Two control strategies have been proposed to reproduce the friction contrast one based on the coefficient of friction control, the other on the vibration amplitude control. Despite the advantage of the method based on the coefficient of friction control which is the adaptation on the user s' fingers, this method presents some limits on precision and dynamics. So we used a direct link between the friction contrast and the wave amplitude to perform our experiments.

A multilevel approach for the surface characterization has been described, based on the friction profile measured by a tribometer. The approach is divided into two steps. Two types of "sliders" are used in each step; first, the real finger is used to characterize the shape of the friction signal, and second a slider made of an aluminium fine rigid tool is used to characterize the fine details of the surfaces. A psychophysical experiment has been carried out to validate the capability of the SmartTac to simulate a level of the texture amplitude which can simulate accurately the real fabrics. After that, another psychophysical experiment has been done on 21 volunteers to evaluate the quality and the capability to simulate and discriminate the fabrics. Three textile fabrics were chosen which are a velvet fabric, a cotton and a polyester twill woven fabrics. This experiment gives satisfactory results with an average of 78% of correct answers, which validates our approach.

The second approach using the direct control of the μ coefficient has not been experimented but it would be interesting to go on improving the control structure and the device to compare the results we may obtain with new psychophysics experiments.

# Conclusion and Perspectives

This thesis is focused on the simulation of the touch properties of textile fabrics. This kind of surfaces is hard to simulate due to the difficulty to have a superficial hairiness and/or the anisotropy of the surface during tactile task. In addition, a difference can be felt between the two directions of motion for some types of fabrics when sliding the finger on the surfaces.

From a tribological perspective, it can be noted that different factors can influence this interaction between the finger and the surfaces such as the applied normal force, the hydrophilic film composition, the relative humidity, temperature and the sliding velocity.

Three important axes were developed to reach the objective of the thesis. The first research axis was to improve the stimulator capability and its robustness on an electrical and control point of view. The second research axis was, on the one hand, to study the interaction between the fingers' subjects and the tactile stimulator in term of tactile threshold, while, on the other hand was to investigate the relation between the finger tribological behaviour and the perception, i.e. the relation between the reduced friction produced by the tactile display and the stimulus perceived by the subjects. The third axis was to choose various textile fabrics and to extract the accurate haptic signal from the surfaces to be simulated by operating a multilevel extraction method.

Finally, the validation of the simulated surfaces was done using a psychophysical experiment to evaluate the capability of the subjects to match the simulated surfaces with the real ones. The success rate of the fabrics discrimination was between 75% and 81% for the three surfaces.

## Original contribution

The main contributions of this research work are gathered here:

- A new approach to control the wave amplitude of the vibration created for tactile stimulation has been developed. To do that, a new modelling has been developed analytically in a d-q frame. This modelling allows to control the vibration amplitude and to track the resonant frequency and has been validated experimentally in the useful range of work. The closed loop control results show a high robustness of the control strategy against the disturbing factors. The objective was to make the tactile feedback insensitive to external disturbances such as the fingertip normal force and the temperature variation.
- A study of the influence of the vibration amplitude (VA) inducing the tactile stimulation on the perception of stimuli. Thus, we conducted a psychophysical experiment on 25 subjects to determine the friction threshold as a function of

the VA. We found an average threshold of vibration amplitude equal to 0.7 µm peak to peak. We observed that the tactile threshold depends on the age of the subjects and not influenced by their gender. In a second experiment, a statistical analysis conducted on 21 subjects was undertaken to determine the criterion affecting the perception of friction reduction on subjects. This experiment leads to the conclusion that the friction contrast criterion ($FC = 1 - \mu_1/\mu_0$), based on the ratio between the reduced and the initial friction, is the most discriminated parameter when comparing the detected and undetected tactile stimulations. The dependence of the friction contrast criterion on the initial coefficient of friction $\mu_0$ was also analysed and related to the stimulus detection. In fact, when $\mu_0$ increases, the friction contrast decreases, and therefore the friction discrimination also decreases.

- A new high fidelity smart tactile stimulator called "SmartTac" has been designed. The capability of this tactile stimulator to control in real time the coefficient of friction (COF) in addition to the closed loop control of the VA was described and performed thanks to the sensors implemented in the stimulator. Tribological validation of the COF control was proved by repeated experiments showing a stable and desired level of friction with a low response time of about 4 ms. After that, a first approach to control the friction contrast has been shown and a limitation of using the SmartTac has appeared, which is the variability of the initial coefficient of friction of the subjects. A solution to reduce this variability has been proposed based on the talc powder and a comparison has been done to evaluate its use.
- An experimental validation of SmartTac by simulating real fabrics and investigation of the effect of the perceived stimuli by the users. Two control structures were summarized to reproduce the friction contrast between the finger and the textures, but only one control strategy was used when simulating the fabrics. The other method based on the control of the µ presented some limits of the control precision which needs more improvement in the control strategy. A multilevel approach to evaluate the surfaces has been shown based on the friction profile measured with a tribometer.

  Two types of sliders were used to characterize the fine details and to characterize the shape of the friction signal. A psychophysical experiment was carried out to validate the capability to find a level of the texture amplitude which can simulate correctly the real fabrics. After that, another psychophysical experiment was done on 21 volunteers to validate the simulated fabrics. Three textile fabrics were chosen for their specificity: a pile fabric (velvet), a fabric with a texture and a standard hairiness (cotton twill woven fabric) and a fabric with a fine texture and without hairiness (polyester twill woven fabric). This experiment gave satisfactory results with an average of 78% of correct answers which validates the simulated surfaces strategy.

## Future work and perspectives

From the presented results, further improvement can be done at different levels:

The improvement of the control strategy of the SmartTac should be performed to use all the capacity of the stimulator, in particular the capability to adapt the simulated signals depending on the users' fingers. The real time closed loop control of the friction must be studied further in order to minimize the noise in the control and to decrease the response time. After that, it should be verified if the real time control can be better at a perceptual level.

The operated approach to extract the fabrics' features based on the multilevel extraction was applied to construct the haptic signals of the textures. This method was validated by conducting a psychophysical experiment with a percentage of success rates of 78% when matching the simulated surfaces to the real surfaces. It may be necessary to have a repeatable measurement of the haptic signals of the surfaces by working further in the improvement of the slider. The improvement can be made on the design of the slider which must be closer to the friction characteristics of a real finger, and at the same time able to detect the fine texture of the surfaces. This development can provide an automated method to extract the essential features of the surfaces for the use in an industrial process. Accordingly, a virtual textile material library could be built without any need to experimental tests with a cohort of users.

Coupling the tactile feedback with the visual display of the texture is also envisaged to have a realistic simulation of the textile fabrics which allows simultaneously touching and seeing the simulated surface.

# Publications

## International Journals

1. **W. Ben Messaoud**, F. Giraud, B. Semail, M. Amberg, and M. A. Bueno, "Amplitude control of an ultrasonic vibration for a tactile stimulator," IEEE/ASME Transactions on Mechatronics, vol. 21, no. 3, pp. 1692–1701, Jun. 2016.
2. **W. Ben Messaoud**, M.-A. Bueno, and B. Lemaire-Semail, "Relation between human perceived friction and finger friction characteristics," Tribology International, vol. 98, pp. 261–269, Jun. 2016.
3. E. Vezzoli, **W. Ben Messaoud**, M. Amberg, F. Giraud, B. Lemaire-Semail, and M. Bueno, "Physical and perceptual independence of ultrasonic vibration and electrovibration for friction modulation," IEEE Transactions on Haptics, vol. 8, no. 2, pp. 235–239, Jun. 2015.
4. E. Vezzoli, **W. Ben Messaoud**, C. Nadal, F. Giraud, M. Amberg, B. Lemaire-Semail, and M.-A. BUENO, "Coupling of ultrasonic vibration and electrovibration for tactile stimulation," European Journal of Electrical Engineering, vol. 17, no. 5–6, pp. 377–395, Nov. 2015.

## International conferences

5. **W. Ben Messaoud**, B. Lemaire-Semail, and M.-A. BUENO, "Textile Fabrics' Texture: from Multi-Level Feature Extraction to Tactile Simulation," presented at the International Conference EuroHaptics 2016, London, UK, 2016.
6. **W. Ben Messaoud**, B. Lemaire-Semail, M.-A. Bueno, M. Amberg, and F. Giraud, "Closed-Loop Control for Squeeze Film Effect in Tactile Stimulator," presented at the International Conference and exhibition on new actuators and drives, (Actuator 2014), Bremen, Germany, 2014, pp. 245–248.
7. **W. Ben Messaoud**, M. Amberg, B. Lemaire-Semail, F. Giraud, and M.-A. Bueno, "High fidelity closed loop controlled friction in SMARTTAC tactile stimulator," presented at the 17th European Conference on Power Electronics and Applications (EPE'15 ECCE-Europe), Genève, Suisse, 2015.
8. **W. Ben Messaoud**, M.-A. Bueno, and B. Lemaire-Semail, "Tribological Analysis Of The Friction Reduction In Tactile Stimulation," presented at the 42nd Leeds-Lyon Symposium on Tribology, Lyon, France, 2015.
9. **W. Ben Messaoud**, E. Vezzoli, F. Giraud, and B. Lemaire-Semail, "Pressure dependence of friction modulation in ultrasonic devices," presented at the IEEE World Haptics Conference (WHC2015), Chicago, USA, 2015.

## National conferences

10. **W. Ben Messaoud**, E. Vezzoli, M.-A. Bueno, and B. Lemaire-Semail, "Analyse des modulations de frottement par effet squeeze film et électrovibration: validité de la complémentarité," presented at the Journées Internationales Francophones de Tribologie (JIFT 2014), Mulhouse, France, 2014.
11. E. Vezzoli, **W. Ben Messaoud**, C. Nadal, F. Giraud, M. Amberg, B. Lemaire-Semail, and M.-A. Bueno, "Couplage vibration ultrasonique et électro-vibration pour la stimulation tactile," presented at the Symposium de Génie Electrique (SGE 2014), Cachan, France, 2014.
12. P. Melchior, **W. Ben Messaoud**, S. Victor, F. Cazaurang, and C. Goetz, "Plateforme AEROfan, Plateforme Aquitaine pour l'Enseignement et la Recherche sur les mOteurs aéronatiques turbofan : un exemple d'utilisation en automatique à travers l'identification et la commande du moteur DGEN 380," presented at the Quatrièmes Journées des Démonstrateurs en Automatique, Section automatique du club EEA, Angers, France, 2013.

# Bibliography


## [A]

Adams, M.J., Johnson, S.A., Lefèvre, P., Lévesque, V., Hayward, V., André, T., Thonnard, J.-L., 2013. Finger pad friction and its role in grip and touch. J R Soc Interface 10, 20120467. doi:10.1098/rsif.2012.0467

Al-Samarai, R.A., Haftirman, K.R.A., Al-Douri, Y., 2012. Effect of Load and Sliding Speed on Wear and Friction of Aluminum–Silicon Casting Alloy. International J. of Scientific and Research Publications 2, 1–4.

Amberg, M., Giraud, F., Semail, B., Olivo, P., Casiez, G., Roussel, N., 2011. STIMTAC: a tactile input device with programmable friction, in: Proceedings of the 24th Annual ACM Symposium Adjunct on User Interface Software and Technology, UIST '11 Adjunct. ACM, New York, NY, USA, pp. 7–8. doi:10.1145/2046396.2046401

Asamura, N., Tomori, N., Shinoda, H., 1998. A tactile feeling display based on selective stimulation to skin receptors. Presented at the Virtual Reality Annual International Symposium, pp. 36–42. doi:10.1109/VRAIS.1998.658420

## [B]

Bark, K., Wheeler, J., Lee, G., Savall, J., Cutkosky, M., 2009. A wearable skin stretch device for haptic feedback, in: EuroHaptics Conference, 2009 and Symposium on Haptic Interfaces for Virtual Environment and Teleoperator Systems. World Haptics 2009. Third Joint. Presented at the EuroHaptics conference, 2009 and Symposium on Haptic Interfaces for Virtual Environment and Teleoperator Systems. World Haptics 2009. Third Joint, pp. 464–469. doi:10.1109/WHC.2009.4810850

Bau, O., Poupyrev, I., Israr, A., Harrison, C., 2010. TeslaTouch: electrovibration for touch surfaces, in: Proceedings of the 23nd Annual ACM Symposium on User Interface Software and Technology, UIST '10. ACM, New York, NY, USA, pp. 283–292. doi:10.1145/1866029.1866074

Benali-Khoudja, M., Hafez, M., Alexandre, J.-M., Kheddar, A., Moreau, V., 2004. VITAL: A New Low-Cost VIbro-TActiLe Display System. Presented at the IEEE International Conference on Robotics & Automation, New Orleans, USA.

Ben Messaoud, W., Bueno, M.-A., Lemaire-Semail, B., 2016a. Relation between human perceived friction and finger friction characteristics. Tribology International 98, 261–269. doi:10.1016/j.triboint.2016.02.031

Ben Messaoud, W., Bueno, M.-A., Lemaire-Semail, B., 2015a. Tribological Analysis Of The Friction Reduction In Tactile Stimulation. Presented at the 42nd Leeds-Lyon Symposium on Tribology, Lyon, France.

Ben Messaoud, W., Giraud, F., Lemaire-Semail, B., Amberg, M., Bueno, M.A., 2016b. Amplitude Control of an Ultrasonic Vibration for a Tactile Stimulator. IEEE/ASME Transactions on Mechatronics 21, 1692–1701. doi:10.1109/TMECH.2016.2535300

Ben Messaoud, W., Lemaire-Semail, B., Bueno, M.-A., Amberg, M., Giraud, F., 2014a. Closed-Loop Control for Squeeze Film Effect in Tactile Stimulator. Presented at the International Conference and exhibition on new actuators and drives, (Actuator 2014), Bremen, Germany, pp. 245–248. doi:10.13140/2.1.2461.0086

Ben Messaoud, W., Vezzoli, E., Bueno, M.-A., Lemaire-Semail, B., 2014b. Analyse des modulations de frottement par effet squeeze film et électrovibration: validité de la complémentarité. Presented at the Journées Internationales Francophones de Tribologie (JIFT 2014), Mulhouse, France.

Ben Messaoud, W., Vezzoli, E., Giraud, F., Lemaire-Semail, B., 2015b. Pressure dependence of friction modulation in ultrasonic devices. Presented at the IEEE World Haptics Conference (WHC2015), Chicago, USA.

Bergmann Tiest, W.M., 2010. Tactual perception of material properties. Vision Research, Perception and Action: Part I 50, 2775–2782. doi:10.1016/j.visres.2010.10.005

Biet, M., 2007. Conception et contrôle d'actionneurs électro-actifs dédiés à la simulation tactile. Université Lille1, Lille.

Biet, M., Giraud, F., Lemaire-Semail, B., 2008. Implementation of tactile feedback by modifying the perceived friction. The European Physical Journal - Applied Physics 43, 123–135. doi:10.1051/epjap:2008093

Biet, M., Giraud, F., Lemaire-Semail, B., 2007. Squeeze film effect for the design of an ultrasonic tactile plate. IEEE Trans Ultrason Ferroelectr Freq Control 54, 2678–2688. doi:10.1109/TUFFC.2007.596

Bingi, P., Mir, A., Khamalah, J., 2000. The Challenges Facing Global E-Commerce. Information Systems Management 17, 22–30. doi:10.1201/1078/43193.17.4.20000901/31249.5

Bouscayrol, A., Davat, B., de Fornel, B., François, B., Hautier, J.P., Meibody-Tabar, F., Monmasson, E., Pietrzak-David, M., Razik, H., Semail, E., Benkhoris, F., 2003. Control structures for multi-machine multi-converter systems with upstream coupling. Mathematics and Computers in Simulation, Modelling and Simulation of Electric Machines, Converters and Systems 63, 261–270. doi:10.1016/S0378-4754(03)00074-0

Bowden, F.P., Young, J.E., 1951. Friction of Diamond, Graphite, and Carbon and the Influence of Surface Films. Proceedings of the Royal Society of London. Series A, Mathematical and Physical Sciences 208, 444–455.

Breugnot, C., 2005. Contribution à la caractérisation mécanique du toucher des surfaces textiles à partir de critères neurosensoriels (PhD Thesis). Université de Haute Alsace, Mulhouse.

Bueno, M.-A., Lemaire-Semail, B., Amberg, M., Giraud, F., 2015. Pile surface tactile simulation: role of the slider shape, texture close to fingerprints and the joint-stiffness. Tribology Letters.

Bueno, M.-A., Lemaire-Semail, B., Amberg, M., Giraud, F., 2014. A simulation from a tactile device to render the touch of textile fabrics: a preliminary study on velvet. Textile Research Journal 40517514521116. doi:10.1177/0040517514521116

Bueno, M.-A., Viallier, P., Durand, B., Renner, M., Lamy, B., 1997. Instrumental Measurement and Macroscopical Study of Sanding and Raising. Textile Research Journal 67, 779–787.

Bueno, M.-A., Crest, M., Monteil, G., Berthier, Y., Lemaire-Semail, B., Massi, F., Vinter, A., Aimonetti, J.-M., Carpentier, L., Cornuault, P.-H., Giraud, F., Camillieri, B., Ribot-Ciscar, E., Witt, A., Gentaz, E., Mith, S., 2015. COSTaM: Tool Design for a Controlled Tactile Stimulation. AMSE Journals-AMSE IFRATH Publication _ Modelling C 75, 31–42.

**[C]**

Camillieri, B., Buneo, M.-A., 2015. Doigt artificiel pour frottement sur surfaces pileuses. Presented at the 22ème Congrès Français de Mécanique, Lyon, France.

Cornuault, P.-H., Carpentier, L., Bueno, M.-A., Cote, J.-M., Monteil, G., 2015. Influence of physico-chemical, mechanical and morphological fingerpad properties on the frictional distinction of sticky/slippery surfaces. Journal of The Royal Society Interface 12, 20150495. doi:10.1098/rsif.2015.0495

Coutinho, L.R.R., Girão, A.M., Frota, J.B.B., Jr, E.T.S., 2012. Device to Assist the Visually Impaired in Reading Printed or Scanned Documents, in: 2012 Brazilian Symposium on Computing System Engineering (SBESC). Presented at the 2012 Brazilian Symposium on Computing System Engineering (SBESC), pp. 25–30. doi:10.1109/SBESC.2012.14

**[D]**

Dai, X., Colgate, J.E., Peshkin, M.A., 2012. LateralPaD: A surface-haptic device that produces lateral forces on a bare finger. Presented at the 2012 IEEE Haptics Symposium (HAPTICS), pp. 7–14. doi:10.1109/HAPTIC.2012.6183753

Darden, M.A., Schwartz, C.J., 2013. Investigation of friction mechanisms during the sliding of elastomers against hard parallel-ridge textures. Tribology International, The International Conference on BioTribology 2011 63, 2–7. doi:10.1016/j.triboint.2012.01.005

Darian-Smith, I., 1984. The Sense of Touch: Performance and Peripheral Neural Processes, in: Handbook of Physiology, William and Wilkins. John Wiley & Sons, Inc., Baltimore, pp. 739–788.

Delhaye, B., Lefèvre, P., Thonnard, J.-L., 2014. Dynamics of fingertip contact during the onset of tangential slip. Journal of The Royal Society Interface 11. doi:10.1098/rsif.2014.0698

Derler, S., Gerhardt, L.-C., 2011. Tribology of Skin: Review and Analysis of Experimental Results for the Friction Coefficient of Human Skin. Tribol Lett 45, 1–27. doi:10.1007/s11249-011-9854-y

Derler, S., Gerhardt, L.-C., Lenz, A., Bertaux, E., Hadad, M., 2009. Friction of human skin against smooth and rough glass as a function of the contact pressure. Tribology International, Special Issue: 35th Leeds-Lyon Symposium 42, 1565–1574. doi:10.1016/j.triboint.2008.11.009

Derler, S., Rotaru, G.-M., 2013. Stick–slip phenomena in the friction of human skin. Wear, Wear of Materials 2013 301, 324–329. doi:10.1016/j.wear.2012.11.030

**[E]**

Echenique, A.M., Graffigna, J.P., Mut, V., 2010. Electrocutaneous stimulation system for Braille reading, in: 2010 Annual International Conference of the IEEE Engineering in Medicine and Biology Society (EMBC). Presented at the 2010 Annual International Conference of the IEEE Engineering in Medicine and Biology Society (EMBC), pp. 5827–5830. doi:10.1109/IEMBS.2010.5627501

Efron, N., 1977. OPTACON—A REPLACEMENT FOR BRAILLE?*. The Australian Journal of Optometry 60, 118–129.

**[F]**

Fagiani, R., Massi, F., Chatelet, E., Costes, J.P., Berthier, Y., 2012. Contact of a Finger on Rigid Surfaces and Textiles: Friction Coefficient and Induced Vibrations. Tribol Lett 48, 145–158. doi:10.1007/s11249-012-0010-0

Fontana, M., Rizzi, C., Cugini, U., 2004. Physics-based modelling and simulation of functional cloth for virtual prototyping applications, in: Proceedings of the Ninth ACM Symposium on Solid Modeling and Applications. Eurographics Association, Genoa, Italy, pp. 267–272.

**[G]**

Gee, M.G., Tomlins, P., Calver, A., Darling, R.H., Rides, M., 2005. A new friction measurement system for the frictional component of touch. Wear, 15th International Conference on Wear of Materials 259, 1437–1442. doi:10.1016/j.wear.2005.02.053

Gerhardt, L.-C., Strässle, V., Lenz, A., Spencer, N.D., Derler, S., 2008. Influence of epidermal hydration on the friction of human skin against textiles. Journal of The Royal Society Interface 5, 1317–1328. doi:10.1098/rsif.2008.0034

Ghenna, S., Giraud, F., Giraud-Audine, C., Amberg, M., Lemaire-Semail, B., 2015. Preliminary design of a multi-touch ultrasonic tactile stimulator, in: 2015 IEEE World Haptics Conference (WHC). Presented at the 2015 IEEE World Haptics Conference (WHC), pp. 31–36. doi:10.1109/WHC.2015.7177687

Giraud, F., Amberg, M., Lemaire-Semail, B., 2013. Merging two tactile stimulation principles: electrovibration and squeeze film effect, in: World Haptics Conference (WHC), 2013. Presented at the World Haptics Conference (WHC), 2013, pp. 199–203. doi:10.1109/WHC.2013.6548408

Giraud, F., Amberg, M., Lemaire-Semail, B., 2013. Design and control of a haptic knob. Sensors and Actuators A: Physical 196, 78–85. doi:10.1016/j.sna.2013.03.012

Giraud, F., Amberg, M., Lemaire-Semail, B., Casiez, G., 2012. Design of a transparent tactile stimulator, in: 2012 IEEE Haptics Symposium (HAPTICS). Presented at the 2012 IEEE Haptics Symposium (HAPTICS), pp. 485–489. doi:10.1109/HAPTIC.2012.6183835

Giraud, F., Amberg, M., Vanbelleghem, R., Lemaire-Semail, B., 2010. Power Consumption Reduction of a Controlled Friction Tactile Plate, in: Kappers, A.L., van Erp, J.F., Bergmann Tiest, W., van der Helm, F.T. (Eds.), Haptics: Generating and Perceiving Tangible Sensations, Lecture Notes in Computer Science. Springer Berlin Heidelberg, pp. 44–49.

Gokcek, C., 2003. Tracking the resonance frequency of a series RLC circuit using a phase locked loop, in: Proceedings of 2003 IEEE Conference on Control Applications, 2003. CCA 2003. Presented at the Proceedings of 2003 IEEE Conference on Control Applications, 2003. CCA 2003, pp. 609–613 vol.1. doi:10.1109/CCA.2003.1223506

Goldfarb, M., Celanovic, N., 1997. A Lumped Parameter Electromechanical Model for Describing the Nonlinear Behavior of Piezoelectric Actuators. J. Dyn. Sys., Meas., Control 119, 478–485. doi:10.1115/1.2801282

**[H]**

Han, H.-Y., Shimada, A., Kawamura, S., 1996. Analysis of friction on human fingers and design of artificial fingers, in: , 1996 IEEE International Conference on Robotics and Automation, 1996. Proceedings. Presented at the , 1996 IEEE International Confer-

ence on Robotics and Automation, 1996. Proceedings, pp. 3061–3066 vol.4. doi:10.1109/ROBOT.1996.509177

Hayward, V., Cruz-Hernandez, M., 2000. Tactile Display Device Using Distributed Lateral Skin Stretch, in: Proc. of the Haptic Interfaces for Virtual Environment and Teleoperator Systems Symposium. Presented at the ASME IMECE2000, Proc. ASME, Orlando, Florida, USA, pp. 1309–1314.

Hendriks, C.P., Franklin, S.E., 2009. Influence of Surface Roughness, Material and Climate Conditions on the Friction of Human Skin. Tribol Lett 37, 361–373. doi:10.1007/s11249-009-9530-7

Horrein, L., Bouscayrol, A., Cheng, Y., El Fassi, M., 2015. Dynamical and quasi-static multi-physical models of a diesel internal combustion engine using Energetic Macroscopic Representation. Energy Conversion and Management 91, 280–291. doi:10.1016/j.enconman.2014.12.022

**[I,J]**

Ilkhani, G., Aziziaghdam, M., Samur, E., 2014. Data-Driven Texture Rendering with Electrostatic Attraction, in: Auvray, M., Duriez, C. (Eds.), Haptics: Neuroscience, Devices, Modeling, and Applications, Lecture Notes in Computer Science. Springer Berlin Heidelberg, pp. 496–504.

Jiang, H., Browning, R., Fincher, J., Gasbarro, A., Jones, S., Sue, H.-J., 2008. Influence of surface roughness and contact load on friction coefficient and scratch behavior of thermoplastic olefins. Applied Surface Science 254, 4494–4499. doi:10.1016/j.apsusc.2008.01.067

**[K]**

Kaczmarek, K.A., Nammi, K., Agarwal, A.K., Tyler, M.E., Haase, S.J., Beebe, D.J., 2006. Polarity effect in electrovibration for tactile display. IEEE Trans Biomed Eng 53, 2047–2054. doi:10.1109/TBME.2006.881804

Kang, J., Lee, J., Kim, H., Cho, K., Wang, S., Ryu, J., 2012. Smooth Vibrotactile Flow Generation Using Two Piezoelectric Actuators. IEEE Transactions on Haptics 5, 21–32. doi:10.1109/TOH.2012.1

Kim, S.-C., Israr, A., Poupyrev, I., 2013. Tactile Rendering of 3D Features on Touch Surfaces, in: Proceedings of the 26th Annual ACM Symposium on User Interface Software and Technology, UIST '13. ACM, New York, NY, USA, pp. 531–538. doi:10.1145/2501988.2502020

Klatzky, R.L., Lederman, S.J., Reed, C., 1987. There's more to touch than meets the eye: The salience of object attributes for haptics with and without vision. Journal of experimental psychology: general 116, 356.

Koudine, A.A., Barquins, M., Anthoine, P.H., Aubert, L., Lévêque, J.L., 2000. Frictional properties of skin: proposal of a new approach. Int J Cosmet Sci 22, 11–20. doi:10.1046/j.1467-2494.2000.00006.x

**[L]**

Lee, J.-H., Ahn, I.-S., Park, J.-O., 1999. Design and implementation of tactile feedback device using electromagnetic type. Presented at the IEEE/RSJ International Conference on Intelligent Robots and Systems, IROS'99, pp. 1549–1554 vol.3. doi:10.1109/IROS.1999.811699

Lee, P.-M., 2002. Behavioral Model of Online Purchasers in E-Commerce Environment. Electronic Commerce Research 2, 75–85. doi:10.1023/A:1013340118965

Lin, C.-M., 2012. Temperature Compensation of Aluminum Nitride Lamb Wave Resonators Utilizing the Lowest-Order Symmetric Mode. EECS Department, University of California, Berkeley.

Liu, X., Colli-Menchi, A., Gilbert, J., Friedrichs, D.A., Malang, K., Sanchez-Sinencio, E., 2015. An Automatic Resonance Tracking Scheme With Maximum Power Transfer for Piezoelectric Transducers. IEEE Transactions on Industrial Electronics PP, 1–1. doi:10.1109/TIE.2015.2436874

Liu, X., Lu, Z., Lewis, R., Carré, M.J., Matcher, S.J., 2013. Feasibility of using optical coherence tomography to study the influence of skin structure on finger friction. Tribology International, The International Conference on BioTribology 2011 63, 34–44. doi:10.1016/j.triboint.2012.08.020

Ljung, L., 1998. System Identification, in: Procházka, A., Uhlíř, J., Rayner, P.W.J., Kingsbury, N.G. (Eds.), Signal Analysis and Prediction, Applied and Numerical Harmonic Analysis. Birkhäuser Boston, pp. 163–173.

Loker, S., Ashdown, S., Carnrite, E., 2008. Dress in the Third Dimension Online Interactivity and Its New Horizons. Clothing and Textiles Research Journal 26, 164–176. doi:10.1177/0887302X08315176

Luginbühl, T., Delattre, L., Gagalowicz, A., 2011. Towards the Automatic Generation of 3D Photo-Realistic Avatars Using 3D Scanned Data, in: Gagalowicz, A., Philips, W. (Eds.), Computer Vision/Computer Graphics Collaboration Techniques, Lecture Notes in Computer Science. Springer Berlin Heidelberg, pp. 192–203.

**[M]**

Magnenat-Thalmann, N., Volino, P., Bonanni, U., Summers, I., Bergamasco, M., Salsedo, F., Wolter, F., 2007. From physics-based simulation to the touching of textiles: The haptex project. The International Journal of Virtual Reality 35–44.

Marshall, R.A., 1990. Moisture absorption by PVC plastisol components. Journal of Vinyl Technology 12, 195–197.

Martinot, F., 2006. Caractérisation du rôle de la dynamique du toucher dans la perception de textures. Lille 1.

Martinot, F., Houzefa, A., Biet, M., Chaillou, C., 2006. Mechanical Responses of the Fingerpad and Distal Phalanx to Friction of a Grooved Surface: Effect of the Contact Angle, in: 2006 14th Symposium on Haptic Interfaces for Virtual Environment and Teleoperator Systems. Presented at the 2006 14th Symposium on Haptic Interfaces for Virtual Environment and Teleoperator Systems, pp. 297–300. doi:10.1109/HAPTIC.2006.1627119

Masen, M.A., 2011. A systems based experimental approach to tactile friction. J Mech Behav Biomed Mater 4, 1620–1626. doi:10.1016/j.jmbbm.2011.04.007

McGill, R., Tukey, J.W., Larsen, W.A., 1978. Variations of box plots. The American Statistician 32, 12–16.

Meyer, D.J., Wiertlewski, M., Peshkin, M.A., Colgate, J.E., 2014. Dynamics of ultrasonic and electrostatic friction modulation for rendering texture on haptic surfaces., in: HAPTICS. pp. 63–67.

Mortimer, B., du Bruyn, T., Davies, J., Tapson, J., 2001. High power resonant tracking amplifier using admittance locking. Ultrasonics 39, 257–261. doi:10.1016/S0041-624X(01)00060-9

Mullenbach, J., Shultz, C., Piper, A.M., Peshkin, M., Colgate, J.E., 2013. Surface Haptic Interactions with a TPad Tablet, in: Proceedings of the Adjunct Publication of the 26th Annual ACM Symposium on User Interface Software and Technology, UIST '13 Adjunct. ACM, New York, NY, USA, pp. 7–8. doi:10.1145/2508468.2514929

**[N]**

Nakamura, T., Yamamoto, A., 2014. Position and Force-direction Detection for Multi-finger Electrostatic Haptic System Using a Vision-based Touch Panel, in: ACHI 2014. Presented at the The Seventh International Conference on Advances in Computer-Human Interactions, Barcelona, Spain, pp. 160–165.

Nakazawa, N., Ikeura, R., Inooka, H., 2000. Characteristics of human fingertips in the shearing direction. Biol Cybern 82, 207–214. doi:10.1007/s004220050020

Nye, P.W., 1976. Reading devices for blind people. Med. Progr. Technol 4, 2.

**[P]**

Pai, D.K., Rizun, P., 2003. The WHaT: a wireless haptic texture sensor, in: 11th Symposium on Haptic Interfaces for Virtual Environment and Teleoperator Systems, 2003. HAPTICS 2003. Proceedings. Presented at the 11th Symposium on Haptic Interfaces for Virtual Environment and Teleoperator Systems, 2003. HAPTICS 2003. Proceedings, pp. 3–9. doi:10.1109/HAPTIC.2003.1191210

Pascoe, M.W., Tabor, D., 1956. The Friction and Deformation of Polymers. Proceedings of the Royal Society of London A: Mathematical, Physical and Engineering Sciences 235, 210–224. doi:10.1098/rspa.1956.0077

Pasumarty, S.M., Johnson, S.A., Watson, S.A., Adams, M.J., 2011. Friction of the Human Finger Pad: Influence of Moisture, Occlusion and Velocity. Tribol Lett 44, 117–137. doi:10.1007/s11249-011-9828-0

Pawluk, D.T., Howe, R.D., 1999. Dynamic lumped element response of the human fingerpad. J Biomech Eng 121, 178–183.

Peck, J., Childers, T.L., 2003. To Have and to Hold: The Influence of Haptic Information on Product Judgments. Journal of Marketing 67, 35–48.

Pigache, F., Giraud, F., Lemaire-Semail, B., 2006. Modelling and identification of a planar standing wave ultrasonic motor. The European Physical Journal - Applied Physics 34, 55–65. doi:10.1051/epjap:2006033

**[R]**

Reuter, E.-M., Voelcker-Rehage, C., Vieluf, S., Godde, B., 2011. Touch perception throughout working life: effects of age and expertise. Exp Brain Res 216, 287–297. doi:10.1007/s00221-011-2931-5

Russomanno, A., O'Modhrain, S., Gillespie, R.B., Rodger, M.W.M., 2015. Refreshing Refreshable Braille Displays. IEEE Transactions on Haptics 8, 287–297. doi:10.1109/TOH.2015.2423492

**[S]**

Samur, E., Colgate, J.E., Peshkin, M.A., 2009. Psychophysical evaluation of a variable friction tactile interface. p. 72400J–72400J–7. doi:10.1117/12.817170

Shi, E., Hu, C., Xu, Y.S., 2015. An Enhanced Ultrasonic Frequency Closed-Loop Control System for Biological Decomposition, in: International Conference on Electrical, Automation and Mechanical Engineering (EAME2015). Atlantis Press, Phuket, Thailand. doi:10.2991/eame-15.2015.13

Shtessel, Y., Edwards, C., Fridman, L., Levant, A., 2014. Introduction: Intuitive Theory of Sliding Mode Control, in: Sliding Mode Control and Observation, Control Engineering. Springer New York, pp. 1–42.

Sivamani, R.K., Goodman, J., Gitis, N.V., Maibach, H.I., 2003. Friction coefficient of skin in real-time. Skin Research and Technology 9, 235–239. doi:10.1034/j.1600-0846.2003.20361.x

Skedung, L., Danerlöv, K., Olofsson, U., Aikala, M., Niemi, K., Kettle, J., Rutland, M.W., 2009. Finger Friction Measurements on Coated and Uncoated Printing Papers. Tribol Lett 37, 389–399. doi:10.1007/s11249-009-9538-z

Skedung, L., Danerlöv, K., Olofsson, U., Michael Johannesson, C., Aikala, M., Kettle, J., Arvidsson, M., Berglund, B., Rutland, M.W., 2011. Tactile perception: Finger friction, surface roughness and perceived coarseness. Tribology International, Special Issue: ECOTRIB 2009 44, 505–512. doi:10.1016/j.triboint.2010.04.010

Smith, A.M., Scott, S.H., 1996. Subjective scaling of smooth surface friction. J. Neurophysiol. 75, 1957–1962.

Souza, J.R., Silva, R.C., Silva, L.V., Medeiros, J.T., Amico, S.C., Brostow, W., 2014. Tribology of composites produced with recycled GFRP waste. Journal of Composite Materials 21998314557296. doi:10.1177/0021998314557296

Streque, J., Talbi, A., Pernod, P., Preobrazhensky, V., 2010. New Magnetic Microactuator Design Based on PDMS Elastomer and MEMS Technologies for Tactile Display. IEEE Transactions on Haptics 3, 88–97. doi:10.1109/TOH.2009.61

Strese, M., Schuwerk, C., Steinbach, E., 2015. On the retrieval of perceptually similar haptic surfaces, in: 2015 Seventh International Workshop on Quality of Multimedia Experience (QoMEX). Presented at the 2015 Seventh International Workshop on Quality of Multimedia Experience (QoMEX), pp. 1–6. doi:10.1109/QoMEX.2015.7148141

Supriya, S., Senthilkumar, A., 2009. Electronic Braille pad, in: 2009 International Conference on Control, Automation, Communication and Energy Conservation, 2009. INCACEC 2009. Presented at the 2009 International Conference on Control, Automation, Communication and Energy Conservation, 2009. INCACEC 2009, pp. 1–5.

Sylvester, N.D., Provancher, W.R., 2007. Effects of Longitudinal Skin Stretch on the Perception of Friction, in: EuroHaptics Conference, 2007 and Symposium on Haptic Interfaces for Virtual Environment and Teleoperator Systems. World Haptics 2007. Second Joint. Presented at the EuroHaptics Conference, 2007 and Symposium on Haptic Interfaces for Virtual Environment and Teleoperator Systems. World Haptics 2007. Second Joint, pp. 373–378. doi:10.1109/WHC.2007.45

## [T]

Takasaki, M., Maruyama, Y., Mizuno, T., 2007. Resonance Frequency Tracing System for Langevin Type Ultrasonic Transducers, in: International Conference on Mechatronics and Automation, 2007. ICMA 2007. Presented at the International Conference on Mechatronics and Automation, 2007. ICMA 2007, pp. 3817–3822. doi:10.1109/ICMA.2007.4304183

Tang, W., Ge, S., Zhu, H., Cao, X., Li, N., 2008. The Influence of Normal Load and Sliding Speed on Frictional Properties of Skin. Journal of Bionic Engineering 5, 33–38. doi:10.1016/S1672-6529(08)60004-9

Tomlinson, S.E., Carré, M.J., Lewis, R., Franklin, S.E., 2011a. Human finger contact with small, triangular ridged surfaces. Wear, 18th International Conference on Wear of Materials 271, 2346–2353. doi:10.1016/j.wear.2010.12.055

Tomlinson, S.E., Lewis, R., Carré, M.J., Franklin, S.E., 2013. Human finger friction in contacts with ridged surfaces. Wear, Wear of Materials 2013 301, 330–337. doi:10.1016/j.wear.2012.12.039

Tomlinson, S.E., Lewis, R., Liu, X., Texier, C., Carré, M.J., 2011b. Understanding the Friction Mechanisms Between the Human Finger and Flat Contacting Surfaces in Moist Conditions. Tribol Lett 41, 283–294. doi:10.1007/s11249-010-9709-y

## [U, V]

Utkin, V., Lee, H., 2006. Chattering Problem in Sliding Mode Control Systems. Presented at the International Workshop on Variable Structure Systems, VSS'06, pp. 346–350. doi:10.1109/VSS.2006.1644542

van Kuilenburg, J., Masen, M.A., Groenendijk, M.N.W., Bana, V., van der Heide, E., 2012. An experimental study on the relation between surface texture and tactile friction. Tribology International, 14th Nordic Symposium on Tribology, NORDTRIB 2010 48, 15–21. doi:10.1016/j.triboint.2011.06.003

Varadarajan, P.R., Yadav, M., 2002. Marketing strategy and the internet: An organizing framework. J. of the Acad. Mark. Sci. 30, 296–312. doi:10.1177/009207002236907

Varao Sousa, T.L., Carriere, J.S.A., Smilek, D., 2013. The way we encounter reading material influences how frequently we mind wander. Front Psychol 4, 892. doi:10.3389/fpsyg.2013.00892

Velazquez, R., Pissaloux, E., Szewczyk, J., Hafez, M., 2005. Miniature Shape Memory Alloy Actuator for Tactile Binary Information Display, in: Proceedings of the 2005 IEEE International Conference on Robotics and Automation, 2005. ICRA 2005. Presented at the Proceedings of the 2005 IEEE International Conference on Robotics and Automation, 2005. ICRA 2005, pp. 1344–1349. doi:10.1109/ROBOT.2005.1570302

Vezzoli, E., Amberg, M., Giraud, F., Lemaire-Semail, B., 2014. Electrovibration Modeling Analysis, in: Auvray, M., Duriez, C. (Eds.), Haptics: Neuroscience, Devices, Modeling, and Applications, Lecture Notes in Computer Science. Springer Berlin Heidelberg, pp. 369–376.

Vezzoli, E., Ben Messaoud, W., Amberg, M., Giraud, F., Lemaire-Semail, B., Bueno, M., 2015a. Physical and perceptual independence of ultrasonic vibration and electrovibration for friction modulation. IEEE Transactions on Haptics 8, 235–239. doi:10.1109/TOH.2015.2430353

Vezzoli, E., Ben Messaoud, W., Nadal, C., Giraud, F., Amberg, M., Lemaire-Semail, B., BUENO, M.-A., 2015a. Coupling of ultrasonic vibration and electrovibration for tactile stimulation. European Journal of Electrical Engineering 17, 377–395. doi:10.3166/ejee.17.377-395

Vezzoli, E., Dzidek, B., Sednaoui, T., Giraud, F., Adams, M., Lemaire-Semail, B., 2015b. Role of fingerprint mechanics and non-Coulombic friction in ultrasonic devices, in: 2015 IEEE World Haptics Conference (WHC). Presented at the 2015 IEEE World Haptics Conference (WHC), pp. 43–48. doi:10.1109/WHC.2015.7177689

Vezzoli, E., Dzidek, B., Sednaoui, T., Giraud, F., Adams, M., Lemaire-Semail, B., 2015b. Role of fingerprint mechanics and non-Coulombic friction in ultrasonic devices. World Haptics Conference (WHC), 2015 IEEE 43–48. doi:10.1109/WHC.2015.7177689

## [W]

Wang, Q., Hayward, V., 2007. In vivo biomechanics of the fingerpad skin under local tangential traction. J Biomech 40, 851–860. doi:10.1016/j.jbiomech.2006.03.004

Watanabe, T., Fukui, S., 1995. A method for controlling tactile sensation of surface roughness using ultrasonic vibration. Presented at the IEEE International Conference on Robotics and Automation, pp. 1134–1139. doi:10.1109/ROBOT.1995.525433

Wiertlewski, M., Hayward, V., 2012. Mechanical behavior of the fingertip in the range of frequencies and displacements relevant to touch. Journal of Biomechanics 45, 1869–1874. doi:10.1016/j.jbiomech.2012.05.045

Wiertlewski, M., Leonardis, D., Meyer, D.J., Peshkin, M.A., Colgate, J.E., 2014. A High-Fidelity Surface-Haptic Device for Texture Rendering on Bare Finger, in: Auvray, M., Duriez, C. (Eds.), Haptics: Neuroscience, Devices, Modeling, and Applications, Lecture Notes in Computer Science. Springer Berlin Heidelberg, pp. 241–248.

Wiertlewski, M., Lozada, J., Hayward, V., 2011. The Spatial Spectrum of Tangential Skin Displacement Can Encode Tactual Texture. IEEE Transactions on Robotics 27, 461–472. doi:10.1109/TRO.2011.2132830

Wiesendanger, M., 2001. Squeeze film air bearings using piezoelectric bending elements (PhD Thesis). École polytechnique fédérale de Lausanne EPFL, Lausanne.

Wijekoon, D., Cecchinato, M.E., Hoggan, E., Linjama, J., 2012. Electrostatic Modulated Friction as Tactile Feedback: Intensity Perception, in: Isokoski, P., Springare, J. (Eds.), Haptics: Perception, Devices, Mobility, and Communication, Lecture Notes in Computer Science. Springer Berlin Heidelberg, pp. 613–624.

Winfield, L., Glassmire, J., Colgate, J.E., Peshkin, M., 2007. T-PaD: Tactile Pattern Display through Variable Friction Reduction, in: EuroHaptics Conference, 2007 and Symposium on Haptic Interfaces for Virtual Environment and Teleoperator Systems. World Haptics 2007. Second Joint. pp. 421–426. doi:10.1109/WHC.2007.105

Winter, C., Civet, Y., Perriard, Y., 2013. Optimal design of a squeeze film actuator for friction feedback. Presented at the Electric Machines Drives Conference (IEMDC), 2013 IEEE International, pp. 1466–1470. doi:10.1109/IEMDC.2013.6556336

Winter, C., Perriard, Y., 2013. Haptic tactile interface: A novel click-wheel user experience, in: 2013 International Conference on Electrical Machines and Systems (ICEMS). Presented at the 2013 International Conference on Electrical Machines and Systems (ICEMS), pp. 1383–1387. doi:10.1109/ICEMS.2013.6713252

Woodward, K.L., 1993. The relationship between skin compliance, age, gender, and tactile discriminative thresholds in humans. Somatosensory & motor research 10, 63–67.

## [X, Y]

Xiaowei Dai, Colgate, J.E., Peshkin, M.A., 2012. LateralPaD: A surface-haptic device that produces lateral forces on a bare finger. Haptics Symposium (HAPTICS), 2012 IEEE 7–14. doi:10.1109/HAPTIC.2012.6183753

Yang, Y., 2013. Design And Control Of An Integrated Haptic Interface For Touch Screen Applications (PhD Thesis). University lille 1, Beihang University, Beijing.

Yang, Y., Lemaire-Semail, B., Giraud, F., Amberg, M., Zhang, Y., Giraud-Audine, C., 2015. Power analysis for the design of a large area ultrasonic tactile touch panel. The European Physical Journal Applied Physics 72, 11101. doi:10.1051/epjap/2015150051

# Appendix

## A1 Control scheme of the inverter

In order to produce a three level signal using the inverter, we operate two PWM (Pulse Width Modulation) signals. These signals are shifted by T/2 and their parameters are tuned thanks to the timer of the DSP. If we want to vary the excitation frequency, the maximum value of the timer of the DSP $TIM_M$ must be tuned and if we want to modify the duty cycle, we should tune the values of $TIM_1$ and $TIM_2$. In this configuration, we chose to use the same duty cycle for the two signals. Then, the three level signal is constructed by subtracting the channel 1 from channel 2. This operated method to generate the sinusoidal voltage is utilized also to synchronize the measurement of the vibration vector at four defined instants of the voltage, [0, T/4, T/2, 3T/4] which are helpful to make the system modelling easier by making $V_d = 0$.

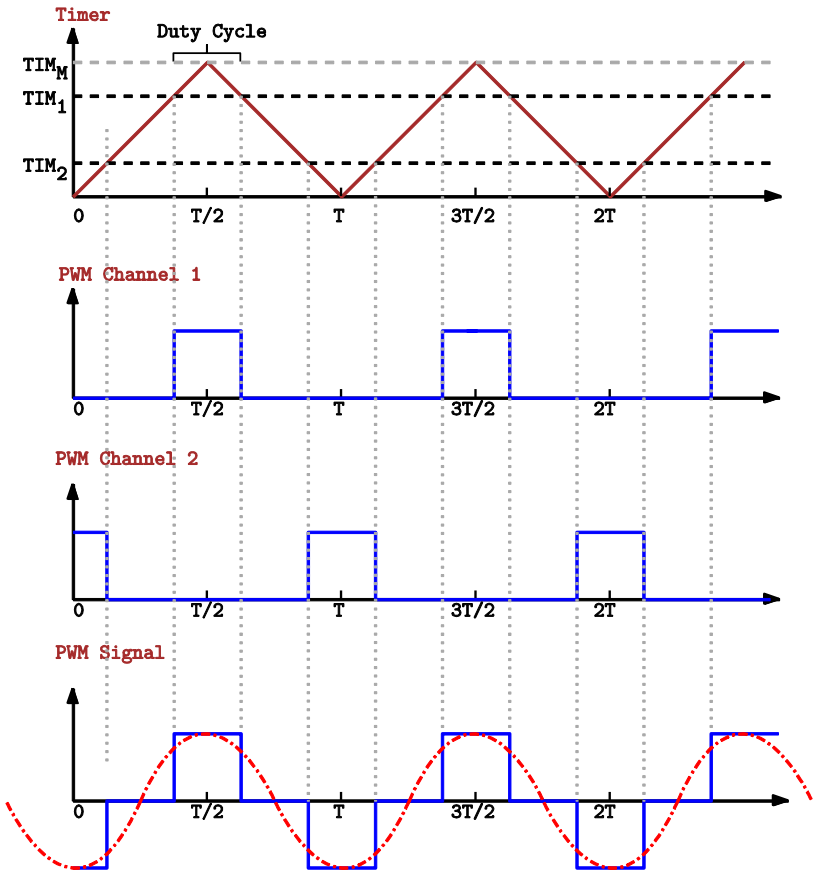


Figure A.1: The used method to create a three level PWM signal by the mean of two PWM signals with the same duty cycle and shifted by T/2. The sinusoidal voltage to be applied to the piezoceramics is filtered using a RL filter.

## A2 Measurement instants

The excitation voltage for the piezoelectric actuator, comes from the three level signal generated in the output of the inverter then filtered and amplified. This sinusoidal signal $\underline{V}$ is phase shifted comparing to the three level signal due to the electrical components in the inverter structure. This phase shift is constant and can be compensated using a rotation matrix. On a practical point of view, the tracking of the resonant frequency is performed with two steps. The first one is to look for the transformation matrix which allows the definition of $V_d$, $V_q$ and the adjustment of $V_d = 0$. This can be done by a primarily measurement offline at the resonance of $\underline{W}$ vector. This vector is first decomposed in $W_d$ and $W_q$ considering as a reference axis the three level signal of the inverter. In that case, even if we are at the resonance $W_q$ is nonzero. But from this vector $\underline{W}$, it is possible to define the transformation matrix which allows to recover the $\underline{W}$ in the new frame with $W_q = 0$. Once this transformation is defined, it is applied online on the measured $\underline{W}$ vector to determine the online values of $W_d$ and $W_q$ and the algorithm aims at minimizing the $W_q$ value by tuning the frequency.

After aligning the vector $\underline{V}$ on the q axis, the voltage vector is become in phase with the three level signal. The resonance is reached when the phase shift between $\underline{W}$ and $\underline{V}$ is $\pi/2$. The resonance is detected by the measuring the values of the vector $\underline{W}$ in 4 instant [0, T/4, T/2, T/4]. Then the real and imaginary parts of the vector $\underline{W}$ ($W_d$ and $W_q$) are determined from $a$ and $b$.

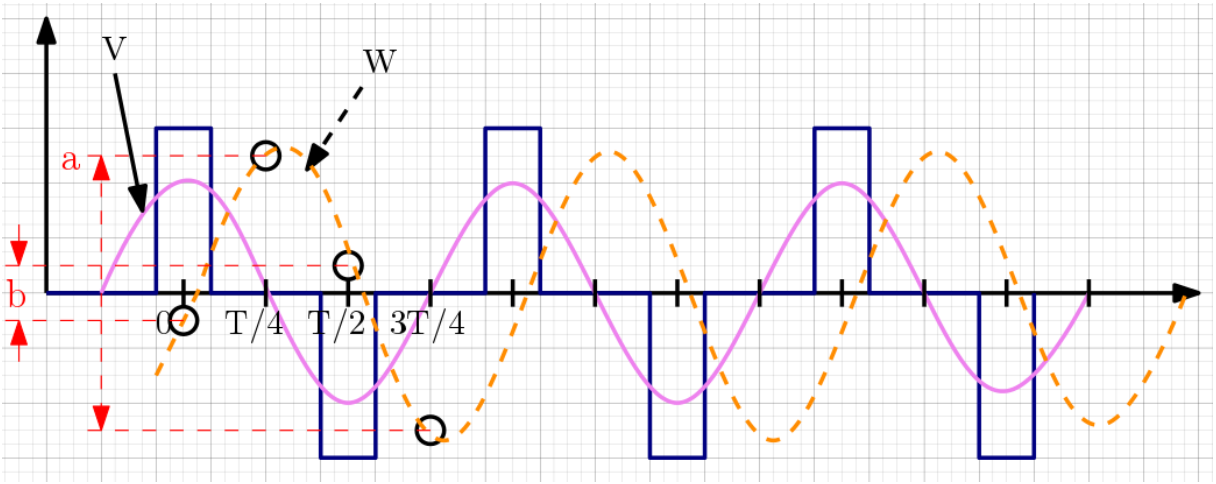


Figure A.2: The defined way to measure the real and imaginary parts of the vector $\underline{W}$ after aligning the voltage applied to the ceramics vector to the three level PWM signal.